Inaugural dissertation

for

obtaining the doctoral degree

of the

Combined Faculty of Mathematics, Engineering and Natural Sciences

of the

Ruprecht – Karls – University

Heidelberg

Presented by

M. Sc. Karolina Kuodytė

Born in Pasvalys, Lithuania

Oral examination: May 16th, 2023

The Golgi complex as a regulatory platform for DNA Damage Response pathways

Referees: Prof. Dr. Britta Brügger

Dr. Simone Köhler

I dedicate this to my loving parents.

Summary

DNA damage response (DDR) is a well-characterised process, however, the majority of studies so far focus specifically on nuclear events, while the cytoplasmic and endomembrane response to DNA damage remains largely unexplored. Although to date there exists little experimental work providing evidence to suggest a role of the Golgi complex as part of the cellular DNA damage response (DDR), a few and far in-between studies have alluded to this function (Farber-Katz *et al.*, 2014). In line with this, previous work from our lab identified a network of 15 proteins that function in various distinct DNA repair pathways, along with cell cycle and other regulatory proteins, that localise to the Golgi and the nucleus. A first in-depth characterisation of the dual-localising DDR protein RAD51C has shed some light on the potential role the Golgi complex might play in DDR (Galea *et al.*, 2022). This work has revealed that the Golgi localisation of RAD51C is dependent on the Golgin Giantin, and strongly reduced upon DNA damage coincident with its increase in nuclear DNA damage sites. The loss of this Giantin-RAD51C interaction by siRNA-mediated depletion of Giantin leads to genomic instability and aberrant DNA repair.

In light of these findings and the wide array of DDR proteins identified at the Golgi, I hypothesised that similar regulatory mechanisms would be present for various other DNA repair pathways. To assess the role of the DDR Golgi population in DNA repair response, various types of DNA lesions were induced utilising DNA damaging agents, while monitoring for any change in distribution patterns of the investigated DDR proteins. The dual-localised DDR proteins were found to change in localisation in a bi-directional manner, showing distribution from the Golgi to the nucleus or from the nucleus to the Golgi depending on the DNA damage induced and based on the proteins' role in specific DDR pathways.

A sub-organelle distribution analysis of DDR proteins within the Golgi was then performed, speculating that specific sub-organelle distribution could be important for

the activation and regulation of these proteins at the organelle. The dual-localised DDR proteins were found to be heterogeneously distributed throughout the Golgi stacks and their position on the organelle was found to be correlated to their function in DDR. Additionally, this work identified several Golgins acting as anchors and regulators of these DDR proteins at the Golgi. Furthermore, proteomic-scale interaction analysis of DDR and Golgin family proteins revealed the new interactions between the Golgin and DDR proteomes, suggesting that the network of interactions between the Golgi proteins and DDR proteins might be more extensive than previously found.

Altogether, the results described in this work demonstrate the presence of a complex relationship between the Golgi and DDR, identifying new interacting pathways between the Golgi proteins, in particular Golgins and DDR. These findings expand on our current knowledge of how DDR is regulated, showcasing the Golgi as a regulatory hub for DNA damage response. These findings are a beginning of a new direction in the DNA damage repair field, shifting from a nuclear-centric to a more global picture of how DNA damage response is regulated, opening up possibilities for finding new therapeutic targets.

Zusammenfassung

„DNA Damage Response“ (DDR) ist ein gut charakterisierter zellulärer Prozess. Die meisten bisher bekannten wissenschaftlichen Studien zu diesem Prozess fokussieren sich allerdings auf molekulare Ereignisse im Zellkern. Zelluläre Antworten auf DDR, die im Zytoplasma oder auf dem Endomembransystem stattfinden sind dagegen kaum untersucht. Obwohl es gegenwärtig wenig experimentelle Befunde gibt, die auf eine Rolle des Golgi Komplex als Teil der DDR hinweisen, haben einige wenige Studien solch eine Funktion vorgeschlagen (Farber-Katz *et al.*, 2014). In Übereinstimmung mit diesen Studien haben Arbeiten in unserem Labor ein Netzwerk von 15 Proteinen entdeckt, die zusammen mit Zellzyklus und anderen regulatorischen Proteinen eine Funktion bei der Reparatur von DNA haben und sowohl am Golgi Komplex und im Zellkern lokalisieren. Eine erste detailliertere Untersuchung des doppelt lokalisierenden DDR Proteins RAD51C hat erste Hinweise auf eine mögliche Rolle des Golgi Komplexes bei der DDR hervorgebracht (Galea et al., 2022). Diese Arbeit hat gezeigt, dass die Lokalisierung von RAD51C an den Golgi von dem Golgin Giantin abhängig ist, und nach DNA- Schädigungen dort stark reduziert wird, wobei es gleichzeitig vermehrt an Stellen der DNA- Schädigung im Zellkern auftritt. Ein Verlust der Interaktion zwischen Giantin und Rad51C, durch siRNA induzierte Herunterregulierung von Giantin führt zu einer genomischen Instabilität und fehlerhaften Reparatur der DNA.

Aufgrund dieser Befunde und der großen Anzahl von DDR-Proteinen am Golgi Komplex habe ich die Hypothese aufgestellt, dass ähnliche regulatorische Prozesse für verschiedene DNA-Reparaturmechanismen existieren. Um die Rolle der am Golgi lokalisierten DDR-Proteine zu untersuchen wurden verschiedenartige Schädigungen der DNA in Zellen induziert und mögliche Veränderungen der Lokalisierung der DDR-Proteine untersucht. Diese Experimente zeigten, dass sich Lokalisierung der doppelt

lokalisierten DDR- Proteine abhängig von ihrer Funktion bei der DDR und der DNA-Schädigung in beide Richtungen verändert, vom Golgi zum Zellkern und umgekehrt. Eine feinere Lokalisierungsstudie der DDR-Proteine auf den Golgi Membranen wurde dann aufgrund der spekulativen Hypothese, dass eine spezifische Feinlokalisierung im Golgi für die Aktivität und Regulierung dieser Proteine wichtig ist, durchgeführt. Das Ergebnis dieser Experimente zeigte, dass die doppelt lokalisierenden DDR-Proteine über den Golgi Komplex verteilt sind, ihre Lokalisierung allerdings auf dem Organell eng mit ihrer Funktion korreliert. Weiterhin hat die hier vorliegende Arbeit gezeigt, dass mehrere Golgin Proteine als Anker für die DDR-Proteine am Golgi notwendig sind. Bindungsstudien von DDR und Golgin Proteinen mittels Proteom-weiter Massenspektrometrie entschlüsselten weitere neuartige Wechselwirkungen zwischen Golgi und DDR-Proteinen und zeigen, dass das Netzwerk der Wechselwirkungen zwischen Golgi- und DDR-Proteinen wesentlich komplexer ist als bisher angenommen.

Zusammengefasst, zeigen die Resultate dieser Arbeit die Existenz einer Komplexen Beziehung zwischen dem Golgi Komplex und DDR, indem sie neuartige Wechselwirkungen zwischen Golgi Proteinen, insbesondere Golgi Proteine, und DDR identifizieren. Diese Befunde erweitern unser gegenwärtiges Verständnis wie DDR reguliert ist und demonstrieren die Rolle des Golgi Komplex als ein Schlüsselorganell für DDR. Diese Befunde stellen auch den Beginn einer neuen Richtung im Feld der DNA-Reparatur dar, eine Verschiebung von einem Zellkern-zentrischen zu einem globalen Bild wie DDR reguliert ist, und eröffnen damit neue Möglichkeiten zum Auffinden von neuen therapeutischen Targets.

List of figures

Acknowledgements

First of all, I would like to thank my supervisor and mentor Rainer Pepperkok, for the opportunity to join his lab and pursue my PhD at EMBL. I am grateful for the chance to work on this challenging and incredibly exciting project and for the scientific independence, to drive it forward. Thank you for the fruitful discussions and helpful suggestions. Your guidance has not only helped me to grow as a scientist but also as a person. Thank you for providing me with both professional and personal advice, as well as being supportive during difficult times by checking on me. Your support has meant a lot to me.

I would also like to thank my TAC committee members Britta Brügger, Simone Köhler and Justin Crocker for their support and guidance throughout my PhD. I am grateful for the insightful discussions and valuable suggestions during and outside the TAC meetings. Additionally, I would like to extend my thanks to Britta Brügger and Simone Köhler for agreeing to be the referees of this thesis, and to Stefan Wiemann for agreeing to be part of my thesis defence committee.

I would also like to acknowledge my very first scientific mentors and supervisors Vaidotas Stankevičius and Kęstutis Sužiedėlis. Thank you for inspiring and encouraging me to pursue a scientific career and giving me the opportunity to work on exciting projects during my bachelor's and master's and allowing me to participate in writing papers. Your support has been crucial in getting me where I am now. I would also like to acknowledge Vytautė Starkuvienė for giving me the chance to an internship in her lab, for the thrilling projects and collaborations that resulted in a publication, and for encouraging me to apply to EMBL for my PhD.

Furthermore, I would like to thank Simone Köhler and Gautam Dey for collaborating on following up on Golgin orthologs in c. elegans and yeast. Additionally, to Gautam, for the chats and career advice over a coffee, I appreciate it. I would also like to thank EMBL Core Facilities, especially Per Haberkant and Frank Stein, for their help with the

proteomics experiments, as well as the whole ALMF team – Alex, Faba, Manuel, Marco, Stefan, Caroline and Christian for the help with the microscopy and valuable feedback during the group meetings. Moreover, I would like to express my appreciation to EMBL cafeteria personnel, for always cheering me up with very essential cups of coffee.

Furthermore, I would like to thank my amazing current and former labmates - Magda, Juan, Sanjana, Muzamil, Joanna, Nadine, Giri, Ann, Chris and George. In particular, I want to give a special thanks to Magda for teaching me how to create CRISPR cell lines, and to Juan for teaching me the VSV-G assay. Muzamil, you've been an invaluable source of help and advice, both in the lab and in my personal life. Joanna and Sanjana, thank you for your countless words of encouragement and support during some of my toughest times. Thank you all for contributing to a great work environment, with stimulating scientific discussions that have enriched both my personal and professional life. Thank you for your patience with me, I know it wasn't always easy.

Special thanks I would like to say to George for his invaluable guidance and support throughout these years. Working with you on these amazing projects has been a pleasure, and I hope to continue collaborating with you in the future, regardless of where our scientific paths take us. Thank you for your patience, countless discussions, arguments and agreements we've had, for helping me navigate my everyday struggles, for serving as my English teacher and grammar advisor. Beyond that, thank you for the friendship we developed, for shared meals and outings, for bike repairs, pranks, woollen jumpers and glasses of Porto. Thank you for helping me survive the quarantine. Thank you for being a true friend, I really appreciate all that you've done for me.

This journey wouldn't have been great without the friendships I made here in Heidelberg. My party people - Jesus, Gilberto, Sebastian, Lucia, Anna, Agata, Matteo, Ana, Maxime, Javier, Ieva and Klaudija – thank you for making Heidelberg feel home, for all the parties, trips, adventures and experiences. Special thanks I would like to say to Aline, for being the best company and support during the thesis writing. Additionally, I would like to thank my friends back home, Judita, Erika, Gintare and Žyge for always being there for me.

At EMBL, I also had the fortune to meet my partner, Alberto. Our journey together has not always been easy, but I am glad that we have managed to build a strong team despite any confusion or challenges that have come our way. I cannot express enough how much your love and support mean to me. Thank you for inspiring me with scientific discussions, for being patient with me, and for never missing any of my talks. Thank you for all those delicious meals, from breakfast burritos and pastor, to crazy spicy enchiladas and the best popcorn. For all the amazing cocktails and countless team carbonaras, for travels and concerts. Like I once said, and I mean it, life with you is like one continuous party. I love you.

Taip pat norėčiau padėkoti Juliui, už meilę ir supratingumą, už padrąsinimus ir įkvėpimus ryžto, už palaikymą siekti svajonių.

Galiausiai, norėčiau padėkoti mano nuostabiai šeimai – sesei Živilei, sūnėnui Ąžuolui, dukterėčiai Rugilei, Aivarui ir, be abejo, mano tėvams - mamai Marinai ir tėčiui Stasiui. Be Jūsų palaikymo ir paramos niekaip nebūčiau ten, kur dabar esu. Ačiū Jums už Jūsų begalinę meilę ir rūpestį, už beribį palaikymą, už lauktuves, kurios man primena apie namus. Ačiū, kad pasidžiaugiant mano mažais pasiekimais. Man tai yra pats didžiausias įvertinimas. Ačiū, kad skatinant siekti svajonių. Labai Jus myliu ir skiriu šią disertaciją Jums.

Contributions

- All experiments presented in this thesis were designed, performed and analysed by me if not otherwise stated.
- Cell Profiler pipelines used in this work were designed by George Galea (Pepperkok lab, EMBL, Heidelberg) and modified by me.
- Proteomic analysis of prepared samples was performed by Per Haberkant (Proteomics Core Facility, EMBL, Heidelberg) and statistical analysis was performed by Frank Stein (Proteomics Core Facility, EMBL, Heidelberg).

List of publications

- **Kuodyte, K.**, Lundberg, E., Galea, G., Pepperkok, R**.** The Golgi complex as platform for DNA Damage Response pathways. (In preparation)
- Galea G; **Kuodyte K**; Khan, M. M., Thu,l P., Neumann, B., Lundberg. E., Pepperkok, R**.** The Golgi complex is a regulatory hub for homologous recombination-mediated DNA repair. *BioRxiv*. (2022)

Abbreviations

ATM	ATM serine/threonine kinase
BER	Base Excision Repair
BRCA1	BRCA1 DNA Repair Associated protein
CCAR1	Cell Division Cycle And Apoptosis Regulator 1
CHK2	Checkpoint Kinase 2
CPT	Camptothecin
ddH2O	Double Distilled Water
DDR	DNA Damage Response
DMEM	Dulbecco's Modified Eagle Medium
DNA	Deoxyribonucleic Acid
DNA-PK	DNA-dependent Protein Kinase
DOX	Doxorubicin
DSB	Double-Strand Break
DTT	Dithiothreitol
EDTA	Ethylenediaminetetraacetic acid
ELM	The Eukaryotic Linear Motif resource
ER	Endoplasmic Reticulum
ESCO2	Establishment Of Sister Chromatid Cohesion N-Acetyltransferase 2
FAM214A	Family With Sequence Similarity 214 Member A
FCS	Fetal Calf Serum
FMN2	Formin 2
GO	Gene Ontology
H2AX	H2A.X Variant Histone
H_2O_2	Hydrogen Peroxide
HeLa cells	Henrietta Lacks Cells
HR	Homologous Recombination
IF	Immunofluorescence

IP	Immunoprecipitation
IPZ	Importazole
$KBrO_3$	Potassium Bromide
LIG1	Ligase 1
LP-BER	Long-Patch Base Excision Repair
LRIG2	Leucine Rich Repeats And Immunoglobulin Like Domains 2 protein
LRRIQ3	Leucine Rich Repeats And IQ Motif Containing 3 protein
MMEJ	Microhomology-Mediated End-Joining
MS	Mass Spectrometry
MS-IP	Immunoprecipitation Mass Spectrometry
MSH6	MutS Homolog 6
NBN	Nibirin
NEG9	Negative Control siRNA
NER	Nucleotide Excision Repair
NES	Nuclear Export Signal
NHEJ	Non-Homologous End-Joining
NHLF	Normal Human Lung Fibroblast cells
NLS	Nuclear Localisation Signal
Noco	Nocodazole
NPC	Nuclear Pore Complex
PARP1	Poly(ADP-Ribose) Polymerase 1
PBS	Phosphate Buffered Saline
PCC	Pearson’s correlation coefficient
PFA	Paraformaldehyde
PFDN6	Prefoldin Subunit 6
POLQ	DNA Polymerase Theta
RAD51C	RAD51 Paralog C
RNA	Ribonucleic acid
ROS	Reactive Oxygen Species
SDCCAG8	SHH Signaling And Ciliogenesis Regulator SDCCAG8
siRNA	Small interfering RNA
SP-BER	Short-Patch Base Excision Repair
SSA	Single Strand Annealing

SSB	Single-Strand Break
TGN	Trans Golgi Network
TGN-46	Trans-Golgi Network Protein 2
TLS	Translesion Synthesis
TOPORS	TOP1 Binding Arginine/Serine Rich Protein, E3 Ubiquitin Ligase
U-2 OS	Human Bone Osteosarcoma Epithelial Cells
USP1	Ubiquitin Specific Peptidase 1
VSV-G	Vesicular stomatitis virus G
XRCC2	X-Ray Repair Cross Complementing 2 protein

List of figures

List of tables

CHAPTER 1

Introduction

Cellular compartmentalisation

Eukaryotes have evolved compartmentalisation into membrane-bound organelles to ensure a way how to achieve higher efficiency and specificity in performing biochemical reactions in a defined space and time. A wide array of membrane-bound organelles, such as the Golgi complex, endoplasmic reticulum, endosomes, lysosomes, and mitochondria were acquired throughout evolution to perform and segregate specific biochemical reactions within the cell in a very efficient and specific manner (Bock *et al.*, 2001; Zhao and Zhang, 2020).

Compartmentalisation is not exclusive to membrane-bond organelles and in recent years, extensive research focus has been dedicated to the characterisation of non-membrane-bound organelles or biomolecular condensates that are assembled via liquid-liquid phase separation (Banani *et al.*, 2017; Wheeler and Hyman, 2018). Molecular condensates like nucleolus, Cajal bodies, PML (Promyelocytic Leukaemia) nuclear bodies, etc. play a vital role in regulating various cellular processes (Musacchio, 2022).

This level of complexity and biochemical segregation has led to the requirement of elaborate signalling pathways to ensure system-wide communication and in turn cellular homeostasis. Even-though, we have a good understanding of how the various organelles function in isolation, the communication and interaction between these cellular compartments and the coordination of signalling remains a poorly understood process. Nevertheless, in the last decade, the development and improvement of new technologies allowed the field to study various processes at more a complex and systematic organelle level.

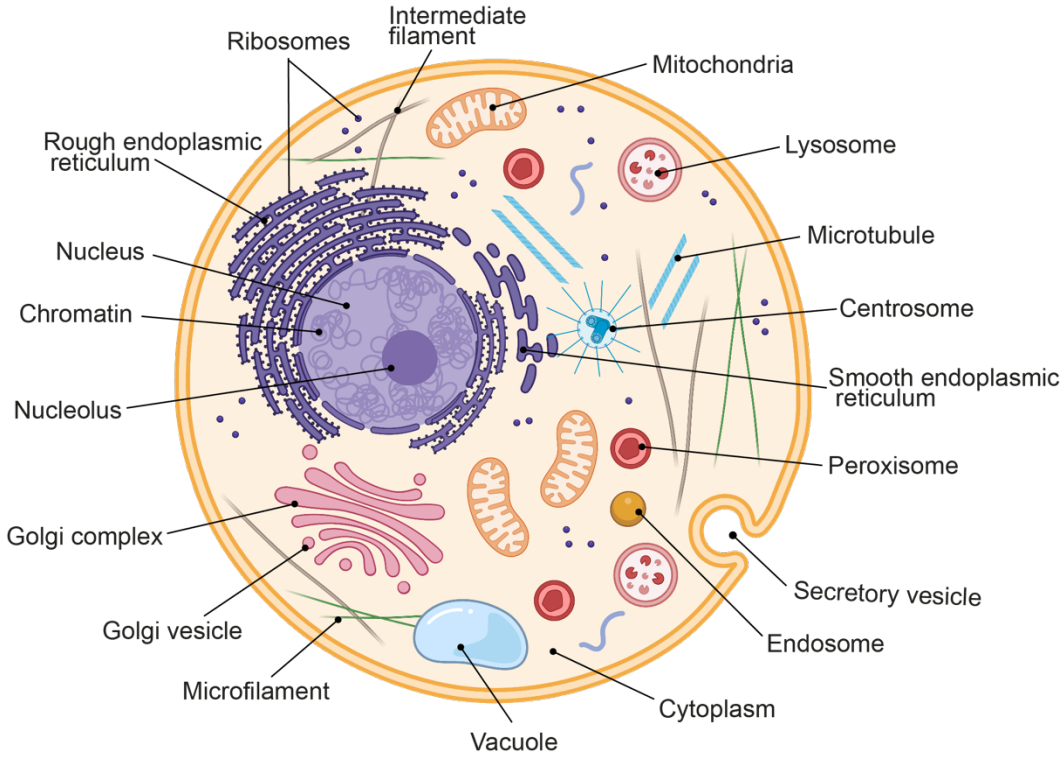

Figure 1. Schematic representation of the compartmentalisation into membrane-bound organelles of the eucaryotic cell. Generated with BioRender.

Communication between different compartments within the cell

A number of new signalling pathways important for organelle coordination have been identified and characterised, among these processes related to the Golgi. Our research team has previously shown that cell surface levels of Epidermal Growth Factor Receptor (EGFRs) are regulated through an elegant feedback loop which requires the transcriptional regulator RNF11 (Scharaw *et al.*, 2016). The study revealed that the continuous stimulation with Epidermal Growth Factor (EGF) increases the transport efficiency of newly synthesised EGFR which is transported via Coat Protein Complex II (COPII) components SEC23B, SEC24B and SEC24D. The upregulation of these transport components is achieved via the ring finger protein RNF11 which localises to early endosomes and appears additionally in the nucleus upon EGF stimulation, highlighting communication between the early secretory pathway and the nucleus.

A similar concept of systemic regulation was found for cholesterol levels via Sterol Regulatory Element-binding Proteins (SREBPs) (Brown and Goldstein, 1997; Sun *et al.*, 2005; Bartz *et al.*, 2009; Ye and DeBose-Boyd, 2011). SREBPs are bound to membranes of the endoplasmic reticulum and are synthesised as inactive precursors. Upon cholesterol deprivation, SREBPs are proteolytically cleaved and migrate to the nucleus to activate the transcription of genes required for lipid synthesis and uptake. These studies highlight the intricate signalling web present between different compartments in the cell and how this communication is accomplished through the spatial-temporal regulation of specific signalling molecules upon distinct physiological stimuli. This work will particularly focus on the communication and signalling cues occurring between the Golgi complex and the cell nucleus, a largely unexplored topic. The two very distinct compartments that play essential roles in eukaryotic cells – the genetic information storage, the 'brain' of the cell – the nucleus and the 'heart' of the cell, the packing and transport station – the Golgi Complex and how the communication between those is achieved.

Molecular transport between the nucleus and the cytoplasm

The development of a very sophisticated way of compartmentalising and concentrating biochemical reactions within the cell comes with the cost that these compartments still need to communicate and coordinate with one another in order to maintain homeostasis. This communication is particularly crucial between the nucleus and the rest of the cytoplasm, to ensure that any transcriptional changes required are communicated quickly between the cytoplasm at the nucleus in response to any cellular stress. This is achieved via a molecular transport system, mainly through the Nuclear Pore Complex (NPC) – a large multimeric structure composed of over 34 nucleoporins (Nups) that dissect the nuclear envelope and allow traffic between the nucleus and the cytoplasm (Neumann, Lundin and Poole, 2010; Strambio-De-Castillia, Niepel and Rout, 2010; Hoelz, Debler and Blobel, 2011; Lu *et al.*, 2021). Salts, nucleotides, and small molecules like ions or small proteins can diffuse freely through the nuclear pore channel, most of the proteins that are larger than 40-65 kDa require the assistance of transport receptors and active transport, to get through the NPC (Timney *et al.*, 2016; Stewart, 2022).

Large proteins requiring transport across the nucleus envelope must have specific motifs encoded in their protein sequence, namely Nuclear Localisation Signal (NLS) and Nuclear Export Signal (NES) (Cautain *et al.*, 2015). These sequences are then directly or via adaptor molecules recognised by transport carriers that bind to the cargoes, diffuse through the nuclear pores and release the cargo (Christie *et al.*, 2016). The transport receptors that are responsible for carrying cargo through NPC belong to the karyopherin-b protein family (Wing, Fung and Chook, 2022). Nuclear import is usually carried out by importin-α and importin-β protein complexes, whereas energy is supplied by the GTP-binding proteins Ran, coordinating the binding and release of the cargo from one to another compartment. In the case of nuclear export, the protein transport is carried out similarly, just in this case NES sequences are recognized and the process is driven by the export protein, CRM1 (Hutten and Kehlenbach, 2007).

The Golgi Complex

At the heart of the cell sits the Golgi complex – a central organelle in the endomembrane trafficking system. The Golgi complex stands out with its unique architecture and is comprised of flattened membrane cisternae that stack together to form a Golgi ribbon (Klumperman, 2011; Lowe, 2011). The Golgi morphology varies in shape and size in different species and cell types, while still containing similar architecture and structural features (Sengupta and Linstedt, 2011; Egea *et al.*, 2015). The Golgi stacks can be sub-categorized into *cis*, *medial* and *trans*-Golgi which further connects to the *Trans Golgi network* (TGN) (Griffiths and Simons, 1986). All of these sub-compartments have distinct compositions, where specific proteins and enzymes localise to ensure to serve a specific function (Mellman and Simons, 1992).

Surrounding the Golgi complex and facing the cytoplasmic face of the Golgi membranes, we find the Golgi matrix. This mesh-like structure composed of various proteins, mainly GRASP and Golgin protein families are believed to contribute to keeping the Golgi structure intact, as well as Golgi's functions like vesicular trafficking (Witkos and Lowe, 2016). Traditionally the Golgi functions as a processing and sorting station in the early secretory pathway. Newly synthesised proteins, lipids and polysaccharides enter the Golgi from the Endoplasmic Reticulum (ER) through the *cis*-

face of the Golgi. The cargos travel through the *cis*, *medial*, to *trans* compartments and get post-translationally modified by the Golgi enzymes. Modifications such as glycosylation, sulfation and proteolytic processing take place at the Golgi (Jamieson, 1998). Finally, the modified soluble protein cargos leave the Golgi complex through the TGN, where they must be properly sorted before reaching the final destination in the cell (Glick, 2002; Boncompain and Perez, 2013).

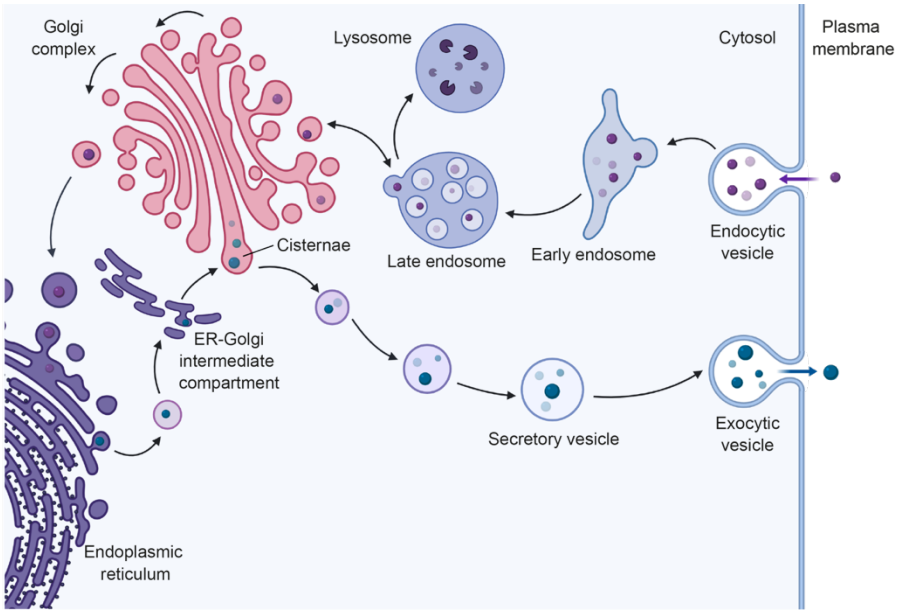

Figure 2. Schematic representation of the Golgi complex as a protein sorting and transport station. Protein cargos move from the ER to the Golgi complex where they are modified, then they are sent to various destinations in the cell, including lysosomes and the cell surface. Generated with BioRender.

In the last two decades, numerous studies have shown that functions of the Golgi complex extend way beyond the classical post-translational modification and sorting (Makhoul, Gosavi and Gleeson, 2019). It was shown that the Golgi plays a role in many more cellular processes such as mitosis (Rabouille and Kondylis, 2007), metabolism (Abdel Rahman *et al.*, 2015), stress (Sasaki and Yoshida, 2015), pro-inflammatory responses and autophagy (Chen *et al.*, 2009; Yamamoto *et al.*, 2012; Lamb, Yoshimori and Tooze, 2013); cytoskeleton organisation and dynamics, calcium homeostasis, growth signalling and energy status regulation (Wilson *et al.*, 2011); while also playing part in processes such as apoptosis and cell migration (Millarte and Farhan, 2012). It is clear that the Golgi complex is a multifunctional organelle that is critical for many cellular processes.

The Golgins

The Golgin family consists of Golgi proteins, that were initially identified as Golgi-localised antigens in patients with autoimmune diseases and classified by their molecular weight (Kooy *et al.*, 1992; Barr and Warren, 1996). Golgins are described as Golgi localised proteins, that are anchored to the Golgi membranes via their carboxy terminus and have long coiled-coil regions at the amino-terminus, positioned to the Golgi's cytoplasmic surface (Cheung *et al.*, 2015; Gillingham and Munro, 2016; Gillingham, 2017; Wong, Gillingham and Munro, 2017). These proteins share similar general structural features, even though they lack significant sequence homology. Golgins are a significant component of the Golgi matrix where they function as membrane tethers and cytoskeletal tethers to maintain the Golgi's structure integrity (Lowe, 2019).

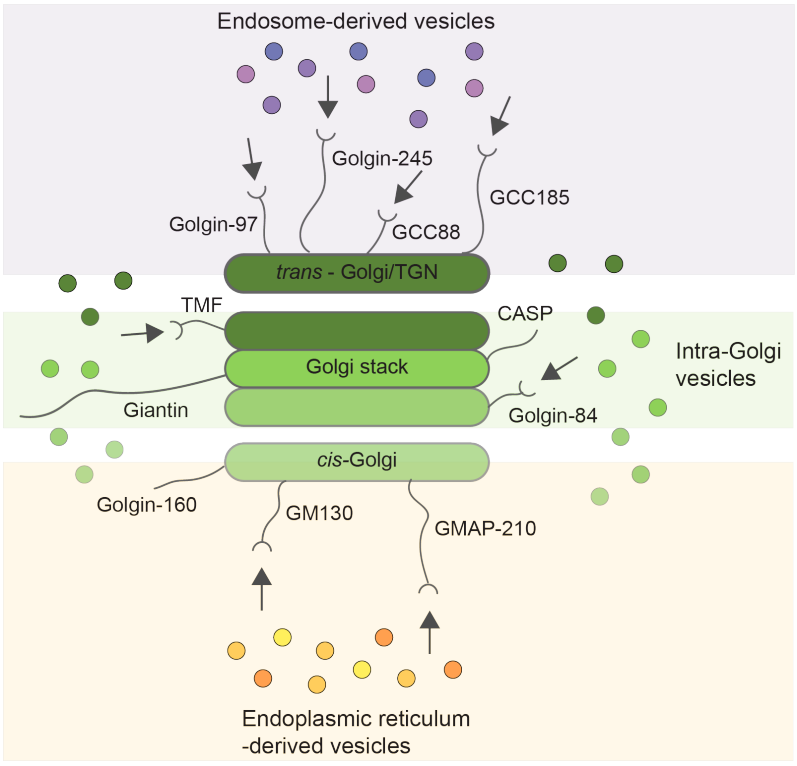

Figure 3. Schematic representation of the Golgins at the Golgi complex. The Golgins that are known to be able to tether vesicles are indicated by arrows. Modified from Lowe, 2019.

The coiled-coil nature of the Golgins allows them to extend to the cytoplasm to between 100 - 600 nm in distance, making it ideal to capture and tether membranes or vesicles from the cytoplasmic surface to the Golgi (Ishida *et al.*, 2015). The

members of this protein family are distributed throughout the Golgi complex where they selectively tether specific types of vesicles. For example, Golgins GMAP210 and GOLGA3 localised at the *cis*-face of the Golgi tether vesicles arriving from the ER or intra-Golgi vesicles; Golgins GOLGIN84 and CUX1 localised within the Golgi catch the intra-Golgi vesicles and Golgins GOLGIN-97 and GOLGIN-245 localised at the trans-face of the Golgi are responsible for tethering endolysosomal system-derived vesicles (Fig. 3) (Gillingham and Munro, 2016; Muschalik and Munro, 2018; Lowe, 2019; Shin *et al.*, 2020). Examples of various Golgins and their localisation at the Golgi are showcased in **Fig. 3** and **Fig. 4**. Golgins have been evolutionary preserved not only in vertebrate species, but also homologs of these proteins are found in worms like *c. elegans*, or single cellular species like fission *s. pombe* or budding yeast *s. cerevisiae*, highlighting their importance in Golgi's structure maintenance as well as membrane trafficking (Witkos and Lowe, 2016).

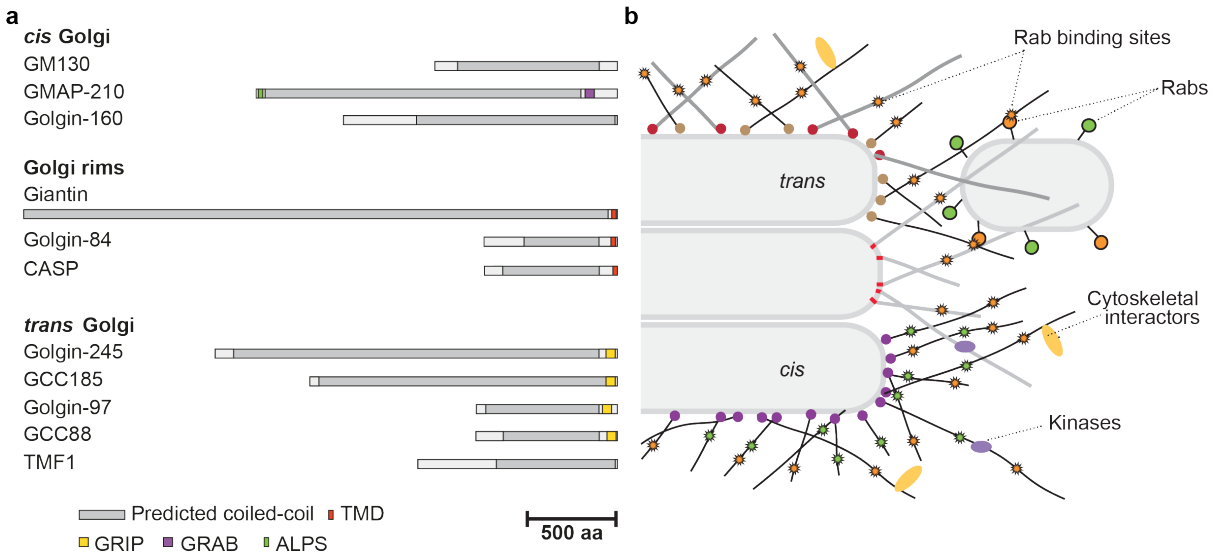

Figure 4. The Golgin protein family. (a) Schematic representation of Golgin family proteins and their functional domains. **(b)** Schematic representation of the proposed model for the Golgin function. The Golgins due to interaction with their binding partners are anchored to particular parts of the Golgi membranes via their carboxy terminus. Cytosolic proteins, such as kinases interacting with Golgins are indicated. Transport vesicles displaying Rab G proteins are captured by directly binding Golgins via Rab binding motifs. Modified from Munro, 2011.

Various Golgins have been shown to cooperate with other Golgi proteins, like small GTPases from the Rab, Arf and Arl families to maintain their localisation and operate as vesicle tethers. For example, *cis*-Golgin GM130 is anchored via protein GASP65,

trans-Golgins GCC185, Golgin-245 GCC88 and Golgin-97 interact with Arl1 via their GRIP domain, GMAP-210 is anchored via its GRAB domain that binds to Arf1; TMF is anchored via binding to Rab6 and Golgin-160 is anchored via binding to Arf1 (Munro, 2011; Witkos and Lowe, 2016). While other Golgins like Giantin, Golgin-84 or CASP are anchored to the Golgi membranes via their carboxy-terminal transmembrane domains. Besides vesicle tethering, Golgins play important in regulating various cellular processes. For example, GM130 have an important role in microtubule nucleation (Rivero *et al.*, 2009) and contributes to microtubule dynamics during mitosis (Wei and Seemann, 2009); GMAP-210 is crucial to ensure the trafficking of cargo to primary cilium (Monis, Faundez and Pazour, 2017); Giantin regulates protein cargo glycosylation at the Golgi (Lan *et al.*, 2016), etc. Considering the importance of the functions of the Golgins it comes as no surprise that the loss of functions results in various disease phenotypes (Zappa, Failli and De Matteis, 2018). For example, mutations in GMAP-210 lead to severe developmental disorders achondrogenesis type 1A (ACG1A) (Smits *et al.*, 2010) or odontochondrodysplasia (ODCD) (Wehrle *et al.*, 2019). Mutations in GM130 genes lead to neuromuscular disorder (Shamseldin *et al.*, 2016). Furthermore, Golgins have been associated with various cancer disease phenotypes (Hsu *et al.*, 2018; Yoon *et al.*, 2021; Spano and Colanzi, 2022).

The Golgi Complex in the DNA Damage Response

It has become evident that the Golgi complex is a multifunctional organelle responsible for regulating various cellular events. Moreover, recent work from the Field's lab reported that Golgi also plays a role (at least partially) in regulating the DNA damage response (DDR) In the work done by Farber-Katz *et al*., the cytoplasmic response on the Golgi after DNA damage was investigated showing that after DNA damage events, the Golgi undergoes a dramatic morphological change from ribbon-like perinuclear stack to dispersed fragments. The mechanism that drives this change requires the Golgi phosphoprotein 3 (GOLPH3) that interacts with the actin cytoskeleton mediated by the myosin protein, MYO18A. The process is initiated a few hours after a DNA damage event by the phosphorylation of the GOLPH3 by the DDR signalling kinase DNA-PK and is important for increased cell survival after DNA damage events. The reasons for this response and its impact on cell survival are unknown (Farber-Katz *et al.*, 2014). Among these, GOLPH3 has been identified as an oncogene amplified in

human cancers (Scott *et al.*, 2009) and is often overexpressed in tumours with poor prognosis (Buschman, Rahajeng and Field, 2015). As Farber-Katz *et al*. have shown, the fragmentation of the Golgi is associated with cell survival and leads to changes in trafficking patterns. These changes might enhance cell survival after DNA damage, although the particular mechanisms are still unknown. Perhaps this links to cancer formation/initiation and the role of GOLPH3 as an oncogene.

Moreover, recent work from our lab highlighted that the Golgi might play a way bigger role in DNA Damage Response (DDR) signalling than previously thought. Our lab has identified a number of DNA damage response proteins that localise both to the Golgi and the nucleus, none of these proteins has been previously described to localise or have any function at the Golgi. This study focused on the characterisation of one of these proteins – RAD51C, which is a Homologous Recombination (HR) double-strand break repair protein. In this work was shown that RAD51C redistributes from the Golgi to the nucleus upon induction of double-strand DNA breaks. The redistribution of this protein is regulated by kinase ATM. This study has also shown that RAD51C localisation at the Golgi is dependent on the Golgi protein Giantin. Disruption of this interaction leads to genomic instability and impaired DNA damage response signalling (Galea *et al.*, 2022). This study highlighted the importance of the Golgi complex in HR repair, but what about the rest of the DDR proteins that were found to localise to the Golgi?

Interestingly, these 15 proteins act in various DNA damage repair pathways, such as Homologous Recombination (HR), Base Excision Repair (BER), Non-Homologous-End-Joining (NHEJ), Mismatch Repair (MMR), not only, some proteins take part not only in DNA repair per se but are crucial for the signalling and cell cycle regulation. This project focuses on the characterisation of these proteins, starting from the hypothesis of whether the Golgi not only plays a role in HR signalling but expands to the other DNA damage repair pathways and acts as a hub for DNA damage response regulation. But first, to better understand the DNA damage response in general, the following sections will be dedicated to describing the processes underlying key players in cell response to DNA damage.

The DNA Damage Response

DNA is the essential genetic information carrier in every living cell and it is vital to maintain its integrity and stability. DNA is exposed to various physical and chemical factors such as Reactive Oxygen Species (ROS) which are endogenous products of cellular metabolism or external environment factors such as ionizing radiation and UV light which eventually lead to several types of DNA damage (Lindahl, 1993; Chatterjee and Walker, 2017). It is estimated that cells could experience around 10^5 DNA lesions daily (Hoeijmakers, 2009). This accumulation of DNA lesions has been associated with neurogenerative disorders (Rass, Ahel and West, 2007; Kulkarni and Wilson, 2008); immunological defects and infertility (Jackson and Bartek, 2009); the process of ageing (Schumacher, Garinis and Hoeijmakers, 2008) and development of cancer (Iyama and Wilson, 2013). To counteract this threat and keep the genome intact, eukaryotic cells have developed a number of mechanisms for the maintenance and repair of DNA which are collectively termed DNA Damage Response (DDR) (Harper and Elledge, 2007; Ciccia and Elledge, 2010).

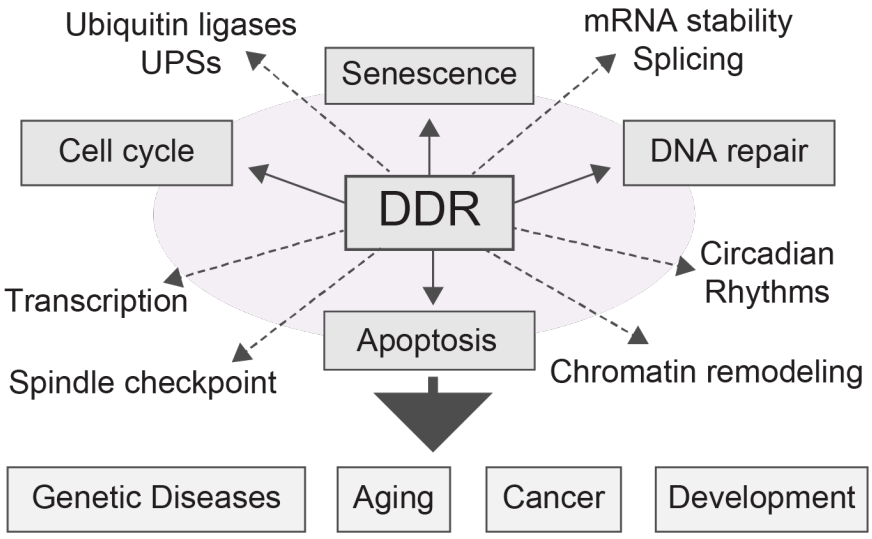

Figure 5. Consequences to DNA Damage Response in biochemical and physiological processes. Modified from Harper and Elledge, 2007.

Process	Key mediators
Nonhomologous end joining (NHEJ)	
Recognition	gH2AX, ATM, ATR, DNA-PK, Ku70, Ku80
DNA end processors	Artemis
DNA ligation	Ligase IV, XRCC4, XLF
Homologous recombination (HR)	
Recognition	gH2AX, ATM, ATR, MRE11, RAD50, NBS1
DNA end sensors	CtIP, EXO1, BLM, RPA
DNA resection/strand invasion	RAD51, RAD52, PARP-1, BRCA1, BRCA2, PALB2
DNA strand resolution	BLM, topoisomerase IIIa, MUS81, EME1, GEN1
Base excision repair (BER)	
Recognition	DNA glycosylases (MUTYH, OGG), Ape1, PARP1
End processors	APE, PNK, Aprataxin
DNA synthesis	DNA polymerase b
DNA ligation	XRCC1, Ligase IIIa, Ligase 1
Nucleotide excision repair (NER)	
Recognition	XPC, XPA, RPA, RAD23, CSA, CSB
DNA unwinding	TFIIH, RNA polymerase II
DNA cleaving	ERCC1, XPF, XPG
DNA repair	DNA polymerase d or e, PCNA, RPA, RFC
Mismatch repair (MMR)	
Recognition	MSH2, MSH6, MSH3
DNA cleaving	MLH1, PMS2, PCNA, EXO1
DNA repair	Polymerase d/e and DNA ligase IV

Table 1. DNA damage repair mechanisms and their key effector proteins. Modified from Weeden and Asselin-Labat, 2018.

The main function of DDR is to detect errors in DNA, signal their presence and lead to their repair (Harper and Elledge, 2007). This requires the tight coordination of several pathways that need to be regulated both spatially and temporally to sustain cell homeostasis There are various types of DNA lesions that occur, namely pyrimidine dimers, DNA adducts and crosslinks, base oxidation, hydrolysis and damage, single and double-strand breaks, replication errors etc. (Weeden and Asselin-Labat, 2018); with each requiring very distinct and specific mechanisms to get repaired. For example, single-strand lesions - the Single-Strand DNA Breaks (SSB) and oxidative

damage of DNA bases are repaired by Base Excision Repair (BER) system (David, O'Shea and Kundu, 2007); errors during DNA replication are fixed by Mismatch Repair (MMR) (Jiricny, 2006); bulky adducts are removed by Nucleotide Excision Repair (NER) (Hoeijmakers, 2001). Each of these systems requires a unique set of proteins for the signalling, the repair machinery recruitment to the site of damage and the repair itself which are summarised in **Table 1.**

Double-strand break repair

Among the various types of DNA damage, Double Strand Breaks (DSB) are perhaps the best characterised as they are considered the most dangerous of all the DNA lesions, resulting in chromosome rearrangements which result in cell death or oncogenesis (Lieber, 2010). The two main pathways that handle the repair of double-strand breaks: Homologous Recombination (HR) and Non-Homologous DNA End-Joining (NHEJ) (Scully *et al.*, 2019). In addition to these, Microhomology-Mediated End-Joining (MMEJ) and Single Strand Annealing (SSA) mechanisms are also responsible for double-strand break repair, however, they are more prone to errors and are rather specific to radiation-induced DSB (Czajkowski, Szmyd and Gee, 2022).

Homologous Recombination

The most accurate mechanism that repairs double-strand DNA breaks is Homologous Recombination (HR). In this case, the information in the repair process is copied from a homologous DNA sequence that is present in another chromosome, avoiding introducing any errors into DNA. However, this mechanism can be active only in the late S/G2 phases of the cell cycle, when the sister chromatid is available as a template (Scully *et al.*, 2019; Burgess *et al.*, 2020). The repair is initiated by activation of the Ataxia-Telangiectasia Mutated (ATM) protein kinase via autophosphorylation (Matsuoka *et al.*, 2007; Maréchal and Zou, 2013), an event, that leads to ATM localisation at the site of DSB. This process is followed by phosphorylation of histone H2AX, known as γH2AX and further downstream substrates that lead to the recruitment of MDC1 (Mediator of DNA Damage, Checkpoint protein 1) and MRE-11-RAD50-NB1 (MRN) complex to the site of DNA damage (Carusillo and Mussolino, 2020; Reginato and Cejka, 2020). These events are followed by further downstream

signalling and recruitment of proteins CtIP, RPA (replication protein A), BRCA1, PALB1, BRCA2 and RAD51 proteins act in repairing double-strand DNA break via HR repair (Lee *et al.*, 2022).

Non-Homologous End Joining

Non-Homologous End Joining DNA repair pathway does not require a sister chromatid as a template for double-strand break repair and occurs throughout the cell cycle (Jazayeri *et al.*, 2006; Czajkowski, Szmyd and Gee, 2022). However, it comes with an expense that repair is not as accurate and can result in added small deletions and insertions into DNA sequence (Symington and Gautier, 2011; Chapman, Taylor and Boulton, 2012). In the NHEJ pathway, the repair is initiated by binding of Ku70/Ku80 protein heterodimer to the site of damage. This leads to the recruitment of the kinase DNA-PK_{cs}, that in turn phosphorylates repair signalling propagator γH2AX, as well as other repair complex components Ku70/Ku80, Artemis, XRCC4, XLF (Hartlerode and Scully, 2015; Chang and Lieber, 2016). The repair process is completed by ligation via DNA ligase IV and XLF (Ma *et al.*, 2004; Deriano and Roth, 2013).

Microhomology-Mediated End Joining

Another, however, even less accurate than the NHEJ alternative double-break repair mechanism is MMEJ (or Alt-EJ) – a pathway, that is often upregulated in cancer cells that are deficient in HR and NHEJ repair and is activated in case of extensive DNA damage (Chang *et al.*, 2017). The repair processed via this pathway can give rise to large chromosomal translocations, deletions, insertions and other complex rearrangements in DNA (Iliakis *et al.*, 2004; Simsek and Jasin, 2010; Iliakis, Murmann and Soni, 2015). The MMEJ pathway is initiated by the binding of ADP-ribose polymerase 1 (PARP1), followed by the assembly of repair complex with the key players in it: MRN, CtIP, X-Ray Repair Cross-complementing protein (XRCC1), Polymerase theta (POLQ) and Ligase 4 (Lig4) (Frit *et al.*, 2014; Sallmyr and Tomkinson, 2018).

Single-strand break repair

Base Excision Repair

Small alterations to the DNA helix caused by oxidation, deamination and alkylation by various environmental factors are repaired via Base-Excision Repair (BER) pathway (Krokan and Bjørås, 2013). The repair is initiated by DNA glycosylases (AP endonucleases) and depending on the damage can proceed in two alternative ways – Short-Patch SP-BER (in case of single nucleotide damage) and Long-Patch LP-BER (in case of damage in 2-10 nucleotide patches). SP-BER is then processed by XRCC1, Pol ß and LIG3 (Hegde, Hazra and Mitra, 2008; Krokan and Bjørås, 2013), whereas LP-BER appears only in proliferating cells, utilizing DNA replication machinery for the repair and involves APE1, PCNA, POLδ and LIG1 for repair to be complete (Woodrick *et al.*, 2017).

Mismatch Repair

The pathway that repairs base mismatches, mutations caused by small deletions/insertions during DNA replication and recombination is named DNA Mismatch Repair (MMR) (Kunkel and Erie, 2005; Li, 2008). The repair is initiated by the ATPase heterodimers MSH2-MSH6 and MSH2-MSH3 binding to the mismatched DNA, followed by recruitment of other factors such as MLH1/PMS2, EXO1, PCNA, POLδ. The repair is finished by the ligation step performed by Lig1 (Li, 2008; Pećina-Šlaus *et al.*, 2020).

Nucleotide Excision Repair

Bulky DNA adducts caused by UV light or other chemical factors are repaired utilizing Nucleotide Excision Repair (NER) pathway. NER can be split into two alternative pathways: Global Genome NER (GG-NER) can act anywhere in the genome, whereas Transcription Coupled NER (TC-NER) occur only in regions with active transcription (Fousteri and Mullenders, 2008; Schärer, 2013). The lesion is detected by Cockayne syndrome proteins CSA and CSB, followed by excision made by ERCC1 complex;

resynthesis by POLδ/ε/κ and ligation by Lig1/3-XRCC1 (Borszéková Pulzová, Ward and Chovanec, 2020).

DNA Damage Response at a broader scale

When it comes to DNA damage response, DNA damage repair tends to take centre stage but it is important to keep in mind that DDR extends way beyond just repair. DNA repair goes hand-in-hand with the regulation of many physiological processes, such as insulin signalling, RNA splicing, kinetochore proteins and mitotic spindle, chromatin remodelling, mitotic checkpoint, as well as a strong connection with the circadian clock (Collis and Boulton, 2007; Harper and Elledge, 2007; Sancar *et al.*, 2010). This is particularly evident in cell cycle regulation, where specific DNA repair pathways can only occur within a short phase of the cell cycle. It is clear that DNA damage response is an extremely broad and physiologically essential process that has an impact on the entire cell. On the other hand, most of the studies in response to DNA damage are focused on following nuclear events, while the response and effects of these events on the cytoplasmic organelles still need to be investigated.

Aims of the study

Previous work carried out in our research team identified 15 DNA damage response (DDR) proteins that localise both to the Golgi and to the nucleus. In-depth characterisation of one of these dual-localised proteins RAD51C revealed that this protein redistributes from the Golgi to the nucleus upon induction of double-strand DNA breaks (DSB) and its localisation at the Golgi is dependent on the Golgin Giantin. Concurrently with this RAD51C redistribution, an increase in genomic instability and inhibition of DSB repair signalling was observed (Galea *et al.*, 2022). These results along with the identification of several Golgi-localising DDR protein functioning in other DNA repair pathways led to the hypothesis that this Golgi regulation could function for other DNA repair pathways in general. Therefore, placing the Golgi as a central platform for DNA damage response regulation.

Project hypothesis:

DNA damage response is a highly regulated process where the Golgi acts as a central regulatory station ensuring that various types of DNA repair machinery are recruited at the sites of DNA damage when required. **With this, the following aims were set:**

I. To test the involvement of the Golgi population of identified DDR proteins in response to various types of DNA damage.
II. To identify key proteins responsible for the localisation of DDR proteins at the Golgi and their regulation.
III. To characterise the role of the Golgi complex in DNA damage response.

CHAPTER 2

Results

Identification of DNA Damage Response proteins at the Golgi

Previous work in the Pepperkok Team identified a network of at least 15 DNA damage response proteins that localise to the nucleus, Golgi complex and further cytoplasmic structures (**Fig. 6**) (Galea *et al.*, 2022). The network consists of proteins that are described to act in various DNA damage repair and DNA damage response associated pathways, for example, Homologous Recombination (HR) - proteins RAD51C and NBN; Non-Homologous End-Joining (NHEJ) – proteins POLQ and LRGI2; Base Excision Repair (BER) - LIG1 and TOPORS; Mismatch Repair (MMR) – MSH6; along with proteins involved in cell cycle regulation – CCAR1 and SDCCAG8. Here I present example images of these dual-localised proteins acquired in Galea et al., 2022 (**Fig. 6b**).

To start understanding the role of these proteins in the DDR pathways and potentially at the Golgi complex I analysed the available literature and summarised the role of the proteins and predicted domains of interest below. I would like to briefly introduce each of these proteins and their relation to DNA damage response. Starting from - RAD51C a protein from the RAD51 recombinase family is characterised as one of the key players acting in homology-mediated double-strand break repair (Rein, Bernstein and Baldock, 2021). Along with RAD51C, another key player of HR is Nibirin (NBN) – a component of the MRE11-RAD50-NBN (MRN complex) that is crucial for the initiation and processing of HR double-strand break repair (Qiu and Huang, 2021). DNA polymerase theta (POLQ) is an enzyme which promotes double-strand DNA break repair via an alternative NHEJ pathway – more specifically via MMEJ (Ceccaldi *et al.*, 2015; Kent *et al.*, 2015). Ubiquitin-specific peptidase 1 (USP1) is an enzyme from the

ubiquitin-specific processing (UBP) family, that is involved in the regulation of HR and NHEJ (Murai *et al.*, 2011), acts in alternative DNA repair pathways such as Fanconi Anemia (FA) pathway (Nijman *et al.*, 2005) and Translesion synthesis (TLS) (Huang *et al.*, 2006). LRIG2 protein has been described to be associated with the NHEJ pathway, however, its specific role in the repair process remains to be elucidated (Fadda *et al.*, 2016). Ligase 1 (LIG1) besides being crucial for joining Okazaki fragments during DNA replication (Maffucci *et al.*, 2018), acts in the final steps of the LP-BER pathway (Balakrishnan *et al.*, 2009). TOPORS – a protein, which functions as E3 ubiquitin and E3 SUMO1 protein ligase, has been described to have a regulatory role in BER (Hu *et al.*, 2018a). Another protein from the dual-localised protein network – MSH6 – is a protein that forms two protein complexes together with MSH2 and the dimer is known to be an essential component of mismatch repair machinery (Pećina-Šlaus *et al.*, 2020).

The identified cluster of DDR proteins consists not only of key DNA damage repair machinery proteins but also important of various signalling regulators that are crucial for ensuring cell responses to DNA damage. Such example is cell cycle regulation. Cell cycle and apoptosis regulatory protein (CCAR1) has been first identified as an apoptosis regulator, but later on, been shown to play an active role in the cell cycle (Rishi *et al.*, 2003; Muthu *et al.*, 2015), transcription and DDR regulation (Kim *et al.*, 2008; Seo *et al.*, 2013). SHH signalling and ciliogenesis regulator (SDCCAG8) has been described to be important for DDR signalling (Airik *et al.*, 2016). Formin 2 (FMN2) – a protein, known to be important for the organization of actin cytoskeleton along with cell polarity, has been shown to have a role in DDR through the regulation of cyclin-dependent kinase inhibitor p21 (Yamada *et al.*, 2013). Establishment of sister chromatid cohesion N-acetyltransferase (ESCO2) is a protein required for cohesion between sister chromatids in particular during DNA replication as well as recombination-mediated DNA repair (Jevitt *et al.*, 2023). Prefoldin subunit 6 (PFDN6) – a subunit of the prefoldin complex, required for actin and tubulin folding (Tahmaz, Shahmoradi Ghahe and Topf, 2022). Some proteins from the network still need to be better characterised. For example, FAM214A, which has been shown in a genome-wide HR screen to affect HR (Adamson *et al.*, 2012), requires further characterisation. Similarly, LRRIQ3 is a not well-characterised protein which is bioinformatically predicted to be associated with DDR.

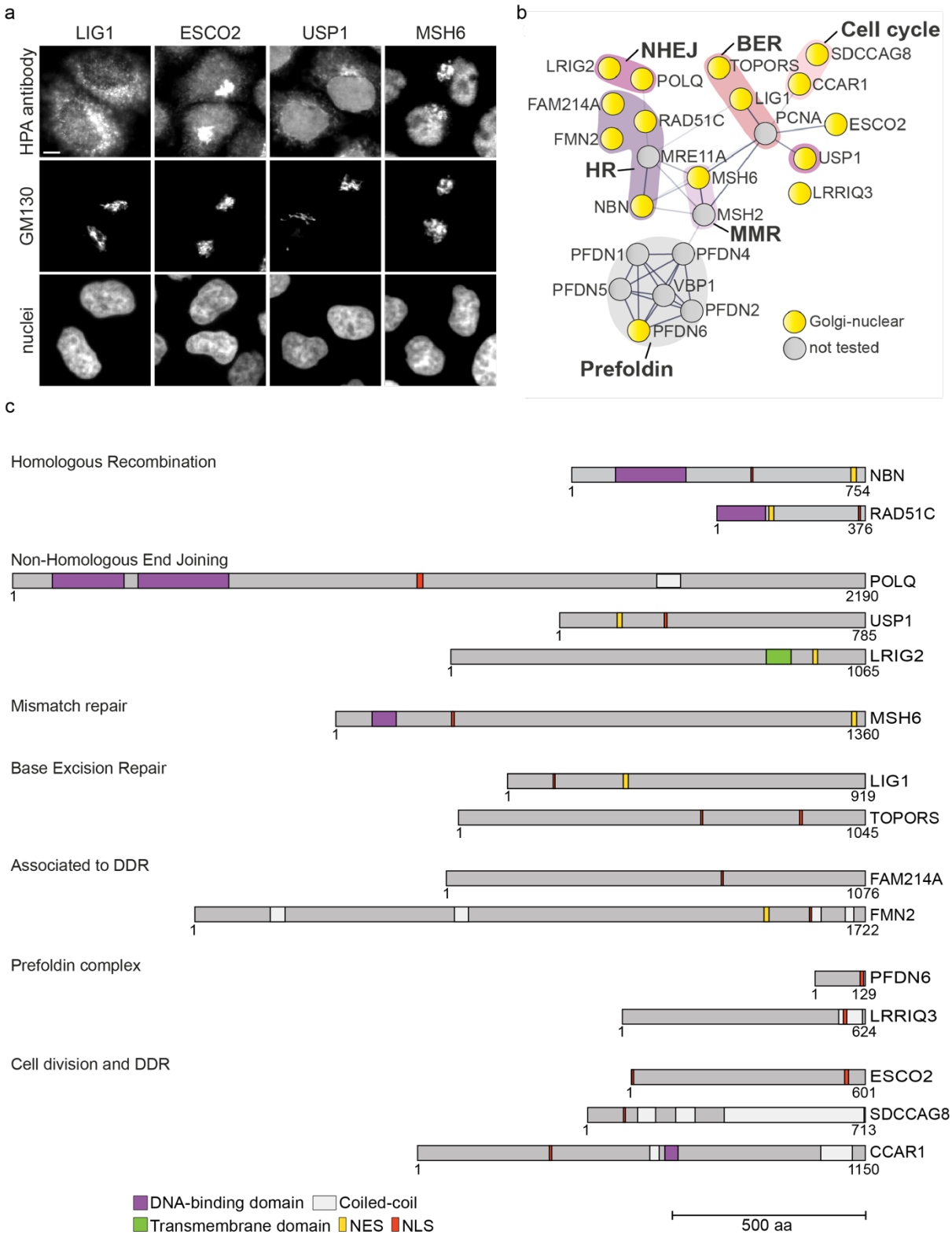

Figure 6. Identified DNA damage response proteins localising at the Golgi and the nucleus.

Legend continues in next page.

Figure 6. Identified DNA damage response proteins localising at the Golgi and the nucleus. (a) Representative images of dual-localised proteins; HeLa Kyoto cells were fixed and stained with antibodies against LIG1, ESCO2, USP1, MSH6 and Golgi marker GM130; nuclei were stained with Hoechst 33342; scale bar, 5 μm. **(b)** STRING protein-protein interaction network of dual-localised DNA damage response proteins; yellow nodes indicate dual-localised DDR proteins; grey nodes are filler nodes; experimental-based network, confidence level > 0.4. **(c)** Schematic representation of the dual-localised DDR proteins. Known functional DNA binding and transmembrane domains are indicated. Predicted Nuclear Localisation Signal (NLS) and Nuclear Export Signal (NES) from ELM resource (Kumar *et al.*, 2022).

Interestingly, none of these proteins has been previously described to localise or have any function in the Golgi. Protein structure analysis revealed that none of these proteins, besides LRIG2, have predicted transmembrane domains which would be one explanation for their localisation at the Golgi (**Fig. 6c**). Altogether this raises questions about why and how these proteins are localised at the Golgi. These questions will be further addressed in the results chapter.

Validation experiments for dual-localised DDR proteins

To start characterising the Golgi-nuclear localised DDR proteins, I first started by validating the localisation of these proteins using different molecular biology methods. To this aim, I utilized three different cell lines - HeLa Kyoto cells, which were previously used in Galea et al., 2022, human osteosarcoma cells U-2 OS, commonly used in the DDR field and normal human lung fibroblasts NHLF and validated DDR protein localisation in these cell lines. Here, as an example, I showcase the cell cycle and apoptosis regulatory protein CCAR1, which was confirmed to localise in addition to the nucleus also to Golgi membranes co-stained with the Golgi marker GM130 (**Fig. 7a**) in all three cell lines. The localisation in different cell lines was also tested for shortlisted proteins from different DDR pathways – RAD51C (HR), and USP1 (NHEJ) (**Appendix Supplementary Fig. 1**). Next, the specificity of antibodies for DDR proteins was tested upon depletion of DDR proteins. An example of a selected protein CCAR1 antibody specificity test is shown in **Fig. 7b**, where it was validated that the fluorescence intensity of CCAR1 antibody staining significantly decreased in both the Golgi and nuclear compartments upon depletion of CCAR1 with siRNA (**Fig. 7b, c**).

The antibody specificity with siRNA knock-down was also validated for proteins RAD51C, NBN, USP1 and LIG1 (**Appendix Supplementary Fig. 1**).

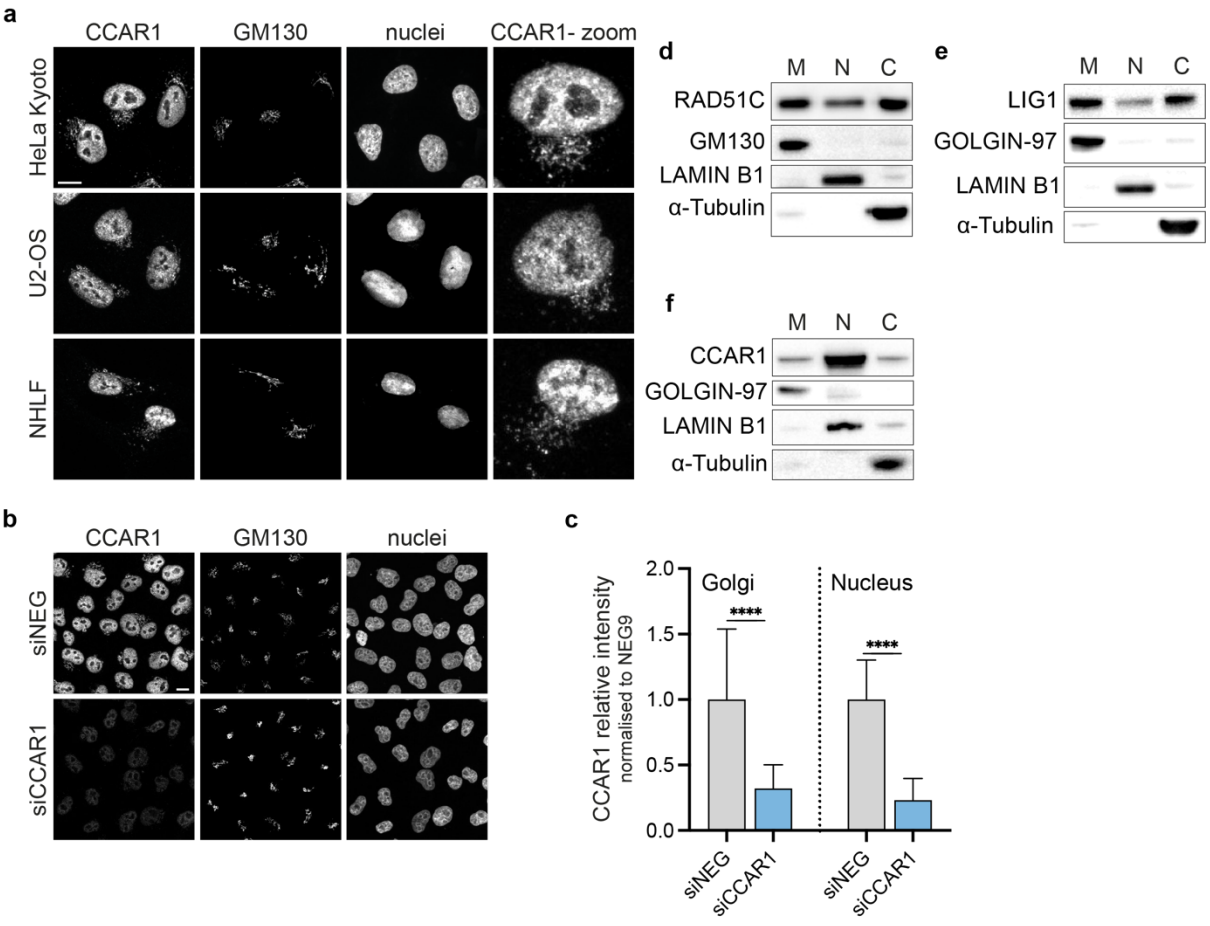

Figure 7. Validation experiments for Golgi-nuclear localised proteins. (a) Representative images of the dual-localised DDR protein CCAR1 in HeLa Kyoto, U2-OS and NHLF cells, which were fixed and stained with antibodies against CCAR1, Golgi marker GM130; nuclei were stained with Hoechst 33342. **(b)** Example images of antibody against CCAR1 validation experiment. HeLa Kyoto cells were transfected with control NEG9, and CCAR1 siRNAs for 72 hours, then fixed and stained with antibodies against CCAR1 and Golgi marker GM130; nuclei were stained with Hoechst 33342, scale bars, 10 μm. **(c)** Quantification of CCAR1 intensity after depletion with siRNA. Error bars represent the mean ± SD (n=3 independent biological replicates). Statistical significance: ****P < 0.0001, compared to untreated control, determined using two-tailed unpaired Student's t-test. **(d, e, f)** Western blots showing the subcellular fractions: membrane (M), nuclear (N) and cytoplasmic (C) of RAD51C, LIG1 and CCAR1, where markers for fractions are: GM130 and GOLGIN-97, for the Golgi membranes, LAMIN B1, for the nuclear compartment and α-Tubulin for the cytoplasmic fraction.

Additionally, the localisation of selected DDR proteins was further validated biochemically, using a subcellular fractionation approach. For this, HeLa Kyoto cells, using a combination of reagents from The Subcellular Protein Fractionation Kit (Thermofisher Scientific) and centrifugation were stepwise lysed into three functional fractions: soluble cytoplasmic, membrane (includes plasma membrane, mitochondria, endoplasmic reticulum and Golgi membranes) and nuclear (soluble and chromatin-bound fractions combined). In this experiment, I tested, whether DDR proteins could be detected in all three subcellular fractions, as it was observed via immunofluorescence. The western blot analysis of subcellular fractionations for proteins RAD51C, LIG1 and CCAR1 is shown in **Fig. 7d-f**. These experiments confirm the localisation of selected proteins RAD51C, LIG1 and CCAR1, where these proteins were found in membrane, nuclear and cytoplasmic fractions. The enrichment of each fraction was tested with marker proteins, GM130 and GOLGIN-97 for enrichment in Golgi membrane proteins, Lamin B1 for nuclear proteins and α-Tubulin – for cytoplasmic proteins. Altogether these experiments validate our approach and confirm the localisation of DDR proteins at the Golgi and the nucleus, both via immunofluorescence and biochemical assays. However, why these proteins localise to both compartments and what the functional role of this localisation is yet to be answered.

DDR protein localisation changes upon DNA damage induced by doxorubicin

Since these 15 proteins that were found to localise to the Golgi are described to have a function in DNA damage response, I first started testing whether these proteins respond to induction of DSBs and whether the Golgi population of the protein is required for this. For this purpose, the DNA-damaging agent, doxorubicin (DOX), a widely used chemotherapeutic drug that predominantly induces double-strand DNA breaks through intercalation of DNA (Tewey *et al.*, 1984; Stingele, Bellelli and Boulton, 2017), was utilized. HeLa Kyoto cells were treated for 3 hours with the DNA damaging agent, then fixed and immunostained for the proteins of interest and the Golgi marker GM130. Treatment with DOX resulted in changes in the subcellular distribution pattern of the majority of the tested proteins (**Fig. 8, 9**). The localisation changes observed were varied but presented two predominant patterns, a distribution change where the

Golgi population of the protein was reduced and the nuclear population increased or the reverse, where the nuclear population decreased with a larger proportion of the protein on the Golgi complex (**Fig. 8b, Fig. 9b**). In order to fully quantify changes in localisation upon treatment and counter any reduction of the overall protein population, a ratio of the total Golgi population against the nuclear population for each protein tested was calculated. These measurements give a better representation of the changes in population dynamics, especially since in most of the cases the overall protein population was observed to reduce over the course of DOX treatment (**Appendix Supplementary Fig. 2a, b**). When the distribution ratio is smaller than one – proteins distribute in a pattern Golgi-to-nucleus, while ratios larger than one denote a nucleus-to-Golgi redistribution pattern. Proteins, directly acting on DNA repair are presented in **Fig. 8** and DDR signalling proteins are presented in **Fig. 9.**

DDR proteins functioning in a specific DNA damage repair pathway displayed a similar redistribution pattern when treated with doxorubicin. For example, HR proteins RAD51C and NBN resulted in distribution ratios 0.27 ± 0.09 and 0.63 ± 0.29, where in the RAD51C case the population of the protein in the Golgi was decreased (**Fig. 8c**) and the population in the nucleus increased, forming distinct nuclear foci (**Fig. 8d**), whereas NBN population in the nucleus did not increase (**Fig. 8d**), however, the population in the Golgi reduced at a higher rate than in the nuclear compartment and resulted in the distribution ratio lower than 1.

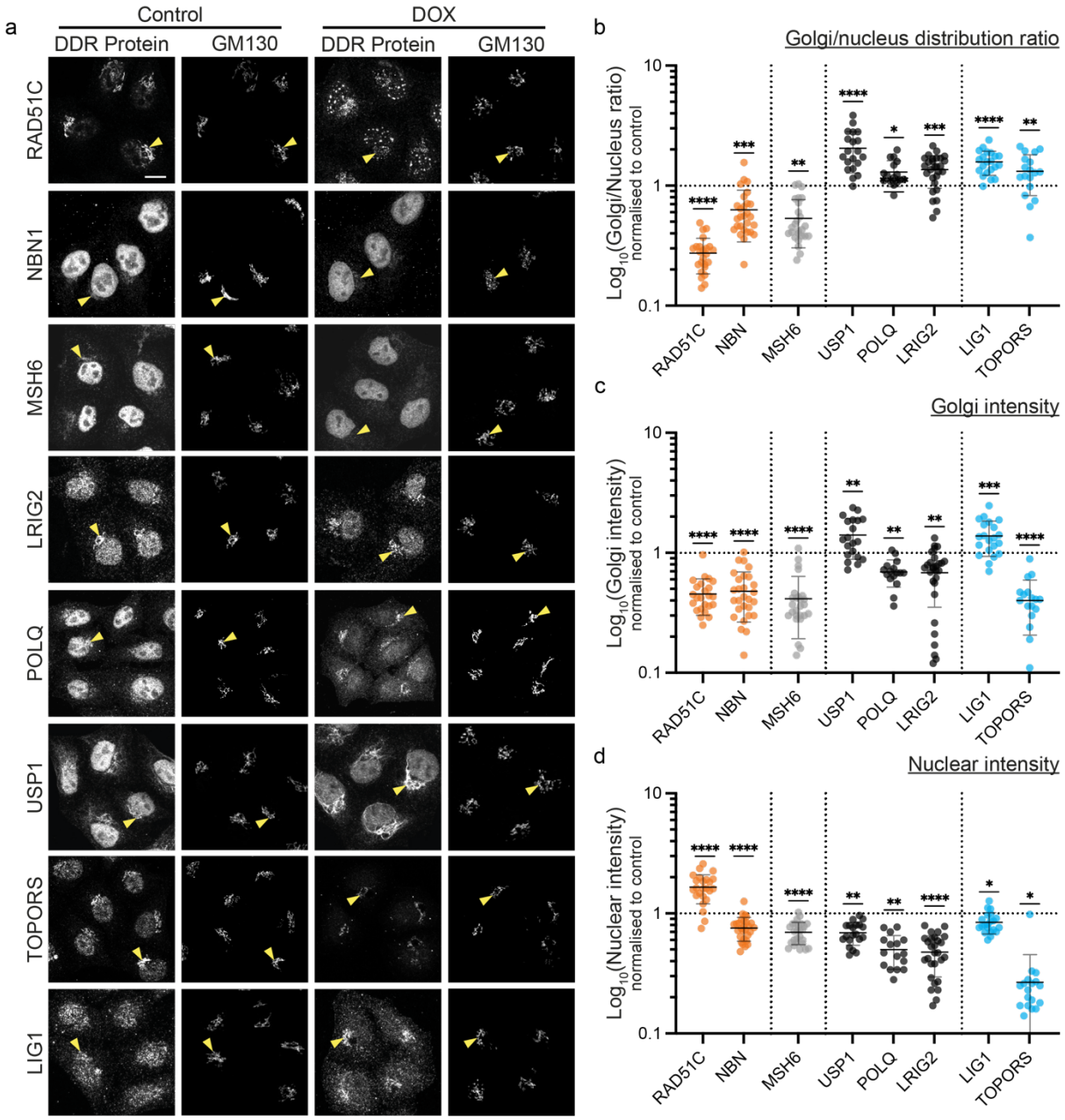

Figure 8. Dual-localising proteins undergo localisation changes upon induction of DNA damage by doxorubicin.

Legend continues in next page.

Figure 8. Dual-localising proteins undergo localisation changes upon induction of DNA damage by doxorubicin. (a) HeLa Kyoto cells were treated with 40 μM Doxorubicin (DOX) for 3 hours prior to cells being fixed and stained with antibodies against RAD51C, NBN, MSH6, LRIG2, POLQ, USP1, TOPORS, LIG1, Golgi marker GM130. Yellow arrows indicate the Golgi membrane, scale bar, 10 μm. **(b)** Quantification of the normalised ratio of Golgi-nuclear distribution of DDR proteins untreated control versus DOX treated. **(c)** Quantification of the relative intensity of DDR proteins at the Golgi, DOX treated normalised to untreated control. **(d)** Quantification of the relative intensity of DDR proteins at the nucleus, DOX treated normalised to untreated control. The proteins are classified according to the DDR pathway they function in. Error bars represent the mean ± SD (n=3 independent biological replicates). Statistical significance: *P < 0.05, **P < 0.01, ***P < 0.001, ****P < 0.0001, compared to untreated control, determined using two-tailed unpaired Student's t-test.

A similar redistribution pattern was observed with the MMR protein MSH6, where in total protein population was reduced (**Appendix Supplementary Fig. 2a**), although at a higher rate in the Golgi than in the nucleus (distribution ratio 0.53 ± 0.23), as well as with cell cycle regulatory protein CCAR1 (distribution ratio 0.47 ± 0.21). This protein, similarly to RAD51C, formed distinct nuclear foci upon the induction of DSB. However, the nature of these structures needs to be further tested. Interestingly, proteins LIG1 and TOPORS, acting in the BER pathway, responded to the DOX oppositely. The LIG1 population in the nucleus was reduced and the Golgi population increased (distribution ratio 1.59 ± 0.35); the TOPORS protein population decreased in both compartments, but at a higher rate in the nucleus (distribution ratio 1.32 ± 0.49). Proteins acting in NHEJ, an alternative pathway for double-strand break repair, also responded in an opposite manner compared to proteins acting in HR. USP1, POLQ and LRIG2 proteins resulted in distribution ratios of 2.05 ± 0.78, 1.3 ± 0.32 and 1.36 ± 0.41, respectively. Taken together, these results suggest that the Golgi population of these DDR proteins respond to induction of double-strand DNA breaks and provides a line of evidence towards the involvement of the Golgi population of these DDR proteins in DNA repair.

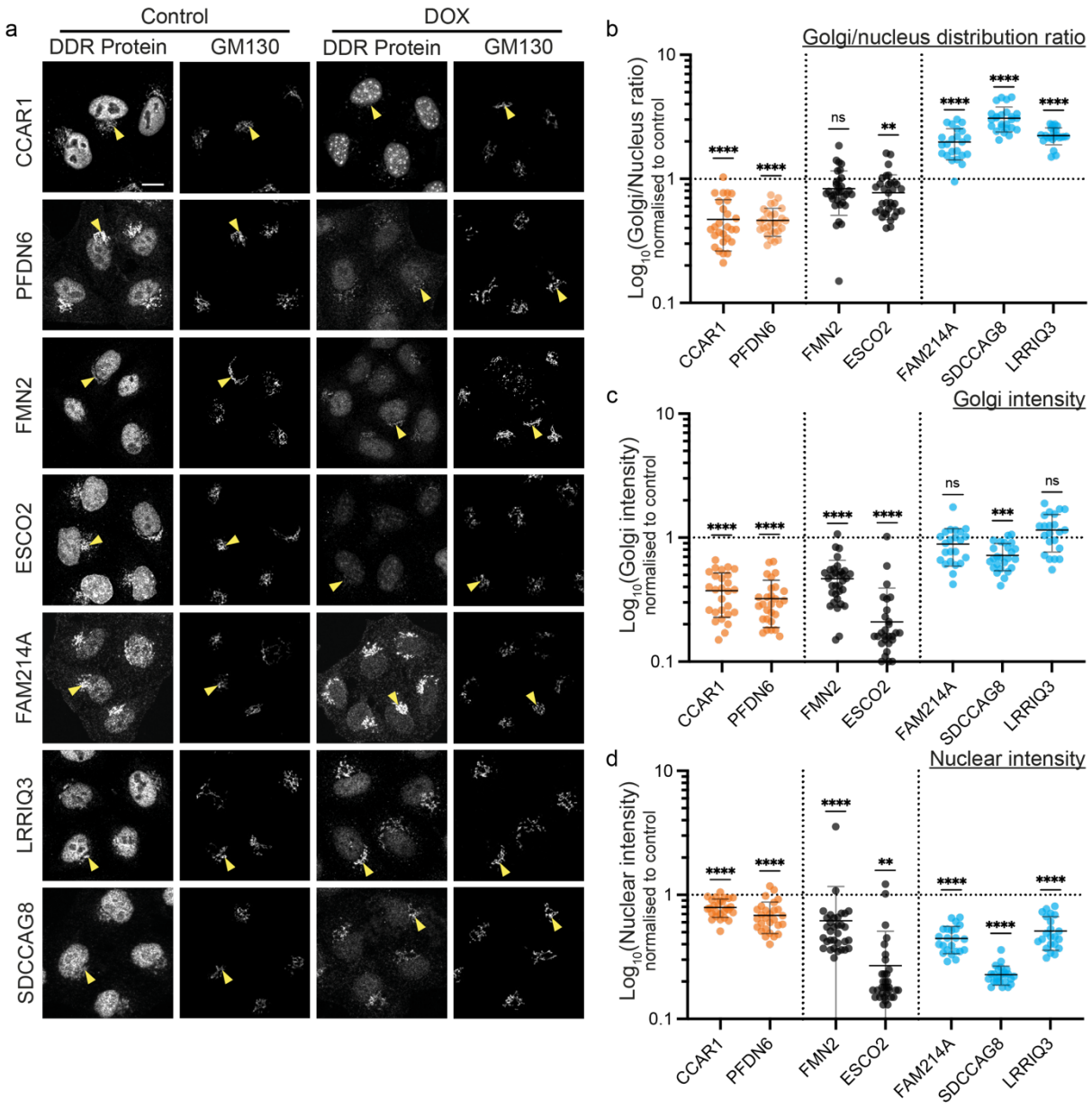

Figure 9. Dual-localising proteins undergo localisation changes upon induction of DNA damage by doxorubicin. (a) HeLa Kyoto cells were treated with 40 μM Doxorubicin (DOX) for 3 hours prior to cells being fixed and stained with antibodies against CCAR1, PFDN6, FMN2, ESCO2, FAM214A, SDCCAG8, LRRIQ3, Golgi marker GM130. Yellow arrows indicate the Golgi membrane, scale bar, 10 μm. **(b)** Quantification of the normalised ratio of Golgi-nuclear distribution of DDR proteins untreated control versus DOX treated. **(c)** Quantification of the relative intensity of DDR proteins at the Golgi, DOX treated normalised to untreated control. **(d)** Quantification of the relative intensity of DDR proteins at the nucleus, DOX treated normalised to untreated control. The proteins are classified according to patterns in the response to the DOX treatment. Error bars represent the mean ± SD (n=3 independent biological replicates). Statistical significance: ns $P > 0.05$, **$P < 0.01$, ***$P < 0.001$, ****$P < 0.0001$, compared to untreated control, determined using two-tailed unpaired Student's t-test.

CCAR1 foci upon induction of DSB by doxorubicin

Previously I observed the formation of distinct CCAR1 nuclear foci upon treatment with doxorubicin. Since this protein hasn't been described to act directly in double-strand DNA break repair and to form such structures, I investigated the nature of these foci through co-localisation with known HR protein markers. Cells treated with doxorubicin were fixed and stained with antibodies against CCAR1 and well-established HR double-strand break repair markers XRCC2 and BRCA1 (Scully *et al.*, 1997; O'Regan *et al.*, 2001). CCAR1 foci that form in the nucleus upon induction of DNA damage were found to co-localise with DSB repair markers (**Fig. 10**), which are known to be recruited to the sites of DNA damage. At this initial stage, the results would suggest a more prominent role for CCAR1 in HR, however, further investigation is required to understand the role of this protein.

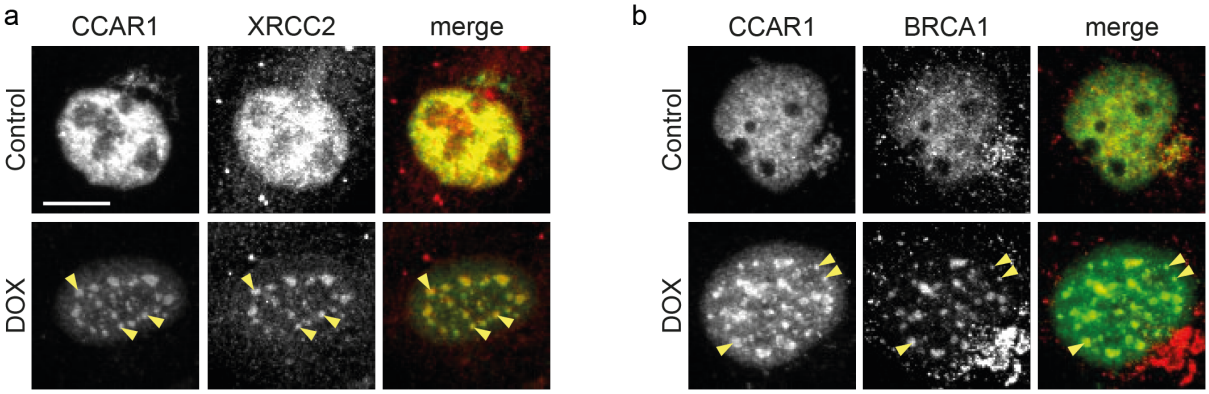

Figure 10. Co-localisation analysis of CCAR1 nuclear foci induced by doxorubicin with DDR markers. (a, b) HeLa Kyoto cells were treated with 40 μM doxorubicin (DOX) for 3 hours prior to cells being fixed and stained with antibodies against CCAR1, and HR DDR markers: **(a)** XRCC2 and **(b)** BRCA1. Yellow arrows indicate nuclear foci, scale bar, 10 μm.

DDR protein localisation changes upon oxidative DNA damage induced by hydrogen peroxide

Doxorubicin predominantly causes double-stranded DNA breaks, which raises the question of whether the protein distribution patterns observed in doxorubicin experiments are dependent on this particular DNA damage process and whether other types of DNA lesions such as single-strand DNA breaks would trigger similar or different types of response. Hydrogen peroxide (H_2O_2), a very commonly used reagent

in the DNA damage field to induce oxidative damage, was utilised to test this. Hydrogen peroxide treatment results predominantly in DNA base lesions (Dirksen *et al.*, 1988; Grollman and Moriya, 1993) which leads to the activation of the Base Excision Repair pathway (Bohr, 2002). Hela Kyoto cells were treated with hydrogen peroxide at a concentration of 5 mM for 20 minutes followed by 15 minutes of recovery. Cells were then fixed and immunostained for the DDR proteins of interest and a Golgi marker GM130 (**Fig. 11, 12**). A ratio of the total Golgi population against the nuclear population was calculated for each protein.

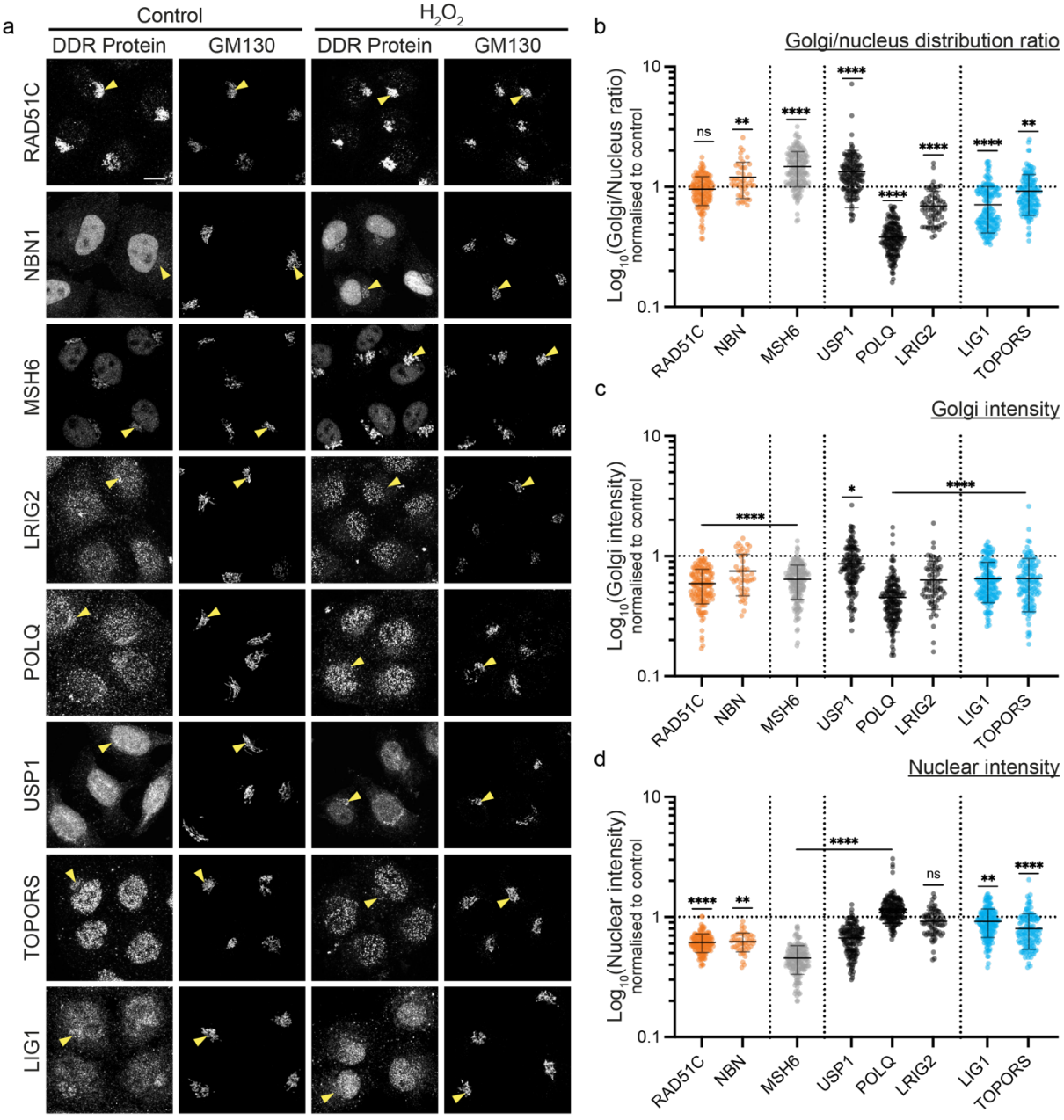

Figure 11. Oxidative DNA damage induced by hydrogen peroxide triggers localisation change of DDR protein. *Legend continues in next page.*

Figure 11. Oxidative DNA damage induced by hydrogen peroxide triggers localisation change of DDR protein. (a) HeLa Kyoto cells were treated with 5 mM H_2O_2 for 20 minutes and let for 15 minutes recover, prior to cells being fixed and stained with antibodies against RAD51C, NBN, MSH6, LRIG2, POLQ, USP1, TOPORS, LIG1, Golgi marker GM130. Yellow arrows indicate the Golgi membrane, scale bar, 10 μm. **(b)** Quantification of the normalised ratio of Golgi-nuclear distribution of DDR proteins untreated control versus H_2O_2 treated. **(c)** Quantification of the relative intensity of DDR proteins at the Golgi, H_2O_2 treated normalised to untreated control. **(d)** Quantification of the relative intensity of DDR proteins at the nucleus, H_2O_2 treated normalised to untreated control. The proteins are classified according to the DDR pathway they function in. Error bars represent the mean ± SD (n=3 independent biological replicates). Statistical significance: ns P > 0.05, *P < 0.05, **P < 0.01, ****P < 0.0001, compared to untreated control, determined using two-tailed unpaired Student's t-test.

The oxidative DNA damage treatment resulted in a significant redistribution of the subcellular distribution of proteins LIG1 and TOPORS (distribution ratios 0.59 ± 0.21 and 0.86 ± 0.17, respectively), proteins, that have been well described to be important in the BER repair pathway (Svilar *et al.*, 2011; Hu *et al.*, 2018b), with an increase in the nuclear population of TOPORS, as well nuclear population redistribution of LIG1 (**Fig. 11**). The localisation pattern changes of the two proteins are the reverse of what was observed after treatment with doxorubicin. Oxidative damage induced with hydrogen peroxide also resulted in a decreased population of the cell cycle and apoptosis regulatory protein CCAR1 at the Golgi at a higher rate when it was observed in the nucleus (distribution ratio 0.69 ± 0.10) (**Fig. 12**), whereas no change in distribution between the two compartments was observed for RAD51C that belongs to HR pathway (**Fig. 11**).

Surprisingly, another HR protein NBN responded in an opposite manner compared to the distribution pattern observed in the doxorubicin experiment. Considering that the total protein population after treatment decreased (**Appendix. Supplementary Fig. 2c**), the protein population in the nucleus decreased at a much higher rate than in the Golgi population, resulting in a distribution ratio of 1.29 ± 0.19 (**Fig. 11**). A similar distribution pattern was observed for MMR repair protein MSH6 (distribution ratio 1.28 ± 0.32), as well as NHEJ proteins POLQ and LRIG2 (**Fig. 11**), which were also observed to distribute in an opposite way compared to doxorubicin treatment.

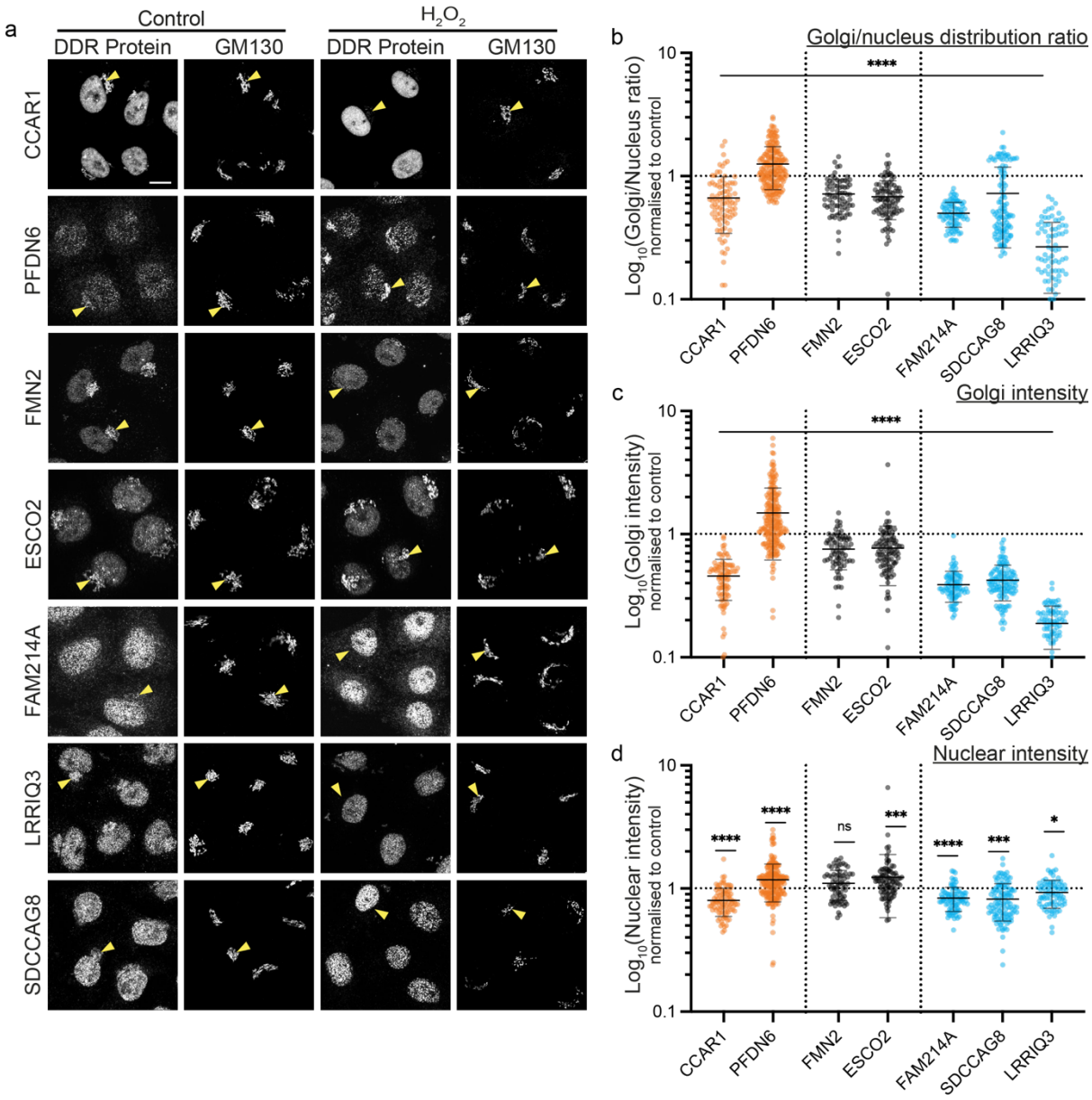

Figure 12. Oxidative DNA damage induced by hydrogen peroxide triggers localisation change of DDR protein. (a) HeLa Kyoto cells were treated with 5 mM H_2O_2 for 20 minutes and let for 15 minutes recover, prior to cells being fixed and stained with antibodies against CCAR1, PFDN6, FMN2, ESCO2, FAM214A, SDCCAG8, LRRIQ3, Golgi marker GM130. Yellow arrows indicate the Golgi membrane, scale bar, 10 µm. Quantification of the normalised ratio of Golgi-nuclear distribution of DDR proteins untreated control versus H_2O_2 treated. **(c)** Quantification of the relative intensity of DDR proteins at the Golgi, H_2O_2 treated normalised to untreated control. **(d)** Quantification of the relative intensity of DDR proteins at the nucleus, H_2O_2 treated normalised to untreated control. The proteins are classified according to the DDR pathway they function in. Error bars represent the mean ± SD (n=3 independent biological replicates). Statistical significance: ns $P > 0.05$, *$P < 0.05$, ***$P < 0.001$, ****$P < 0.0001$, compared to untreated control, determined using two-tailed unpaired Student's t-test.

DDR protein localisation changes upon oxidative DNA damage induced by potassium bromide

Next, to ensure that the results obtained in the previous assays are a direct result of DNA damage and not a side effect of the drug, I tested another DNA-damaging agent potassium bromide ($KBrO_3$) which is also known, similar to hydrogen peroxide, to induce oxidative damage of DNA bases (Borghini *et al.*, 2017; Møller *et al.*, 2018; Vodenkova *et al.*, 2020), however, it's proposed mechanism of base oxidation differs from hydrogen peroxide (Kawanishi and Murata, 2006). To perform the assay, HeLa Kyoto cells were treated with potassium bromide for 3 hours, then fixed and immunostained for DDR proteins of interest and a Golgi marker GM130 (**Fig. 13, 14**). Protein distribution patterns were quantified in the same way as it was done in doxorubicin and hydrogen peroxide experiments.

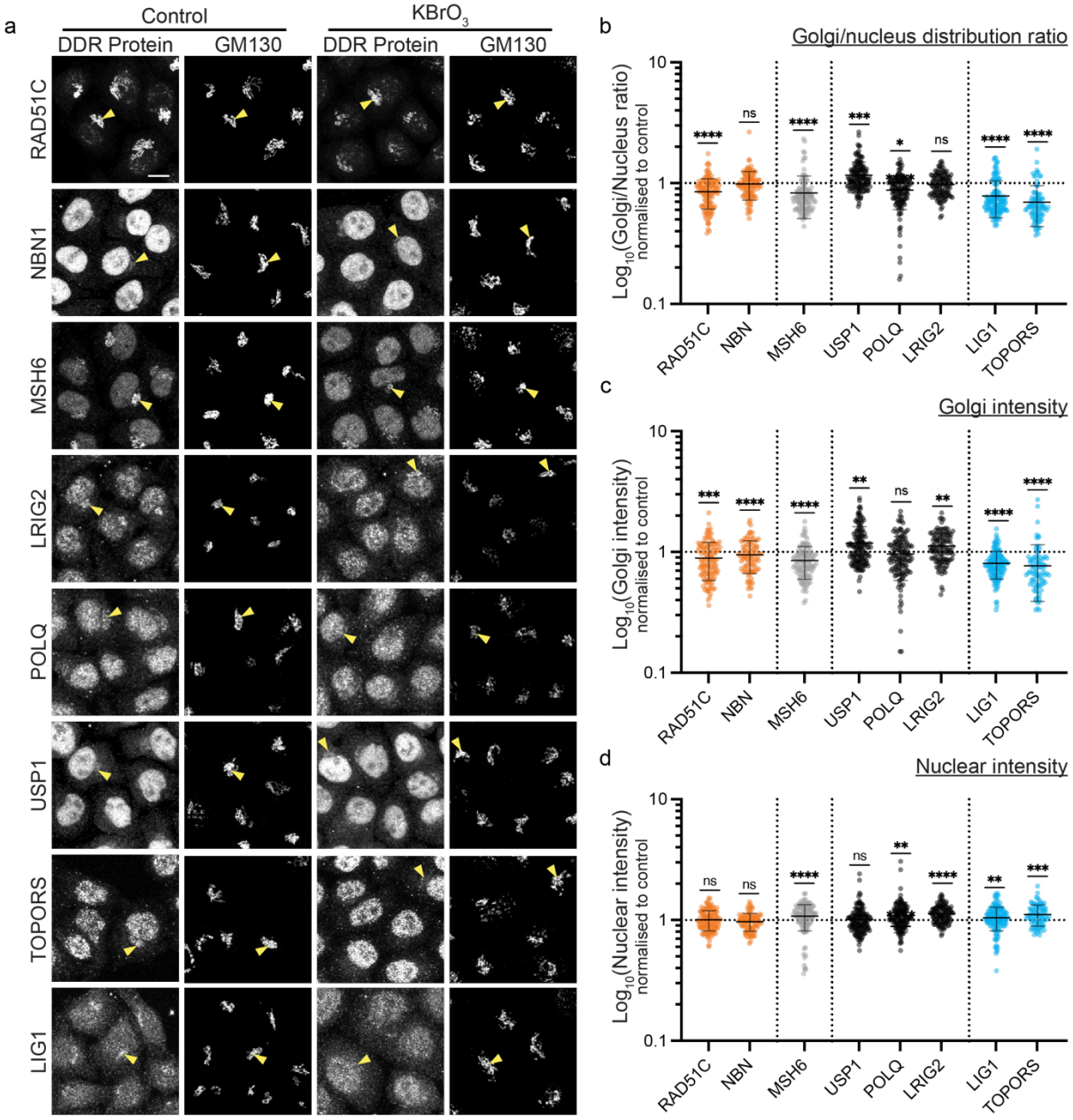

Figure 13. Oxidative DNA damage induced by potassium bromide ($KBrO_3$) triggers localisation change of DDR protein.

Legend continues in next page.

Figure 13. Oxidative DNA damage induced by potassium bromide ($KBrO_3$) triggers localisation change of DDR protein. (a) HeLa Kyoto cells were treated with 5 mM $KBrO_3$ for 3 hours, prior to cells being fixed and stained with antibodies against RAD51C, NBN, MSH6, LRIG2, POLQ, USP1, TOPORS, LIG1, Golgi marker GM130. Yellow arrows indicate the Golgi membrane, scale bar, 10 μm. **(b)** Quantification of the normalised ratio of Golgi-nuclear distribution of DDR proteins untreated control versus $KBrO_3$ treated. **(c)** Quantification of the relative intensity of DDR proteins at the Golgi, $KBrO_3$ treated normalised to untreated control. **(d)** Quantification of the relative intensity of DDR proteins at the nucleus, $KBrO_3$ treated normalised to untreated control. The proteins are classified according to the DDR pathway they function in. Error bars represent the mean ± SD (n=3 independent biological replicates). Statistical significance: ns $P > 0.05$, *$P < 0.05$, **$P < 0.01$, ***$P < 0.001$, ****$P < 0.0001$, compared to untreated control, determined using two-tailed unpaired Student's t-test.

In this experiment, it was observed that BER repair proteins LIG1 and TOPORS responded to oxidative stress induced by potassium bromide and resulted in decreased protein populations at the Golgi and increased protein populations in the nucleus resulted (distribution ratio 0.75 ± 0.11 and 0.67 ± 0.13, respectively) (**Fig. 13b**), similarly as it was observed in hydrogen peroxide treatment. Furthermore, protein FMN2 showed a dramatic change in distribution between organelles, where the protein population in the Golgi was reduced and the protein population in the nucleus increased upon induction of oxidative damage (distribution ratio 0.56 ± 0.06) (**Fig. 14b**). CCAR1 responded similarly to DOX and H_2O_2 treatments – protein population at the Golgi was reduced and the nuclear population did not show significant change, resulting in protein distribution ratio 0.69 ± 0.07 (**Fig. 14**). This experiment confirmed the findings observed in the previous assay, where BER repair proteins are distributing to the nucleus upon induction of DNA base lesions by oxidative stress. Altogether results, obtained in doxorubicin, hydrogen peroxide and potassium bromide treatment experiments suggest that DDR proteins distribute differently between the Golgi and the nucleus depending on the DNA damage that has been induced and the pathway they are acting on.

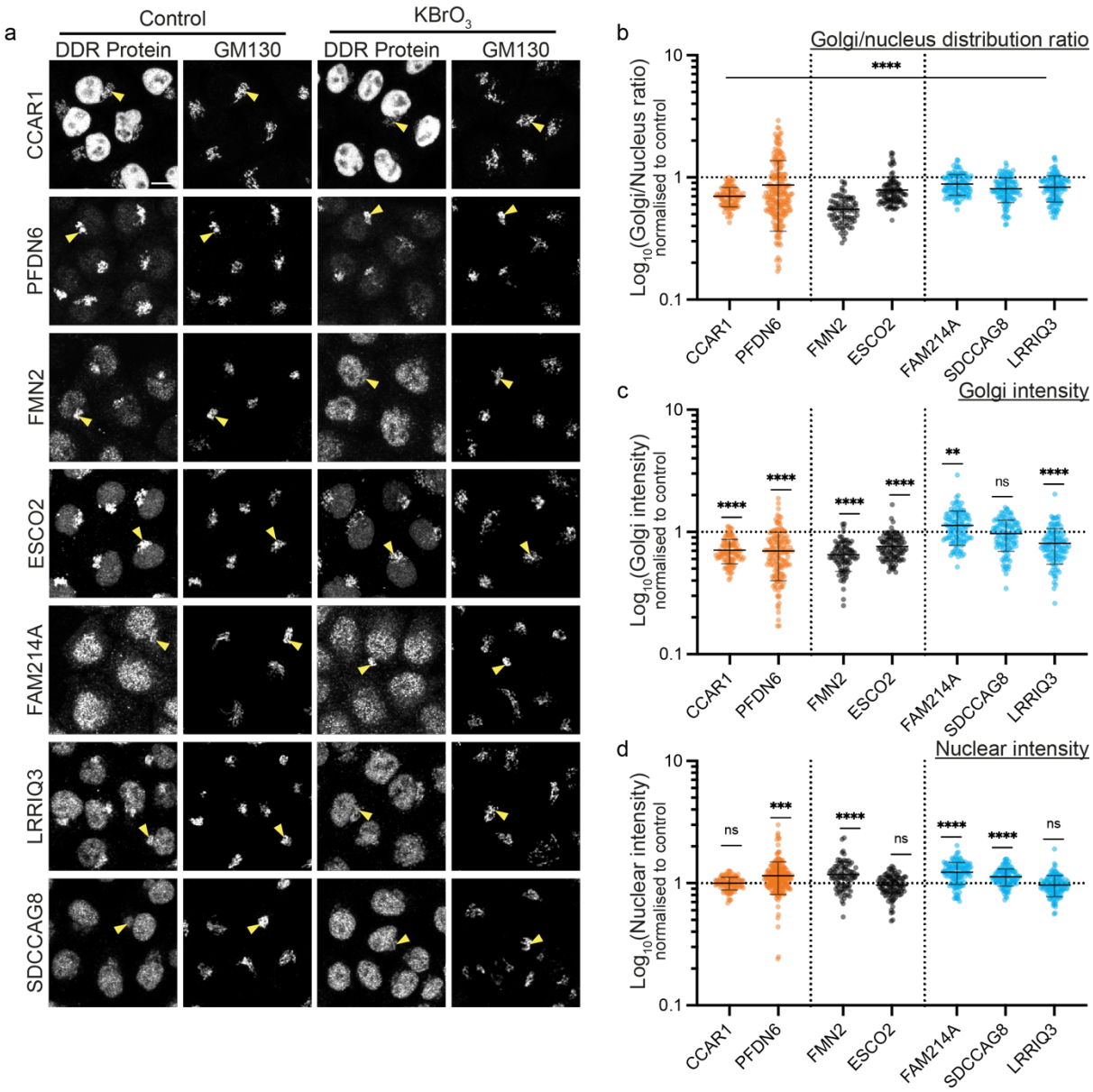

Figure 14. Oxidative DNA damage induced by potassium bromide ($KBrO_3$) triggers localisation change of DDR protein. (a) HeLa Kyoto cells were treated with 5 mM $KBrO_3$ for 3 hours, prior to cells being fixed and stained with antibodies against CCAR1, PFDN6, FMN2, ESCO2, FAM214A, SDCCAG8, LRRIQ3, Golgi marker GM130. Yellow arrows indicate the Golgi membrane, scale bar, 10 μm. **(b)** Quantification of the normalised ratio of Golgi-nuclear distribution of DDR proteins untreated control versus $KBrO_3$ treated. **(c)** Quantification of the relative intensity of DDR proteins at the Golgi, $KBrO_3$ treated normalised to untreated control. **(d)** Quantification of the relative intensity of DDR proteins at the nucleus, $KBrO_3$ treated normalised to untreated control. The proteins are classified according to the DDR pathway they function in. Error bars represent the mean ± SD (n=3 independent biological replicates). Statistical significance: ns P > 0.05, *P < 0.05, **P < 0.01, ***P < 0.001, ****P < 0.0001, compared to untreated control, determined using two-tailed unpaired Student's t-test.

Effect of nuclear import inhibition on DDR protein distribution changes upon DNA damage

Next, I investigated whether the localisation pattern changes of the DDR proteins upon DNA damage events are due to the redistribution of the Golgi population to the nucleus and whether this protein transport is dependent on their Nuclear Localisation Sequence (NLS) motif. Soluble proteins that contain NLS are known to be transported to the nucleus via importin-ß transport receptors (Harel and Forbes, 2004). A small molecule called importazole has been shown to inhibit importin-ß mediated transport from the cytoplasm to the nucleus by altering importin-ß interaction with RanGTP (Soderholm *et al.*, 2011). To test the involvement of importin-ß mediated transport, I selected proteins NBN, MSH6, CCAR1 and PFDN6 based on their redistribution pattern from the Golgi to the nucleus with doxorubicin treatment and having a described or predicted NLS motif in their sequence. Since LIG1 showed an opposite pattern upon doxorubicin treatment, it was selected as a negative control for this experiment. HeLa Kyoto cells were pre-treated with importazole or DMSO control for 20 min followed by 3 h treatment with doxorubicin, then fixed and immunostained against the DDR proteins of interest and the Golgi marker, GM130. Cells co-treated with importazole and doxorubicin showed a reduction in the Golgi-to-nucleus localisation pattern shift of CCAR1, PDFN6, NBN and MSH6 population when compared to the doxorubicin treatment itself (**Fig. 15, 16**).

Initial inspection of the images and quantifications showcase that there is more protein at the Golgi co-localising with the Golgi marker GM130 upon combination treatment with importazole and doxorubicin in comparison with just doxorubicin (**Fig. 15a, b; Fig. 16a, b**). Even though images indicate the increase of protein population at the Golgi upon combination treatment with importazole and doxorubicin for the tested proteins NBN, MSH6, CCAR1 and PFDN6, however, not all cells responded in the same manner. Perhaps due to the variability within the replicates increase of protein population at the Golgi was shown to be statistically significant only for HR protein NBN (**Fig. 15a**). Interestingly, the redistribution of the control protein LIG1 was also shown to be affected by the nuclear import block induced by importazole (**Fig. 16e, f**). LIG1 population at the Golgi increased at a lower rate in cells treated with a combination of importazole and doxorubicin in comparison with just doxorubicin-

treated cells. However, why is this so, needs to be further investigated. Altogether, these results would indicate that Golgi-localised DDR proteins redistribute from the Golgi to the nucleus upon DNA damage in an importin-ß dependent manner.

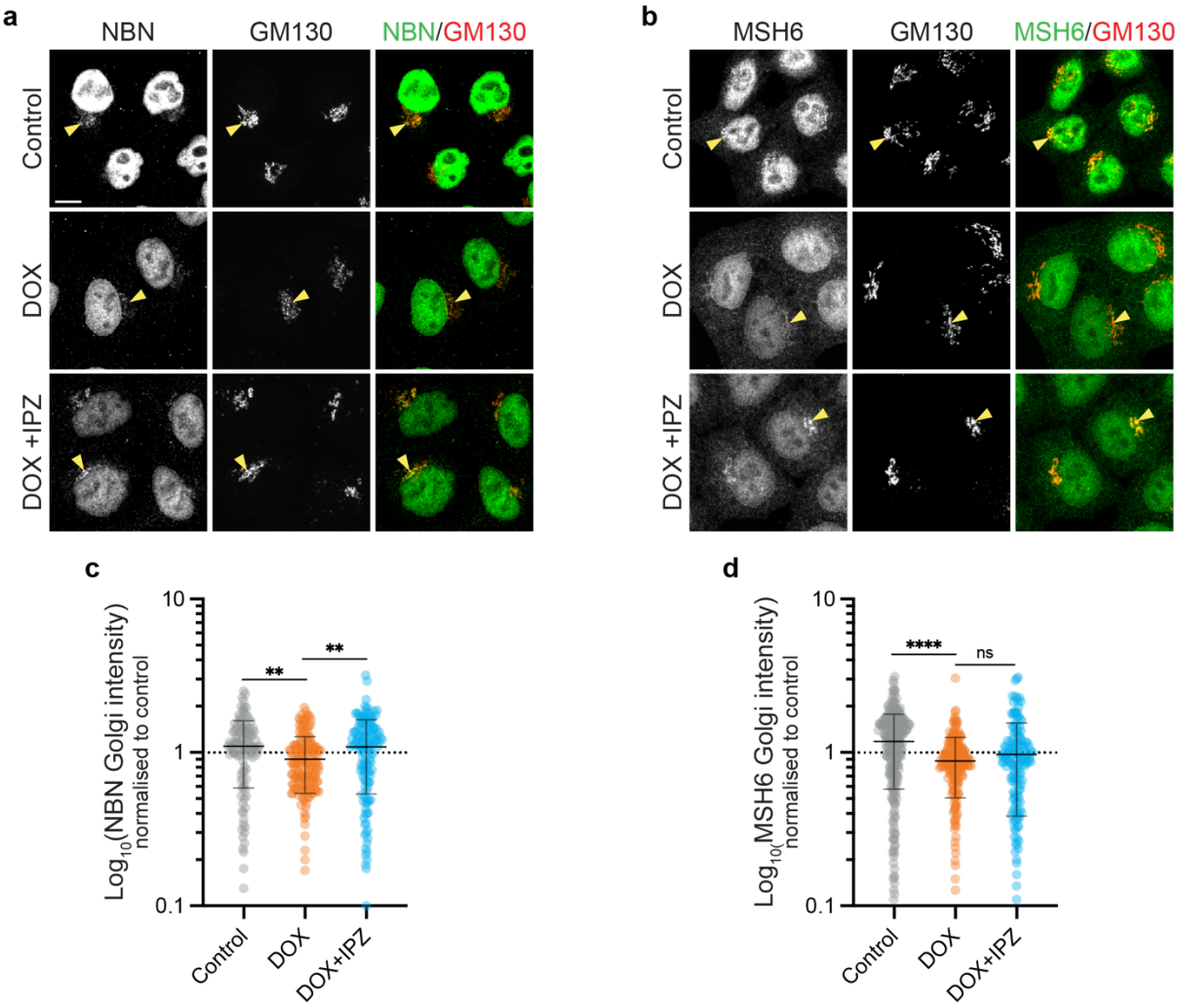

Figure 15. Nuclear import inhibitor importazole inhibits DDR protein distribution from the Golgi to the nucleus. (a-d) HeLa Kyoto cells were treated with 40 µM importazole (IPZ) for 20 min prior to a 3-hour treatment with 40 µM doxorubicin (DOX), followed by fixation and antibody staining against NBN, MSH6 and the Golgi marker GM130. Yellow arrows indicate the Golgi membrane, scale bar, 10 µm. **(a-b)** Representative confocal microscopy images. **(c-d)** Quantification of the relative intensity of DDR proteins at the Golgi, DOX and IPZ+DOX treated normalised to untreated control. Error bars represent the mean ± SD (n=3 independent biological replicates). Statistical significance: ns P > 0.05, *P < 0.05, **P < 0.01, ***P < 0.001, ****P < 0.0001, compared to untreated control, determined using one-way analysis of variance ANOVA.

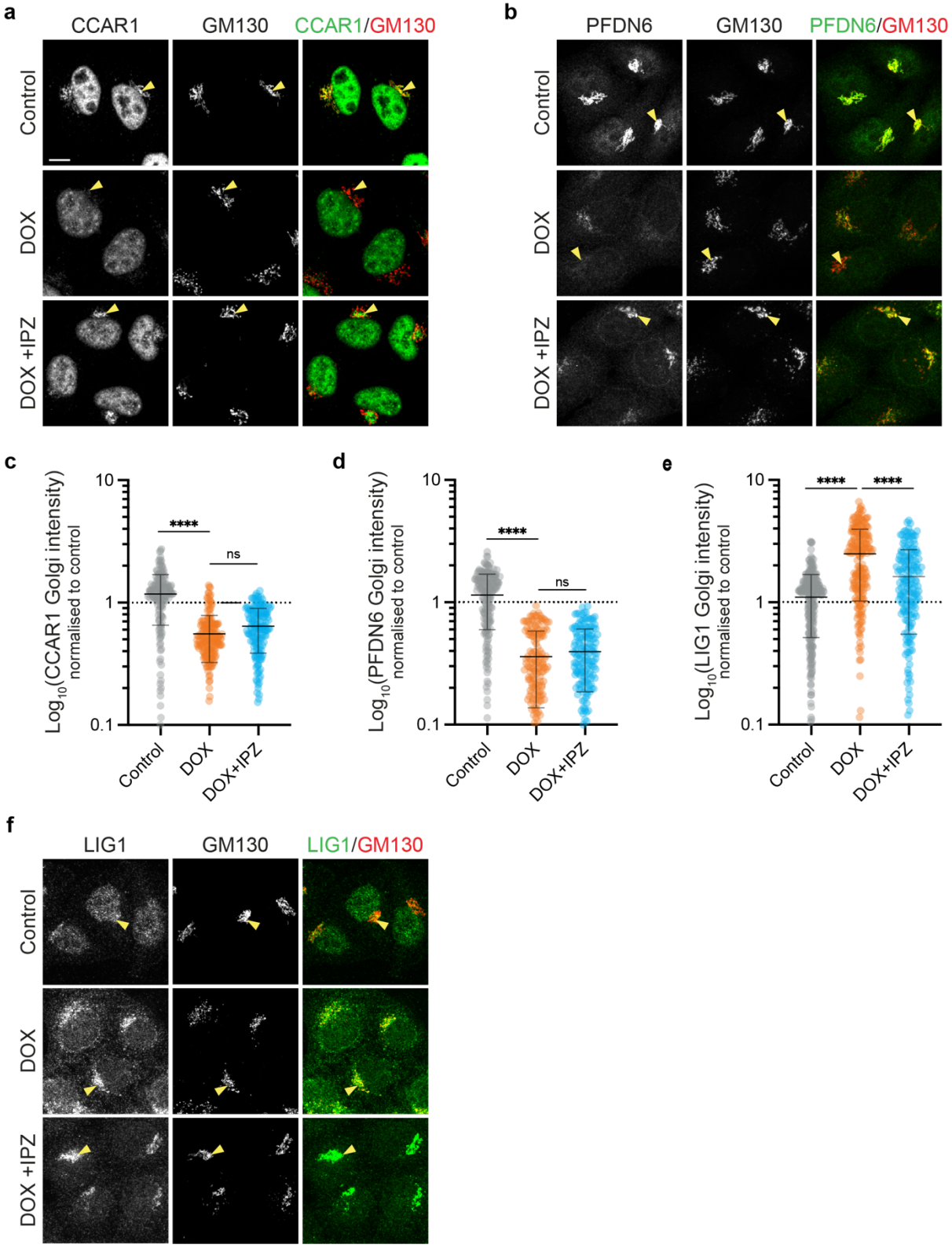

Figure 16. Nuclear import inhibitor importazole inhibits DDR protein distribution from the Golgi to the nucleus.

Legend continues in next page.

Figure 16. Nuclear import inhibitor importazole inhibits DDR protein distribution from the Golgi to the nucleus. (a-d) HeLa Kyoto cells were treated with 40 μM importazole (IPZ) for 20 min prior to a 3-hour treatment with 40 μM doxorubicin (DOX), followed by fixation and antibody staining against CCAR1, PFDN6, LIG1 and the Golgi marker GM130. Yellow arrows indicate the Golgi membrane, scale bar, 10 μm. **(a-b)** Representative confocal microscopy images. **(c-d)** Quantification of the relative intensity of DDR proteins at the Golgi, DOX and IPZ+DOX treated normalised to untreated control. Error bars represent the mean ± SD (n=3 independent biological replicates). Statistical significance: ns P > 0.05, *P < 0.05, **P < 0.01, ***P < 0.001, ****P < 0.0001, compared to untreated control, determined using one-way analysis of variance ANOVA.

Golgi morphology upon knock-down of DDR proteins

Having established that the DDR Golgi protein population is important in DDR, I investigated whether Golgi-localised DDR proteins have other structural or regulatory functions at the Golgi. First, I tested if the systematic depletion of these proteins affects Golgi morphology (**Fig. 17, 18**). HeLa Kyoto cells were transfected with siRNAs targeting DDR proteins for 72 hours, then cells were fixed stained with antibodies against *cis*-Golgi marker GM130 and *trans-Golgi network* marker TGN-46 to observe any Golgi morphological changes. No significant alteration of the Golgi morphology was identified (**Fig. 17, 18**), with the only exemption of NBN and LIG1, where some fragmentation was observed, and minor Golgi compaction with the knock-down of TOPORS (**Fig. 17**). Interestingly, in this experiment it was also observed that depletion of a few DDR proteins, such as NBN, LIG1, FMN2 and ESCO2 (yellow arrows) (**Fig. 17, 18**) resulted in nuclear foci formation of the Golgi protein GM130, that was used as the Golgi marker. This protein was previously reported to accumulate in the nucleus and form molecular condensates upon overexpression conditions (Rebane *et al.*, 2020). However, the nature and functions of the GM130 foci forming in the nucleus upon depletion of DDR proteins and whether it could be related to DNA damage response remain to be investigated.

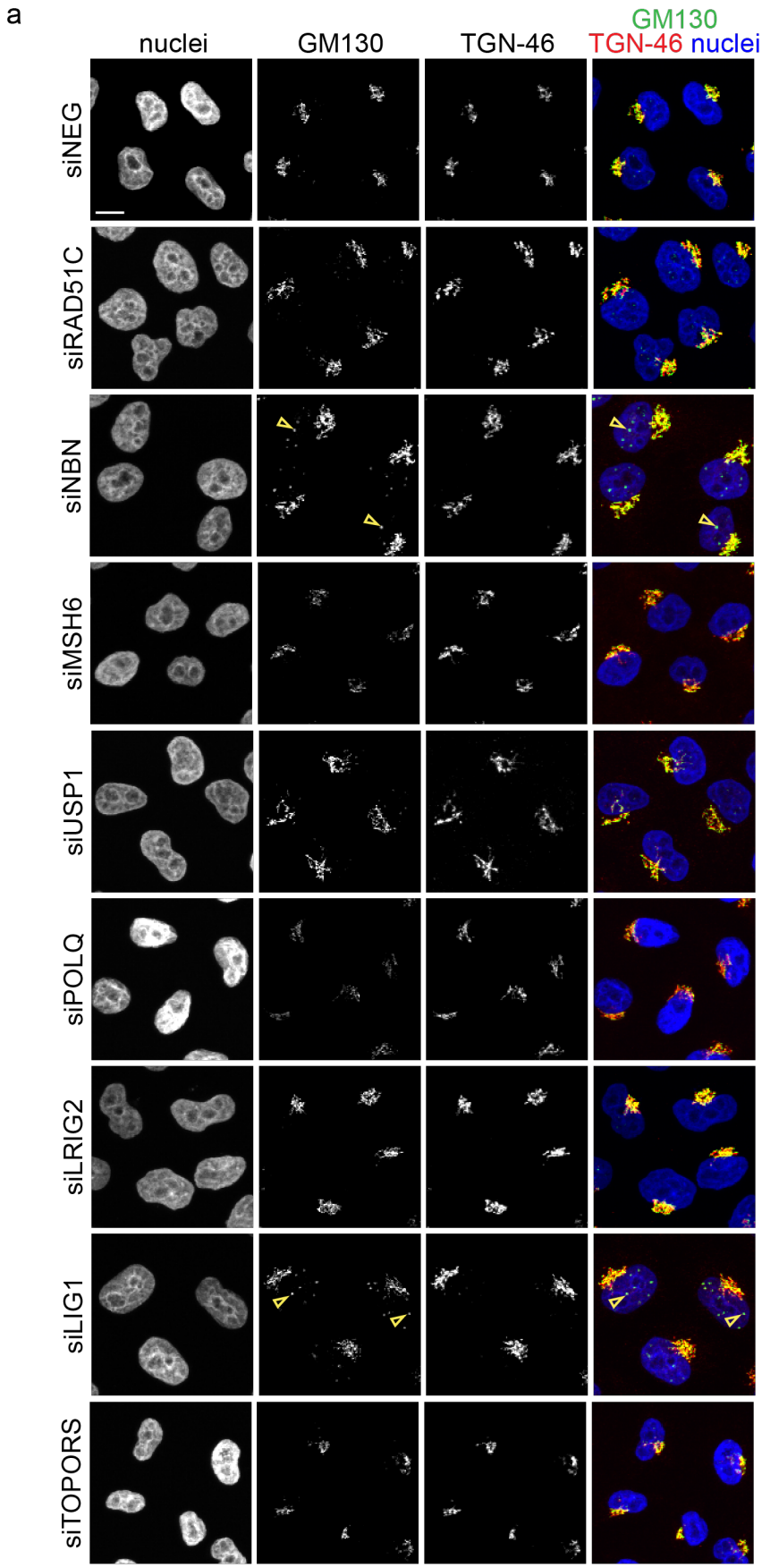

Figure 17. Golgi morphology upon knock-down of Golgi-localised DDR proteins.

Legend continues in next page.

Figure 17. Golgi morphology upon knock-down of Golgi-localised DDR proteins. (a) HeLa Kyoto cells were transfected with control NEG9, RAD51C, NBN, MSH6, USP1, POLQ, LRIG2, LIG1 and TOPORS siRNAs for 72 hours, then fixed and stained with antibodies against *cis*-Golgi marker GM130 (green) and *trans*-Golgi marker TGN46 (red). Nuclei were stained with Hoechst 33342 (blue), scale bar, 10 μm. Yellow arrows indicate the nuclear foci of GM130. Data from biological replicate.

Next, I tested whether shortlisted DDR proteins from different DNA pathways have any regulatory function on membrane traffic passing through the Golgi. For that aim, I performed a VSV-G trafficking assay (Hirschberg *et al.*, 1998) as described (Simpson *et al.*, 2012). No significant alteration of VSV-G trafficking was observed (**Appendix Supplementary Fig. 3**).

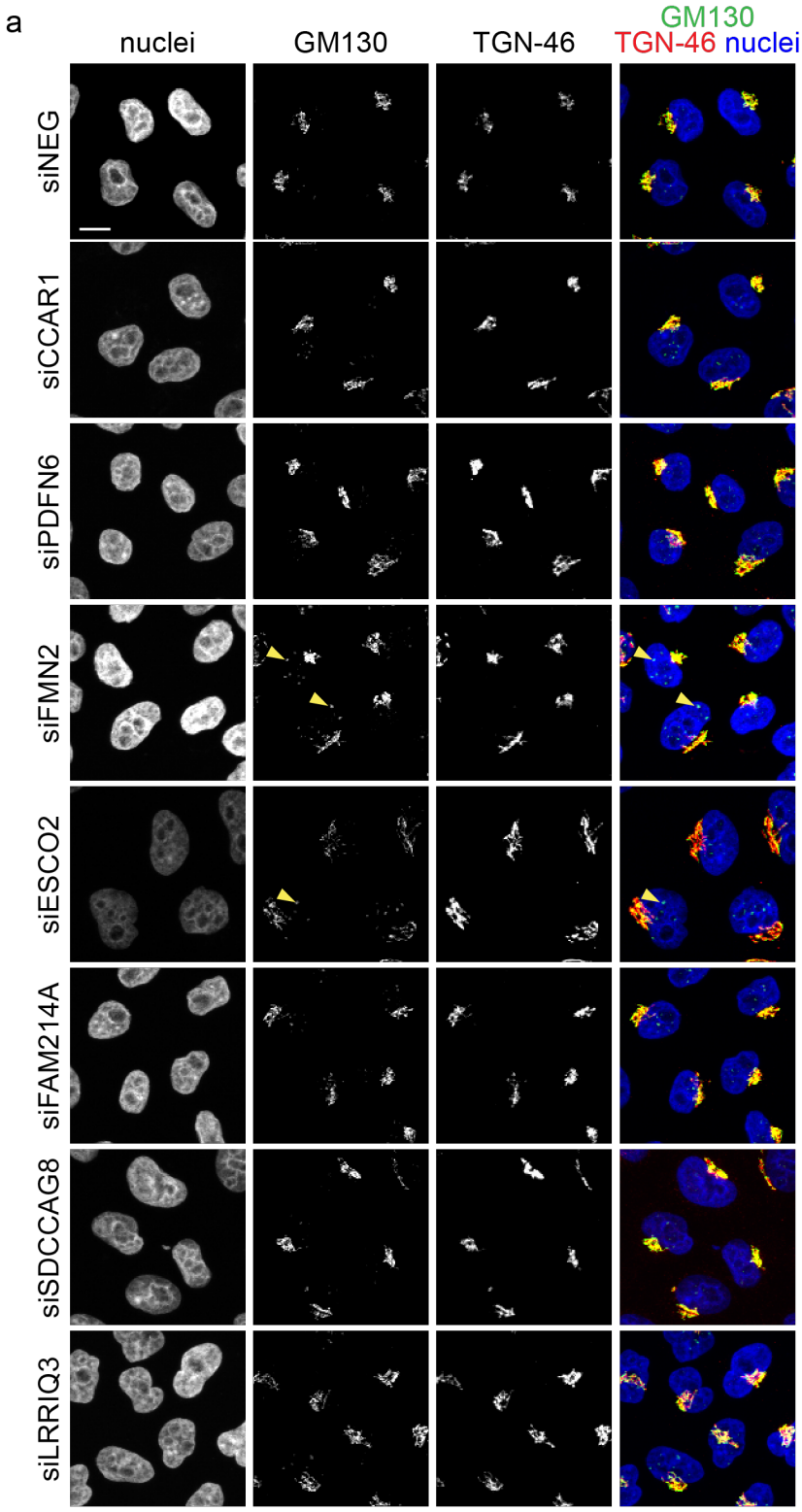

Figure 18. Golgi morphology upon knock-down of Golgi-localised DDR proteins. (a) HeLa Kyoto cells were transfected with control NEG9, CCAR1, PFDN6, FMN2, ESCO2, FAM214A, SDCCAG8, and LRRIQ3 siRNAs for 72 hours, then fixed and stained with antibodies against *cis*-Golgi marker GM130 (green) and *trans*-Golgi marker TGN46 (red). Nuclei were stained with Hoechst 33342 (blue), scale bar, 10 μm. Yellow arrows indicate the nuclear foci of GM130. Data from one biological replicate.

DDR protein distribution at the Golgi

The Golgi complex consists of serially stacked membrane cisternae that are categorised into sub-Golgi regions, namely the *cis*-Golgi, *medial*-Golgi, *trans*-Golgi and *trans-Golgi network* (De Matteis and Luini, 2008). To establish the distribution of these DDR proteins within the Golgi complex, I carried out an analysis of their distribution. For this purpose, HeLa Kyoto cells were treated with the microtubule depolymerisation agent nocodazole at the concentration of 33 μM for 3 h. The depolymerisation of microtubules caused by nocodazole is known to induce disruption of the Golgi ribbon into smaller structures mini-stacks, which allow for more accurate co-localisation measurements of the Golgi membranes (Dejgaard *et al.*, 2007; Rizzo *et al.*, 2013; Beznoussenko *et al.*, 2014). Distribution of DDR proteins across the Golgi stacks was determined utilising Golgi markers for the *cis*-Golgi, GM130 and the *trans*-Golgi network, TGN46 (**Fig. 19**) (Rizzo *et al.*, 2013; Beznoussenko *et al.*, 2014). Acquired images containing Golgi ministacks were analysed manually using Fiji software by obtaining line plots of each mini stack by manually drawing lines throughout the stack. Measurements from each channel were used to calculate Pearson's correlation coefficient (PCC) between *cis*-Golgi and *trans*-Golgi markers and DDR proteins. The quantifications revealed that the DDR proteins were found to distribute across the Golgi in a DDR pathway-specific manner (**Fig. 19a**). BER proteins LIG1 and TOPORS (PCC 0.95 ± 0.04 and 0.88 ± 0.13, respectively); NHEJ proteins POLQ, USP1 and LRIG2 (PCC 0.92 ± 0.06, 0.89 ± 0.10 and 0.88 ± 0.09, respectively); as well as MMR protein MSH6 (PCC 0.84 ± 0.18) co-localise with the *trans*-Golgi network (TGN) marker TGN46, while HR proteins NBN and RAD51C (PCC 0.92 ± 0.06 and 0.76 ± 0.15, respectively) co-localise with *cis*-Golgi marker GM130. No protein has been found to distribute uniformly throughout the Golgi.

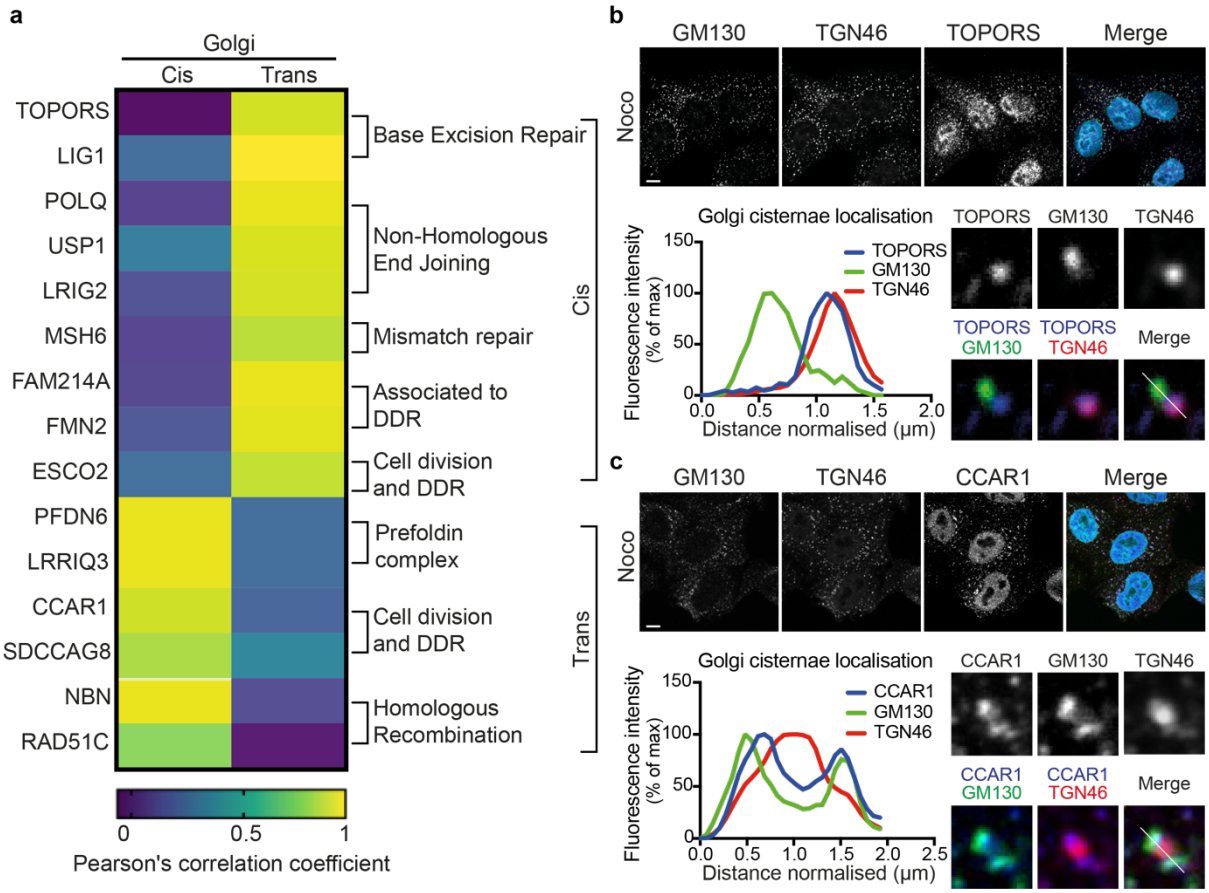

Fig. 19. DDR Golgi-localising proteins are distributed to specific Golgi-cisternae. **(a)** Distribution of DDR proteins on different Golgi compartments. Quantification of Pearson's correlation coefficient (PCC) between *cis*-Golgi and *trans*-Golgi markers and DDR proteins. Scale bar, 5 µm. **(b)** Representative confocal microscopy images of HeLa Kyoto cells treated with Nocodazole, fixed and labelled with anti-TOPORS (blue), anti-GM130 (a *cis*-Golgi marker, green) and anti-TGN-46 (a *TGN*-Golgi marker, red) antibodies; zoom enlarged view of single isolated mini stack, white line across the stack was used for line-scan analysis. **(c)** Representative confocal microscopy images of HeLa Kyoto cells treated with Nocodazole (33 µM, 3 h), fixed and labelled with anti-CCAR1 (blue), anti-GM130 (a *cis*-Golgi marker, green) and anti-TGN-46 (a *TGN*-Golgi marker, red) antibodies; zoom enlarged view of single isolated mini stack, white line across the stack was used for line-scan analysis.

Golgins as potential anchors for DDR proteins at the Golgi

Structure and sequence analysis of the Golgi-localised DDR proteins show that most of these proteins do not have a detectable transmembrane or attachment domain which could explain their localisation to the Golgi membranes (**Fig. 6**), therefore it could be hypothesised that Golgi proteins are responsible for anchoring these proteins on Golgi membranes. In the previous study, George Galea (Pepperkok lab, EMBL Heidelberg) analysed primary data published in two genome-wide screens (Paulsen *et al.*, 2009; Adamson *et al.*, 2012) identifying the Golgin protein family as a candidate for this Golgi anchoring and regulation role. In these two datasets, the depletion of several Golgin family members was shown to significantly affect both the homologous recombination repair rates (**Fig. 20a**) (Adamson *et al.*, 2012), as well as DDR signalling, measured through the phosphorylation levels of DDR regulator H2AX (**Fig. 20b**) (Paulsen *et al.*, 2009). In line with these results, the Golgin Giantin was found to be responsible for anchoring RAD51C to Golgi membranes and in turn regulating HR activity (Galea *et al.*, 2022). Based on these findings, I hypothesised that other Golgins could play similar roles in anchoring various DDR proteins to the Golgi complex and potentially regulating other DNA repair pathways. To test this hypothesis, I systematically depleted various members of the Golgin protein family and monitored for any DDR protein localisation changes at the Golgi.

As a proof-of-concept, I utilised siRNA resources for Golgins that were available in the lab and performed systematic depletion of differently localised Golgins GOLGIN-45 (*medial/cis*-Golgi), GOLGA7 (*trans*-Golgi), GMAP210 (*cis*-Golgi), GOLGA2B (predicted *cis*-Golgi), CUX1 (*medial*-Golgi), GOLGA6A (predicted *cis*-Golgi), Giantin (*medial*-Golgi) and GOLGA4 (*trans*-Golgi) (Barr and Short, 2003; Goud and Gleeson, 2010; Munro, 2011; Witkos and Lowe, 2016; Shin *et al.*, 2017; Ko *et al.*, 2019; Lowe, 2019), while monitoring localisation changes of selected DDR proteins at the Golgi. I selected proteins from different DDR pathways that were shown to distribute to different Golgi cisternae, namely CCAR1 (cell cycle regulatory protein, *cis*-Golgi,), NBN (HR repair pathway, *cis*-Golgi), TOPORS (BER pathway, *trans*-Golgi) and LIG1 (BER pathway, *trans*-Golgi) (**Fig. 19**). HeLa Kyoto cells were transfected with siRNAs targeting the various Golgins for 72 hours, fixed, and stained with antibodies against

DDR proteins and the Golgi marker GM130 followed by measurements of their Golgi localisation patterns (**Fig. 21-23**).

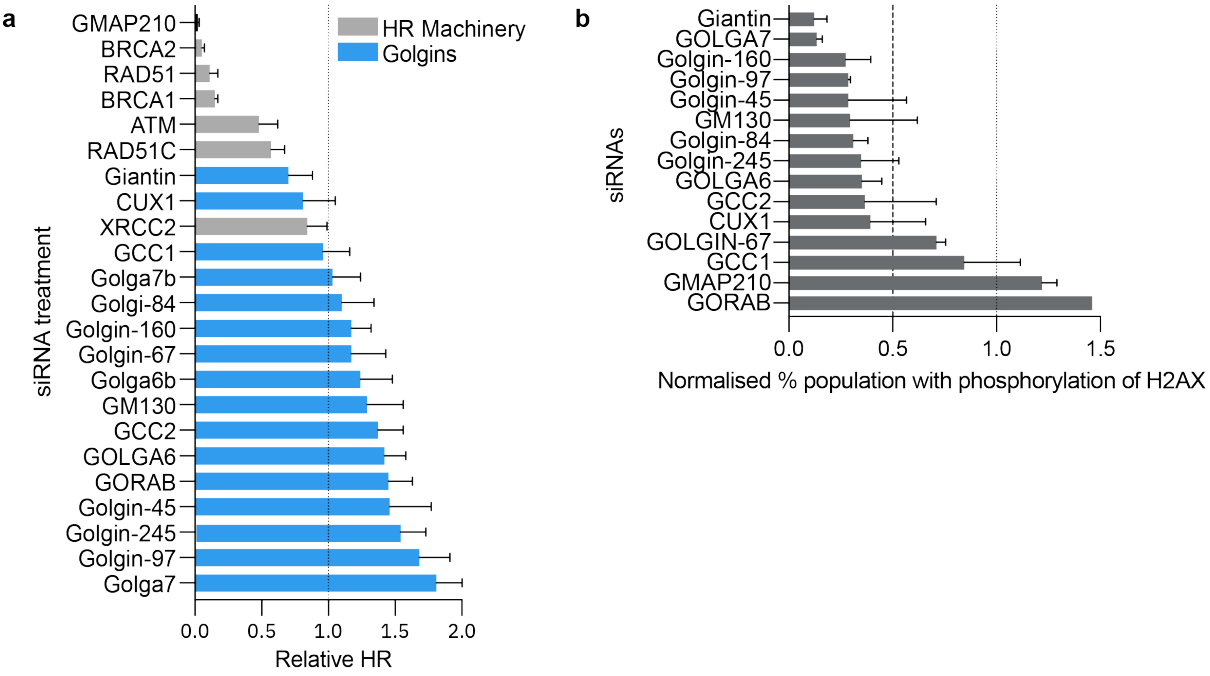

Figure 20. Golgins and DNA damage response. (a) HR siRNA screen data (Adamson *et al.*, 2012) showing relative HR repair rate upon knock-down of Golgin family proteins and HR machinery proteins**. (b)** H2AX phosphorylation siRNA screen data (Paulsen *et al.*, 2009) showing the relative percentage of cell population with phosphorylated H2AX upon knock-down of Golgins. Both datasets are normalised to the negative control.

Statistically significant changes in CCAR1 subcellular distribution were observed with the depletion of 4 out of 8 tested Golgins. The depletion of GOLGA6A and GOLGIN-45 resulted in a reduced CCAR1 protein population at the Golgi, whereas the knock-down of GOLGA7, GMAP-210, CUX1 and Giantin did not result in any significant changes in CCAR1 localisation at the Golgi. Interestingly, the depletion of GOLGA2B and GOLGA4 led to an increase in the CCAR1 protein population at the Golgi (**Fig. 21a**). To test whether these changes in the CCAR1 distribution pattern were a result of interaction between the Golgins and CCAR1, I tested it by performing an immunoprecipitation assay. Since no compatible antibodies for this assay were available for GOLGA6A, the interaction was tested only for GOLGIN-45. For this, HeLa Kyoto cells were lysed and incubated with antibodies against GOLGIN-45; then using A Protein Agarose beads (Roche) antibodies and bound protein complexes were

purified followed by western blot analysis. The immunoprecipitation experiment confirmed the interaction between GOLGIN-45 and CCAR1 (**Fig. 21d**).

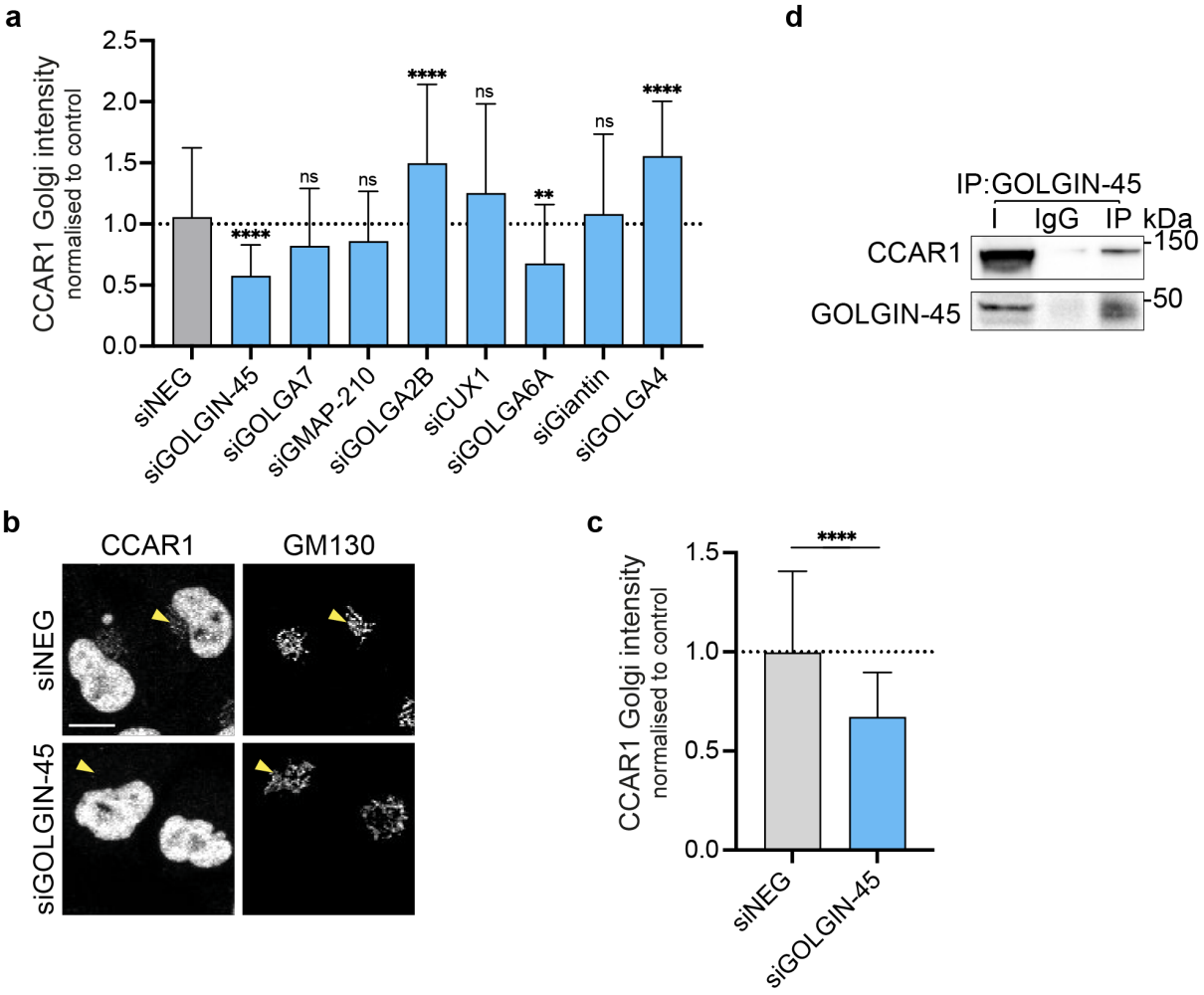

Figure 21. Golgi localisation of CCAR1 is dependent on GOLGIN-45. (a-c) HeLa Kyoto cells were transfected with control NEG9, GOLGIN-45, GOLGA7, GMAP-210, GOLGA2B, CUX1, GOLGA6A, Giantin and GOLGA4 siRNAs for 72 hours, then fixed and stained with antibodies against CCAR1 and Golgi marker GM130. Yellow arrows indicate the Golgi membrane, scale bar, 10 µm. **(a)** Quantification of the relative intensity of CCAR1 protein at the Golgi upon knock-down of Golgins. Error bars represent the mean ± SD (n=3 independent biological replicates). Statistical significance: **P < 0.01, ****P < 0.0001, compared to NEG9 transfected control, determined using one-way analysis of variance ANOVA. **(c)** Quantification of the relative intensity of CCAR1 protein at the Golgi upon knock-down of GOLGIN-45. Statistical significance: ****P < 0.0001, compared to NEG9 transfected control, determined using two-tailed unpaired Student's t-test. **(d)** Immunoprecipitation of GOLGIN-45 with CCAR1.

Analogically, I tested how NBN, TOPORS and LIG1 localisation is affected by depleting selected Golgins (**Fig. 22**). The localisation at the Golgi of NBN and TOPORS was found to be dependent on Golgins GMAP-210 and GOLGA7, respectively. Depletion of GMAP-210 resulted in a significant change in NBN distribution pattern from Golgi-to-nucleus with a quantified decrease of 35% at the Golgi (**Fig. 22b**), while depletion of GOLGA7 led to a decrease of the TOPORS population at the Golgi by 66% (**Fig. 22e**). Similarly, the interactions between NBN and GMAP-210 between TOPORS and GOLGA7 were tested immunoprecipitation by assays. The assay revealed, that NBN protein co-precipitated together with the GMAP-210 and vice versa (**Fig. 22c**). The interaction between TOPORS and GOLGA7 was also confirmed via immunoprecipitation, where TOPORS was found to be present in purified protein lysate bound to GOLGA7 antibody (**Fig. 22f**).

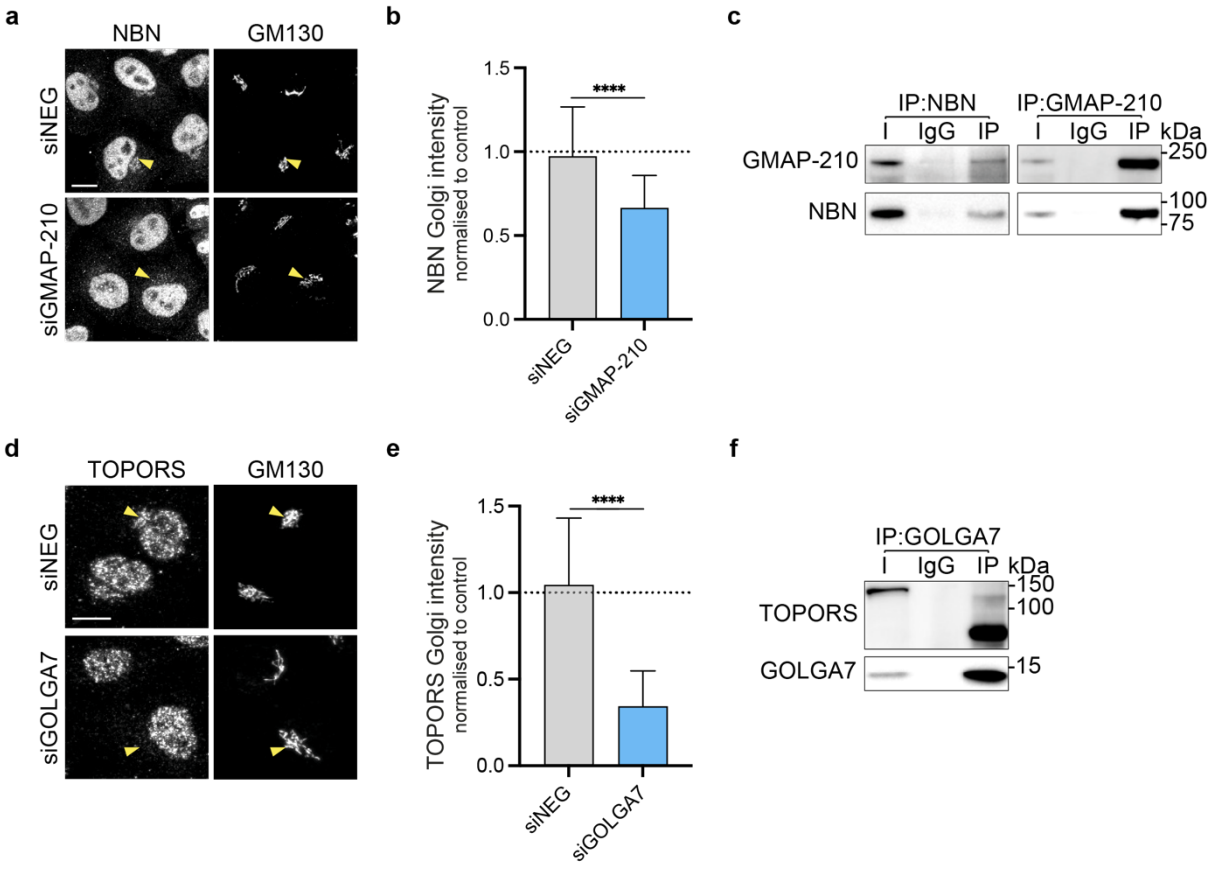

Figure 22. Golgi localisation of NBN and TOPORS is dependent on Golgins GMAP210 and GOLGA7.

Legend continues in next page.

Figure 22. Golgi localisation of NBN and TOPORS is dependent on Golgins GMAP210 and GOLGA7. (a-d) HeLa Kyoto cells were transfected with control NEG9, GMAP-210 and GOLGA7 siRNAs for 72 hours, then fixed and stained with antibodies against NBN, TOPORS and Golgi marker GM130. Yellow arrows indicate the Golgi membrane, scale bars, 10 μm. **(b)** Quantification of the relative intensity of NBN protein at the Golgi upon knock-down of GMAP-210. **(c)** Immunoprecipitation of NBN with GMAP-210 and vice versa. (**e)** Quantification of the relative intensity of TOPORS protein at the Golgi upon knock-down of GOLGA7. **(f)** Immunoprecipitation of GOLGA7 with TOPORS. Error bars represent the mean ± SD (n=3 independent biological replicates). Statistical significance: ****P < 0.0001, compared to NEG9 transfected control, determined using two-tailed unpaired Student's t-test.

Moreover, it was found that the depletion of Golgin Giantin leads to a 33% decrease in the LIG1 protein population at the Golgi in comparison to control NEG9 transfected cells (**Fig. 23a, b**). No interaction of the two proteins could be detected by immunoprecipitation (**Fig. 23c**). This negative result strengthens the positive interactions found between the DDR proteins and Golgins, as not all IPs for Golgins result in interaction with the tested DDR proteins. However, it was curious to test whether this would affect LIG1 response to DNA damage. Following this, I tested whether the effect of Giantin knock-down on the LIG1 population at the Golgi would also be observed after DOX treatment, as it was previously shown that the LIG1 population redistributes between the Golgi and the nucleus upon DOX treatment. Cells depleted of Giantin were treated with doxorubicin for 3 hours, then fixed and stained with antibodies against LIG1 and the Golgi maker GM130 (**Fig. 23d**). Interestingly the LIG1 redistribution observed previously, where the protein population at the Golgi increases upon DOX treatment, was inhibited by depletion of Giantin (**Fig. 23d**). The cells treated with siRNA against Giantin and doxorubicin in combination resulted in reduced Golgi/nucleus distribution ratio (1.3 ± 0.7) in comparison to control siRNA treated cells (1.9 ± 0.9) (**Fig. 23e**).

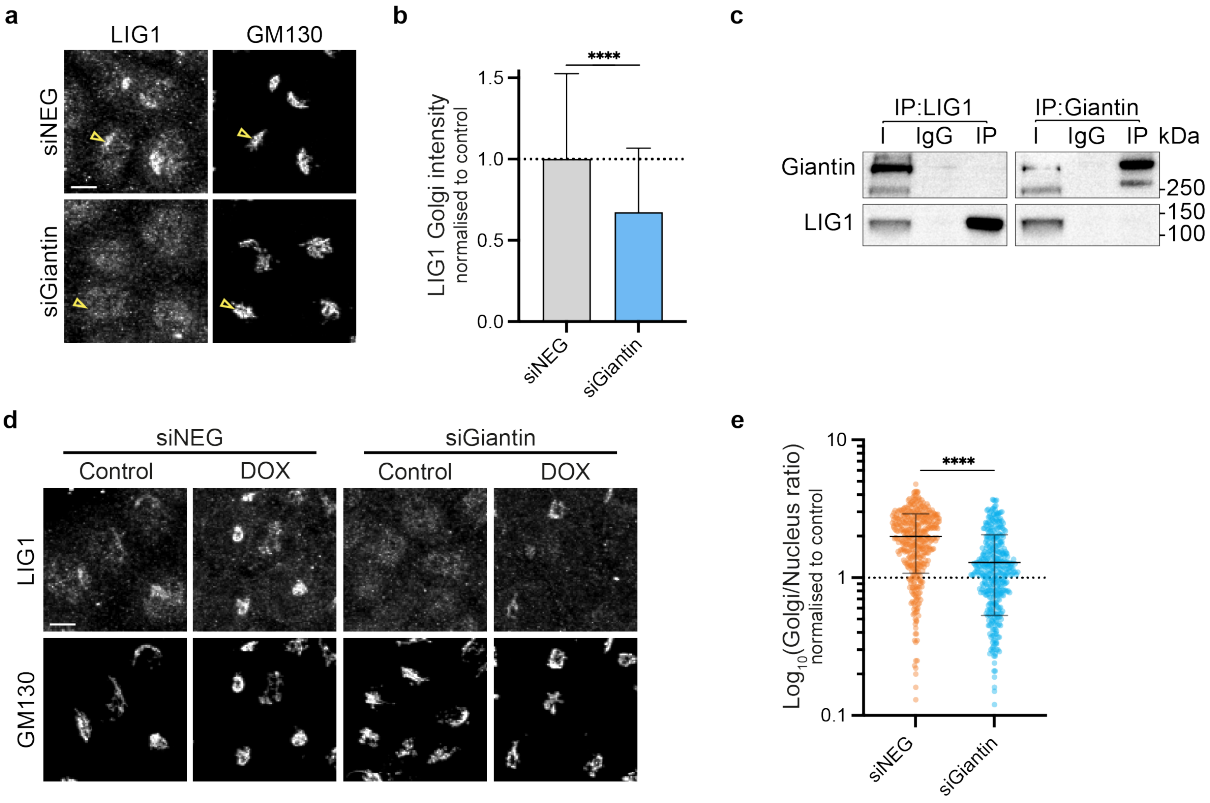

Figure 23. Knock-down of Giantin affect the Golgi localisation of LIG1. (a, b) HeLa Kyoto cells were transfected with control NEG9 and Giantin siRNAs for 72 hours, then fixed and stained with antibodies against LIG1, and the Golgi marker GM130, scale bar, 10 µm. **(b)** Quantification of the relative intensity of LIG1 protein at the Golgi upon knock-down of Giantin. **(c)** Immunoprecipitation of LIG1 and Giantin. (**d)** HeLa Kyoto cells were transfected with control NEG9 and Giantin siRNAs for 72 hours, then treated with 40 µM doxorubicin (DOX) for 3 hours prior to cells being fixed and stained with antibodies against LIG1, and the Golgi marker GM130, scale bar, 10 µm. **(e)** Quantification of the normalised ratio of Golgi-nuclear distribution of LIG1 untreated control versus DOX treated. Error bars represent the mean ± SD (n=3 independent biological replicates). Statistical significance: ****P < 0.0001, compared to NEG9 transfected control, determined using two-tailed unpaired Student's t-test.

Altogether, these results provide a line of evidence that the Golgin family and DDR proteins interact. However, a more systematic approach would be helpful to identify more regulators of DDR proteins at the Golgi and further characterise the interactions and the role of Golgins in DDR response.

Effect of Giantin knock-down on DNA Damage Response

Previously, it was found that the depletion of Golgin Giantin leads to the change in the distribution of the HR repair protein RAD51C where the majority of the Golgi population is lost, leading to the formation of nuclear foci. Co-localisation studies of these nuclear structures highlighted the absence of other DDR machinery suggesting that these structures were not HR DNA repair foci (Galea *et al.*, 2022). It is known that unregulated DNA repair proteins acting when they are not required can be harmful to the cells and lead to genomic instability. To dissect the repercussions of this Giantin-induced RAD51C redistribution together with George Galea, we utilized the comet assay, a classical method in the DDR field for measuring levels of fragmented DNA (Møller, 2018). Briefly, HeLa Kyoto cells were transfected with control and siRNAs targeting Giantin for 72 hours, then bent in agarose and lysed, followed by single-cell electrophoresis. During the electrophoresis damaged and fragmented genomic DNA migrates faster in the electric field and results in the formation of longer comet tails in comparison to genomic DNA, which results in very short or no tail. The experiment revealed that the knock-down of Giantin resulted in longer comet tails compared to the control siRNA-treated cells, suggesting that there is more fragmented DNA, indicating genomic instability (**Fig. 24a**).

To understand if this increase in genomic instability is due to aberrant HR DNA repair, George Galea tested whether the depletion of Giantin and redistribution of RAD51C had repercussions on DDR damage signalling and whether other alternative DNA repair pathways are activated. Standard double-strand break repair signalling markers, such as ATM, CHK2, H2AX and DNA-PK that normally get phosphorylated in response to DNA damage were queried and monitored for changes. Transfected HeLa Kyoto cells with control or Giantin siRNAs were treated cells with double-strand DNA breaks inducing agents – doxorubicin and camptothecin, lysed and probed by western blot analysis. As expected, the phosphorylated levels of ATM, CHK2 and H2AX increased upon induction of DNA damage in control siRNA-treated cells. However, the depletion of Giantin resulted in significantly lower levels of phosphorylation of all the tested signalling proteins, suggesting that the loss of Giantin leads to impaired DDR signalling (**Fig. 24b**). Whether other Golgins, found to be

responsible for anchoring DDR proteins would have similar effects on genomic instability and DDR signalling is still on current investigations.

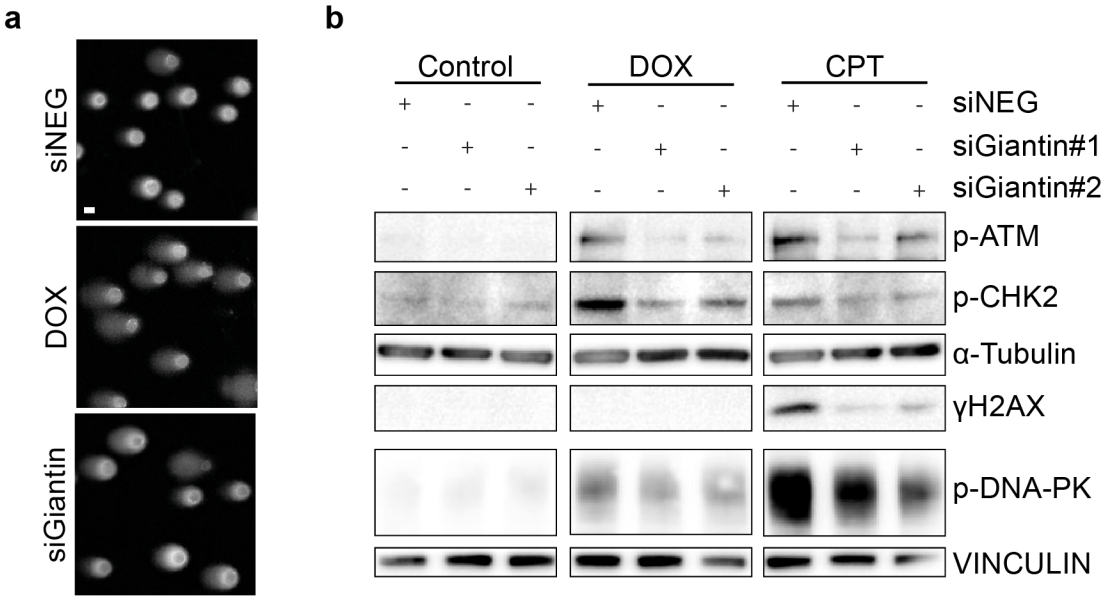

Figure 24. Knock-down of Giantin leads to genomic instability and impaired DDR signalling. (a) Representative images of the comet assay, where HeLa Kyoto cells were transfected with control NEG9 and Giantin siRNA for 72 hours, or treated for 3 hours with DOX, scale bar, 10 μm. **(b)** Western blot analysis of DDR signalling. HeLa Kyoto cells were transfected with NEG9 and Giantin siRNAs for 72 hours and then additionally treated with DOX and CPT. Immunoblotted protein extracts were stained with antibodies against p-ATM, p-CHK2, γ-H2AX and DNA-PK, α-Tubulin and Vinculin were used as markers for protein levels.

Proteomic-scale interaction analysis of DNA Damage Response proteins

The previous experiments showcased that Golgi proteins, in particular, the Golgin protein family are required for anchoring some DDR proteins to the Golgi membranes. Together with George Galea we already showcased 5 pairs of different Golgins and DDR proteins, where the knock-down of specific Golgins led to the loss of the Golgi localisation of DDR protein. Therefore, it would be expected that there might be more Golgi proteins involved in, perhaps, anchoring and regulating DDR proteins at the Golgi. In order to test this hypothesis, I took a systematic approach to identify

interacting proteins, using proteomics. I performed an immunoprecipitation experiment, where HeLa Kyoto cells were lysed and whole cell lysate was incubated with antibodies against all 15 Golgi-localised DDR proteins; then using Protein A Agarose beads (Roche) purified antibodies together with interacting protein complexes. The resulting samples were processed and analysed by the Proteomics Core Facility (EMBL, Heidelberg). The proteomic analysis was performed by Per Haberkant and the statistical analysis of MS data was done by Frank Stein (EMBL, Heidelberg).

As a first step, I tested the compatibility of the available antibodies with IP experiments. The antibodies that successfully presented enrichment of the bait were selected for further experiments. The compatibility was tested for antibodies against all 15 DDR proteins, namely RAD51C, NBN, MSH6, USP1, POLQ, LRIG2, LIG1, TOPORS, CCAR1, PFDN6, FMN2, ESCO2, FAM214A, SDCCAG8 and LRRIQ3. The initial analysis revealed 8 out of 15 samples showed no significant enrichment for the bait protein (RAD51C, POLQ, LRIG2, TOPORS, PFDN6A and FMN2). Following this, I shortlisted antibodies, against NBN, MSH6, USP1, LIG1, CCAR1, ESCO2 and SDCCAG8 that presented enrichment in bait protein and proceeded with further experiments. The results of the MS-IP experiment for DDR interactome are presented in **Fig. 25**. All proteins identified in each sample are denoted in grey, whereas proteins in light blue are the ones that were found to be enriched and resulted in $\log_2$ FC > 1; and were also selected for further characterisation. To analyse the Golgi-interactome of the tested DDR proteins, the identified interactors were annotated using the UniProt subcellular localisation database (**Supplementary Table 1**). Proteins annotated as Golgi-localising are denoted in orange (**Fig. 25**).

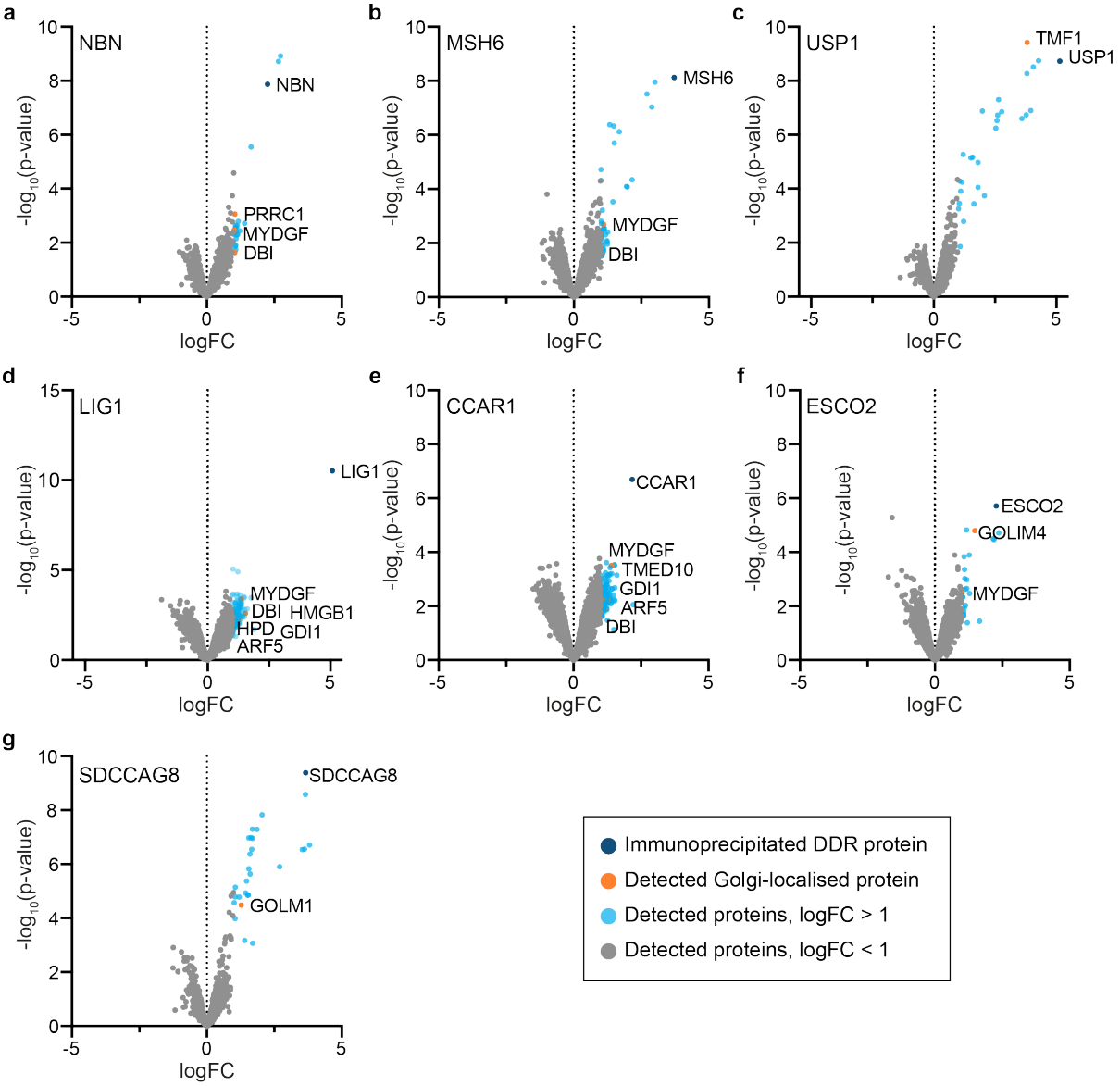

Figure 25. MS-IP analysis of DDR proteins. (a-h) Volcano plots of NBN, MSH6, USP1, LIG1, CCAR1, ESCO2 and SDCCAG8 interaction data from IP samples. The *x*-axis shows the log_2FC of each identified protein, and the *y*-axis the corresponding $-log_{10}$ p-value (Limma statistical analysis). The bait proteins NBN, MSH6, USP1, LIG1, CCAR1, ESCO2 and SDCCAG8 respectively, are marked in dark blue; statistically significant interactions $log_2FC > 1$ depicted in light blue; Golgi-localised proteins (from subcellular localisation analysis) are highlighted in orange. Summarized data of two independent replicates. Data normalised to the control sample without antibodies present.

The analysis revealed, that indeed Golgi-localised proteins could be found in DDR proteins' interacting proteomes. NBN was found to interact with 3 Golgi-localised proteins - PRRC1, MYDGF and DBI (**Fig. 25a**); MSH6 and ESCO2 with pairs of 2 - MYDGF and DBI for MSH6; GOLIM4 and MYDGF for ESCO2 (**Fig. 25b, f**); whereas

USP1 and SDCCAG8 were found to interact with a single Golgi protein - USP1 with TMF1 (**Fig. 25c**) and SDCCAG8 with GOLM1 (**Fig. 25g**). Interestingly, LIG1 and CCAR1 interactomes were found to contain clusters of 5 Golgi-localised proteins (Fig. 20d-e). While proteins, such as MYDGF and DBI, ARF5 and GDI1 were found repeatedly in NBN, MSH6, LIG1 and CCAR1 samples, the rest of the found interactomes between DDR and Golgi-localised proteins were unique for each DDR protein. The Golgin TMF1 was found to be enriched uniquely in the USP1 proteome (**Fig. 25c**). While known Golgin interactors Golgi membrane proteins GOLIM4 and GOLM1 were found to interact with ESCO2 (**Fig. 25f**) and SDCCAG8 (**Fig. 25g**) respectively; transmembrane trafficking protein TMED10 in CCAR1 proteome (**Fig. 25e**) was found to be enriched. Although further testing is required to ensure the identified interaction is confirmed and validated, this experiment highlights that the interaction network between the known Golgi proteins and newly identified Golgi-localised DDR proteins might be even more extensive than previously observed.

Proteomic-scale interaction analysis of Golgins

As a second strategy to explore the Golgin-DDR interactome, I explored the Golgins. Using an analogue approach to the one described above ("Proteomic-scale interaction analysis of DNA damage response proteins"), I investigated whether any DDR proteins can be identified in selected Golgin IP samples. Since DDR proteins were found to be distributed heterogeneously throughout the Golgi (some co-localise with *cis*-Golgi, others *trans*-Golgi markers), I shortlisted Golgins that are known to localise to different Golgi cisternae (**Fig. 3**), as well as been shown to affect H2AX signalling and HR repair rates, as well as Golgins that were shown in my experiments to have an effect on DDR protein localisation at the Golgi. I've selected *cis*-Golgins GMAP-210 and GM130; *medial*-Golgins CUX1; Giantin and GOLGIN-45; *trans*-Golgins GOLGA7, GOLGIN-245 and GOLGIN-97. Using previously used in the lab and validated antibodies for each of the Golgins I performed an immunoprecipitation experiment from whole cell lysates of HeLa Kyoto cells, as explained in the previous section. The MS-IP analysis was done by Per Haberkant in the Proteomics Core Facility (and statistical analysis was done by Frank Stein (EMBL, Heidelberg).

Here I present the preliminary data from one biological replicate. The initial experiment revealed, that all tested antibodies worked well for MS-IP analysis and in each sample, I was able to detect enrichment of the bait protein (**Fig. 26**). All proteins identified in each sample are denoted in grey, whereas proteins in light blue are the ones that were found to be enriched and resulted in $\log_2$ FC > 1. With these I proceeded with further analysis utilizing resources of the UniProt database and GO analysis, to find whether any DDR proteins were enriched in Golgin proteomes. Although in GM130 and GOLGIN-45 proteomes no DDR protein was enriched, the rest of the tested Golgin proteomes contain at least one DDR protein that was enriched and these proteins are depicted in orange (**Fig. 26**). For example, YY1 described to act in HR (Wu *et al.*, 2007) was enriched in GOLGA7 proteome (**Fig. 26d**), DNA damage signalling kinase PLK1 was identified in GOLGIN-245 proteome (**Fig. 26e**); E3 ubiquitin-protein ligase involved in HR (Ismail *et al.*, 2015) identified in GOLGIN-97 proteome (**Fig. 26f**). GMAP-210 proteome was found to be enriched in UBR5, NOP53, and CRIP1 DDR associated proteins (**Fig. 26c**).

What is perhaps even more striking, is that CUX1 and Giantin proteomes were found to be enriched in clusters of DDR proteins (**Fig. 26a, b**). Giantin has been previously shown to be important for RAD51C regulation. In this experiment, it was found to interact with the whole cluster of DDR proteins (**Fig. 26b, 27b**), in particular proteins, acting in the HR DNA repair pathway – MRN complex proteins NBN, RAD50 and MRE11A, a key protein acting in double-strand break repair, as well as HR protein ATRX, along with other proteins involved in DDR. Furthermore, CUX1 was found to interact with a cluster of proteins acting in BER repair, namely RPA3, RPA1, LIG3, XRCC1, as well as TERF2 and TER2IP, which are important in telomere maintenance (**Fig. 26a, 27a**). Although these results are preliminary and require further confirmation, altogether they suggest that Golgins might be interacting not only with single DDR proteins but with whole clusters of proteins from specific DDR pathways. What is the role of these interactions remains to be elucidated.

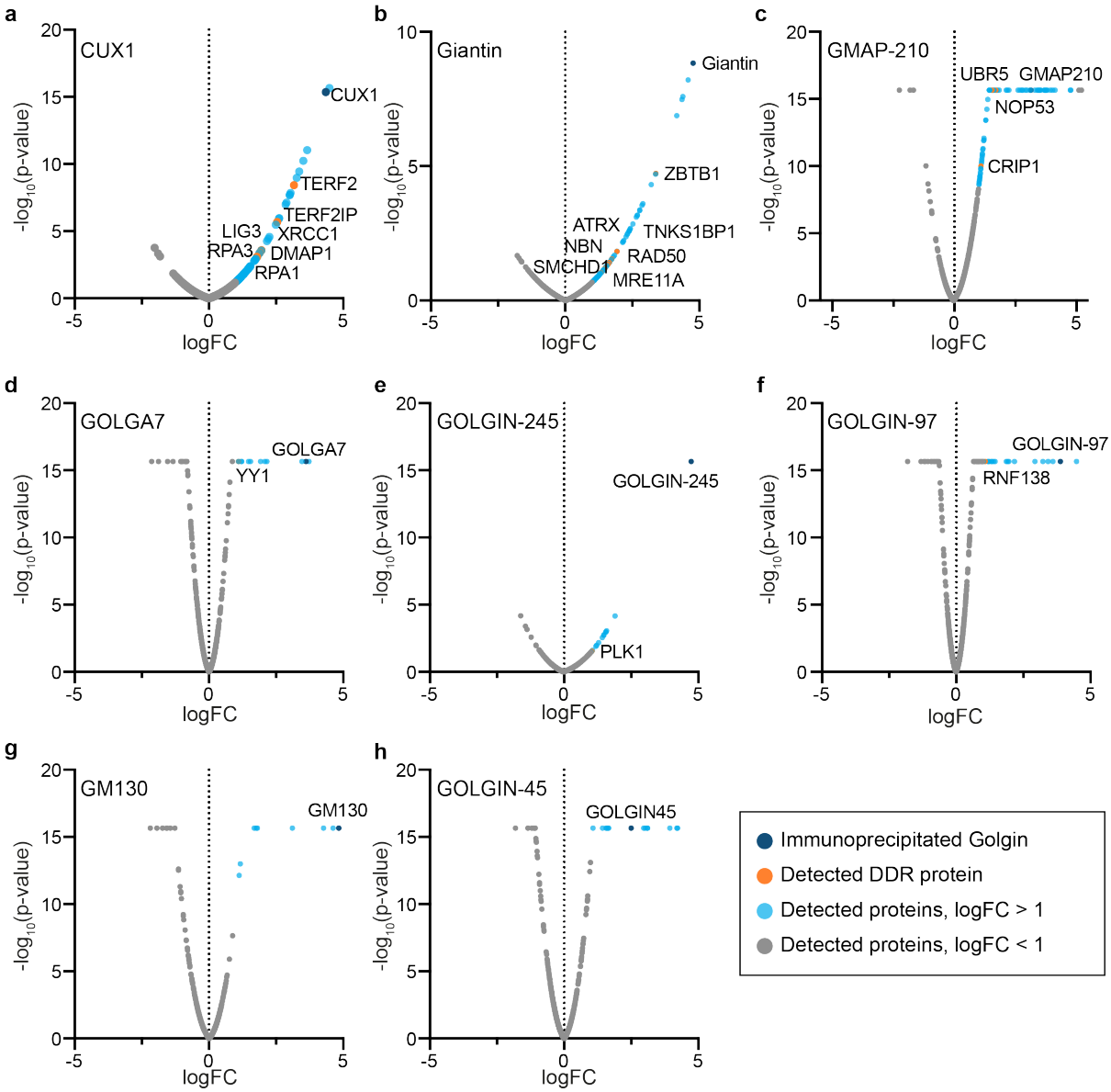

Figure 26. MS-IP analysis of Golgin family proteins. (a-h) Volcano plots of CUX1, Giantin, GMAP-210, GOLGA7, GOLGIN-245, GOLGIN-97, GM130, GOLGIN-45 interaction data from IP samples. The *x*-axis shows the $\log_2$FC of each identified protein, and the *y*-axis the corresponding -$\log_{10}$ p-value. The bait proteins CUX1, Giantin, GMAP-210, GOLGA7, GOLGIN-245, GOLGIN-97, GM130 and GOLGIN-45 respectively, are marked in dark blue; statistically significant interactions $\log_2$FC > 1 depicted in light blue; DDR associated proteins (from GO analysis) are highlighted in orange. Shown preliminary data from one MS-IP experiment. Data normalised to the control sample without antibodies present.

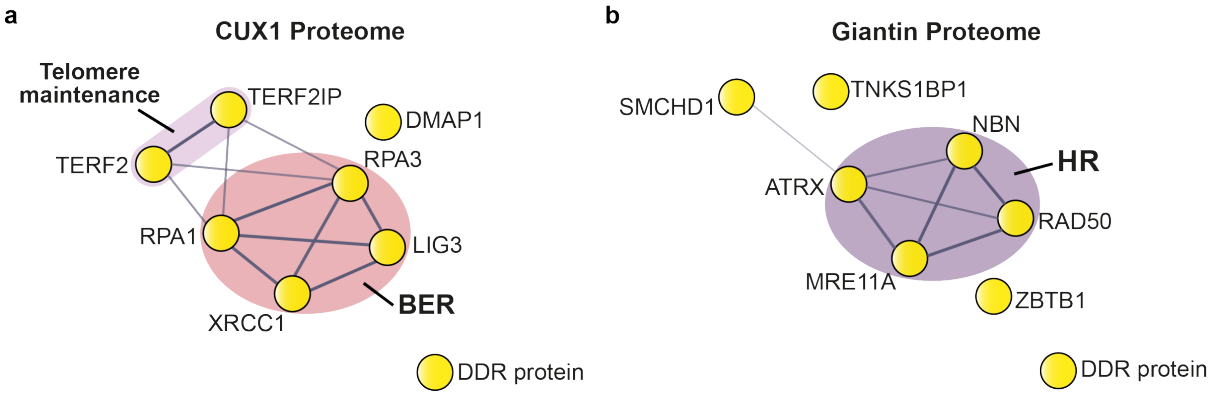

Figure 27. Proteomic-scale interactions of CUX1 and Giantin are enriched in DDR proteins. (a-b) STRING protein-protein interaction networks showcasing CUX1 and Giantin proteomes, where yellow nodes denote: **(a)** DDR proteins from BER and Telomere maintenance pathways detected in CUX1 IP-MS analysis; **(b)** DDR proteins from HR DNA repair pathway which were detected in Giantin IP-MS analysis; experimental-based string network, confidence level > 0.4.

CHAPTER 3

Discussion

Although to date there is not much evidence to point at the role of the Golgi complex as part of the DNA damage response, a few and far in-between studies have alluded to this function. The work carried out by Field's team in 2014 has proposed a mechanism where the Golgi complex alters its structure in response to DNA damage, a process proposed to increase cell survival post-DNA damage events. Although the kinetics of this described process which is in the region of 24 hours would suggest that the Golgi fragmentation observed is part of a recovery process rather than a direct active repair response, although how and whys of this process are still to be described (Farber-Katz *et al.*, 2014). Somehow complementary, our team investigating the Golgi-nuclear interactome, identified a DDR network of 15 proteins that localise to both the Golgi and the nucleus, interestingly, none of these proteins has been previously described to localise or have any function at the Golgi. The identified network was found to be composed of proteins that function in various distinct DNA repair pathways, namely Homologous Recombination, Non-Homologous End-Joining, Mismatch Repair and Base Excision Repair, along with cell cycle and other regulatory proteins. These finding lead to the formation of the hypothesis, that the Golgi complex plays an active role in the DDR, in particular DNA repair regulation.

In-depth characterisation of the dual-localising protein RAD51C has shed some light on the potential role the Golgi complex might play (Galea *et al.*, 2022). This work has revealed that the Golgi population of RAD51C is actively recruited as part of the HR repair mechanism and its localisation at the Golgi is dependent on the Golgin Giantin. Furthermore, the loss of this interaction by depletion of Giantin leads to genomic instability and aberrant DNA repair. Taken together, these first findings have shown active recruitment and regulation acting at the Golgi complex for the functioning of HR.

In light of these findings and the wide array of DDR proteins identified at the Golgi, it is reasonable to postulate that similar regulatory mechanisms would be present for various other DNA repair pathways. In this work, I tested whether the Golgi population of the identified dual-localising DDR cluster have an active role in DDR and if so to start dissecting the mechanisms at play at the Golgi complex.

DDR proteins change localisation upon induction of double-strand breaks with doxorubicin

In order to start testing this hypothesis, I investigated whether the Golgi DDR proteins would respond to the DNA damage by changing their localisation pattern between the Golgi and the nucleus. Following the previous study, DSBs were induced utilising the well-known chemotherapeutic, doxorubicin and the localisation pattern of the protein of interest was monitored. Here I observed, the majority of the proteins changed their localisation pattern (14/15) upon DNA damage by redistributing in Golgi-to-nucleus or perhaps most strikingly from a nucleus-to-Golgi pattern. RAD51C, NBN, MSH6 CCAR1 displayed a localisation pattern Golgi-to-nucleus in response to DNA damage, while USP1, POLQ, LIG1, LRIG2 and TOPORS were found to have a reverse phenotype and distributed in the nucleus-to-Golgi pattern. These changes in distribution patterns were almost always marked by a significant reduction in the protein level. A phenotype I attribute to protein degradation or turnover due to DNA repair although further investigation is warranted to understand the underlying mechanism. Interestingly, the two observed protein redistribution patterns could be clustered based on the pathways the DDR proteins function. Having induced DSBs through the action of doxorubicin (Tewey *et al.*, 1984; Pommier *et al.*, 2010), HR and NHEJ would be expected to be active.

More interestingly, I observed that proteins that belong to the same DDR pathway change their localisation pattern similarly. For example, proteins RAD51C and NBN, which are known to have a direct function in HR, are redistributed to the nucleus, while proteins TOPORS and LIG1, which are known to have a direct function in BER for the repair of single-strand breaks, are distributed oppositely upon induction of DNA damage with doxorubicin. Suggesting that the two BER proteins are translocated away from the nucleus, perhaps to prevent their accidental activation. Based on this

observation, I could postulate these changes in the localisation pattern of these DDR proteins are dependent on the type of DNA lesion induced and in turn, the repair pathway is currently engaged. Additionally, the localisation pattern between these two organelles appears to be bi-directional perhaps suggesting a spatiotemporal regulatory mechanism is in play to ensure the proper regulation of DNA repair pathways.

Contrastingly, in response to doxorubicin treatment non-homology-based double-strand break repair pathways (USP1, POLQ, LRIG2), do not distribute into a Golgi-to-nucleus pattern, what would be expected upon induction of double-strand breaks, but show a redistribution towards the Golgi. Based on what is known in the literature, the choice of which double-strand break repair pathway to be engaged in is highly dependent on the cell cycle phase and cell type (Jazayeri *et al.*, 2006; Scully *et al.*, 2019; Burgess *et al.*, 2020). HeLa Kyoto cells, used in these experiments, are fast proliferating, which would suggest they have an active S cell cycle phase which would justify an overly active HR pathway and would be in line with these findings. Nonetheless, this has to be further investigated, cross-correlated with cell cycle phase, other cell types, and DSBs inducing agents, to ensure that these observations are representative of a “physiological” cellular response.

Similar phenotypes were observed for DDR signalling proteins, perhaps most prominent were the changes observed for the cell cycle and apoptosis regulatory protein CCAR1. The protein was observed to distribute in a nucleus-to-Golgi manner and resulted in the formation of nuclear foci, similar to the ones observed with RAD51C (Galea *et al.*, 2022). These foci were also found to co-localise with a number of HR repair markers. Although CCAR1 has not been previously described to act directly in the repair of double-strand breaks or localise at sites of DNA damage, it has been reported that it interacts with DNA damage-sensing protein H2AX (Sekhar *et al.*, 2019). CCAR1 also has a DNA binding domain which would perhaps explain its presence in these HR-positive nuclear foci. Although without further confirmation we can only speculate that this protein might have an actual role in the double-strand break repair itself, besides being important for DDR signalling and cell cycle regulation.

Nonetheless, these experiments raised important questions regarding the Golgi-nuclear redistribution of these DDR proteins in response to different types of DNA

lesions. Do different DNA lesions such as oxidative stress or single-strand breaks, present different protein distribution patterns?

DDR proteins distribute differently upon induction of oxidative stress

In order to start testing this hypothesis, I utilised hydrogen peroxide, a ROS agent to induce oxidative damage and DNA base lesions and in turn the activation of the BER pathway (Hegde, Hazra and Mitra, 2008). Indeed, after treatment, BER repair proteins LIG1 and TOPORS displayed a shift in localisation pattern in a Golgi-to-nuclear manner, the opposite phenotype observed after doxorubicin treatment. Contrastingly, no localisation change was observed for HR protein RAD51C whereas HR protein NBN showed a nuclear-to-Golgi redistribution, the reverse of what was previously observed after doxorubicin treatment. These findings support the previous observations and my hypothesis that the Golgi localised DDR proteins change their distribution between the Golgi complex and the nucleus in a repair pathway-specific manner. To ensure that the redistribution of DDR proteins is due to the induction of DNA base lesions and not just a consequence of hydrogen peroxide treatment response signalling, I employed potassium bromide, an agent that has been shown to induce similar damage to DNA bases, which would, in turn, activate the BER repair pathway (Borghini *et al.*, 2017; Møller *et al.*, 2018; Vodenkova *et al.*, 2020). Here, BER repair proteins distributed similarly to what was observed in the hydrogen peroxide treatments, while HR proteins did not show a dramatic change in localisation pattern. Overall, the redistribution pattern observed with treatments with hydrogen peroxide was mirrored by potassium bromide treatments. Ideally, to further dissect the redistribution of these DDR proteins in response to various DNA lesions an array of other DNA damage agents should be tested in various other cell types to assess the variability in this response system.

At this point, it cannot be completely excluded that the observed response of these DDR proteins is due to an unknown cellular response although these experiments and a previous study carried out in the lab (Galea *et al.*, 2022) support our current hypothesis. In the case of RAD51C, similar distribution patterns upon induction of double-strand breaks were observed with the treatment of various double-strand

break-inducing drugs, namely doxorubicin, mitomycin, camptothecin and etoposide, suggesting that this is a double-strand break rather than the drug itself-specific response. Nevertheless, further confirmation and characterisation regarding the response of these proteins to specific DNA damage would provide more detail for understanding different types of DNA triggers that would activate different types of DDR pathways. The combination of DDR kinase inhibitors (ATM, ATR and DNA-PK) and DNA damage-inducing agents could be used to ensure that the phenotypes observed are predominately due to DNA damage signalling and not indirect signalling cues such as apoptosis and stress response caused by the drug treatment. Additionally, DNA damage and apoptosis markers should be used to assess the nature of this response.

The redistribution of DDR proteins to the nucleus occurs in an importin-ß specific manner

Next, I examined whether the change in the localisation pattern of DDR proteins is based on the active movement of the protein from one organelle to another and what facilitates this transport. To assess these, an assay was developed combining the nuclear transport inhibitor importazole (Soderholm *et al.*, 2011) and doxorubicin treatment to assess the kinetics of Golgi-nuclear traffic. The drug specifically blocks importin-ß mediated transport from the cytosol to the nucleus. The inhibitor treatment was observed to inhibit the doxorubicin-induced localisation redistribution from the Golgi to the nucleus for all the proteins tested. This resulted in a larger proportion of the protein population at the Golgi when compared with the doxorubicin treatment without importazole. These findings suggest that the observed protein localisation change of the DDR proteins is most likely an active transport of the protein population between the Golgi complex and the nucleus. Nevertheless, only further in-depth investigation and validation would allow more solid conclusions. The systematic depletion of various components of the importin-beta pathway experiment, and deletion mutations of the NLS sequence in these DDR proteins would provide stronger evidence and mechanistic detail in this transport step. Furthermore, it would be ideal to include other DNA-damaging agents, as up to this stage, only doxorubicin-induced redistribution has been tested, it would be interesting to test whether protein

distribution in the Golgi-to-nucleus pattern upon induction of oxidative stress is also achieved via the importin-ß pathway. Additional questions regarding nuclear to Golgi transport are still to be addressed. What are the mechanisms at play regulating this pathway? Are they being affected by nuclear export blockage?

Golgi-localised DDR proteins do not regulate Golgi organisation and anterograde transport of VSV-G

Being established that the Golgi population of DDR proteins is required for DDR, additionally, I studied whether the described DDR proteins would present any moonlighting functions at the Golgi that are not related to DDR but rather important for Golgi morphology or one of the classical functional aspects of the Golgi – anterograde transport. Therefore, I systematically depleted DDR proteins and monitored whether they affected the Golgi structure or anterograde transport of VSV-G. The data showed that the depletion of DDR proteins resulted neither in a significant phenotypical change of Golgi morphology at the light microscopy level nor had a significant impact on the anterograde transport of VSV-G (Hirschberg *et al.*, 1998). These results would suggest that the DDR proteins at the Golgi do not have an observable Golgi structural role. Presently, though it cannot be excluded that knock-down of the investigated DDR proteins may induce Golgi structure changes that may only be detectable by ultrastructural analyses by electron microscopy. Similarly, it can presently not exclude that the knock-downs may have effects on the transport of specific endogenous cargo such as glycosylation enzymes, KDEL receptor or mannose-6-phosphate receptor.

Interestingly, it was observed that upon depletion of DDR proteins such as NBN, LIG1, FMN2 and ESCO2, Golgi marker GM130 forms nuclear foci. GM130 has been recently reported to localise in the nucleus and phase separate when overexpressed (Rebane *et al.*, 2020). Whether the nuclear foci identified upon depletion of DDR proteins are similar to the ones and whether this is somehow related to the DNA damage response, upon loss of DDR protein is unclear.

Localisation of DDR proteins at the Golgi is distributed in a pathway-specific manner

Next, I investigated how these proteins are distributed throughout the Golgi. For that aim, I performed an experiment where I disrupt the Golgi structure into individual stacks using the microtubule depolymerising agent, nocodazole and analysed the distribution of these DDR proteins against two markers sitting at the polar ends of the organelle. Here I observed that the distribution of these proteins on the Golgi stack was correlated to DDR-specific pathways where they function. For example, HR proteins RAD51C and NBN were identified to localise on the *cis*-side of the Golgi, while BER proteins LIG1 and TOPORS localise on the *trans*-side of the Golgi. These results would suggest that DDR proteins are enriched to particular Golgi-cisternae based on their function. Possibly these enriched "domains"/cisternae would allow the quick activation, recruitment and propagation of both DNA repair machinery and DDR signalling. Important mechanistic questions regarding the relevance of the sub-Golgi-localisation of these proteins, and the mechanism by which their localisation is maintained are still to be addressed. Nonetheless, it is important to consider that this assay gives a correlative measure of DDR protein localisation at the Golgi and further confirmation with perhaps electron microscopy imaging should be considered in order to test the hypothesis of DDR protein sub-domain formation at the Golgi.

Golgins as anchors for DDR proteins at the Golgi

All but one of the identified Golgi-localised DDR proteins do not contain a transmembrane or any attachment domain that would explain their localisation at the Golgi. This raised a question, why and how are these proteins localising at the Golgi? Analysis done by George Galea of primary published data from two genome-wide screens (Paulsen *et al.*, 2009; Adamson *et al.*, 2012) identified the Golgin protein family as potential candidates for Golgi-anchoring of DDR proteins. Further characterisation of RAD51C identified the Golgin Giantin as a Golgi anchor for this protein (Galea *et al.*, 2022). Based on these findings, it would be reasonable to suggest that the Golgins may play a similar role in anchoring various DDR proteins to the Golgi complex. To test this, I selected several differently localised Golgins, along with DDR proteins acting in different DDR pathways, and tested whether the depletion of Golgins

would affect their localisation at the Golgi. As a first instance, I identified that knock-down of Golgins GMAP-210, GOLGA7, GOLGIN-45 and Giantin affect the localisation of proteins NBN, TOPORS, CCAR1 and LIG1, respectively. Upon depletion of the Golgins, localisation of these DDR proteins at the Golgi was decreased, raising a question of whether this effect is due to direct interaction between these pairs of Golgins and DDR proteins. I validated these interactions by immunoprecipitation and western blot analysis, confirming the interaction for Golgin and DDR protein pairs of GMAP-210 and NBN, GOLGA7 and TOPORS, CCAR1 and GOLGIN-45. In line with these findings, the identified Golgins are described to also localise to the same Golgi cisternae, as was shown for DDR proteins. For example, NBN was identified to co-localise with the cis-Golgi marker GM130 and GMAP-210 is described as a *cis*-Golgi localised protein (Munro, 2011; Witkos and Lowe, 2016; Lowe, 2019); TOPORS was identified to co-localise with *trans*-Golgi marker, as well as it is described for GOLGA7 (Ko *et al.*, 2019); CCAR1 has been identified to co-localise with *cis*-Golgi marker and GOLGIN-45 is described as *medial-cis* localised Golgin (Barr and Short, 2003).

In contrast, these experiments also indicated that LIG1 and Giantin do not directly interact. Yet, the effect of Giantin knock-down has also resulted in the change of LIG1 Golgi-to-nucleus distribution ratio upon induction of double-strand breaks with doxorubicin, suggesting that the loss of a Golgin can have consequences of localisation of DDR proteins at the Golgi even if these proteins were not shown to directly interact. Altogether, these results present strong evidence that Golgin protein family proteins and DDR proteins interact, and raise more questions regarding the importance of this interaction in the DNA damage response and whether the loss of Golgi localisation of DDR proteins would have any further consequences in DDR.

The knock-down of Giantin leads to genomic instability and inhibition of DDR signalling

To continue to dissect the role of Golgins in DDR, in a previous study it was found that the depletion of the Golgin Giantin leads to a decrease of RAD51C localisation at the Golgi and formation of RAD51C nuclear foci, which resemble DNA repair foci (Galea *et al.*, 2022). Further investigation of these foci revealed that these structures did not co-localise with established HR markers, suggesting that these protein clusters are

not DNA repair foci. Following this, we investigated whether the loss of RAD51C Golgi localisation, leading to nuclear foci formation would have any further consequences on genomic stability or DDR signalling. Indeed, it was shown that the depletion of Giantin resulted in higher levels of fragmented DNA in the cells, indicating genomic instability. It was also observed that the loss of Giantin-RAD51C interaction leads to impaired DDR signalling. These experiments showcased the first instance of the importance of DDR protein localisation at the Golgi and the implications of its loss, letting to speculate, that the Golgi localisation of DDR proteins is part of their regulation. However, whether the depletion of other Golgins results in similar phenotypes and impacts other DDR pathways are under current investigation.

The landscape of Golgin and DDR protein interactions

Having established further that Golgins and DDR proteins interact, it would reasonable to speculate that other members of the Golgin protein family might have a similar function. To investigate the Golgi-DDR interactome I took a systematic approach using proteomics. I carried out immunoprecipitation experiments using antibodies against Golgi-localised DDR proteins followed by proteomic analysis. Unfortunately, this approach is very much dependent on the compatibility of used antibodies and it turned out that not all antibodies against DDR proteins were suitable for this assay - only 7 out of 15 DDR protein proteomes were obtained. As expected, some Golgi proteins, including Golgin family proteins, were enriched in DDR protein proteomes, suggesting that the network of interactions between the Golgi proteins and DDR proteins might be more extensive than previously found.

Following this as a second analogue strategy I also explored selected Golgin proteomes. Although the data presented here is preliminary and still requires further confirmation, a number of DDR proteins were identified in Golgin proteomes. What perhaps is even more exciting, is that in the case of Golgins CUX1 and Giantin, entire clusters of DDR proteins, acting in BER or HR, respectively, were found to interact with these Golgins, confirming the hypothesis that DDR and Golgi protein proteomes interact. However, this study also has limitations, that cannot be excluded. Since the protein extracts used in proteomic analysis experiments are whole-cell lysates, there is a possibility that these proteins interact in other compartments besides the Golgi.

Some Golgins, like CUX1, have been reported to localise also in the nucleus (Krishnan *et al.*, 2022). To test and confirm the compartment in which these Golgi and DDR proteins interact, analogue experiments from fractionated cell lysates are being currently carried out. In addition to that, the already found interactions between the Golgins and DDR proteins were not observed in proteomics data (RAD51C with Giantin, NBN with GMAP-210, GOLGA7 with TOPORS, GOLGIN-45 with CCAR1). Here I suspect these results might be due to another limitation regarding these experiments which is the protocol and used conditions for immunoprecipitation. Since it is not known what kind of interactions are present between these proteins, it might be that because of the used buffer composition, some of these interactions are lost during the lysis and cannot be observed in later analysis. Perhaps, improving the protocol and testing other conditions for the lysis might be beneficial to improve the sensitivity for the detection of these interactions. It cannot also be excluded that some interactions observed via mass spectrometry can be due to unspecific binding and would need further validations, utilising, for example, immunofluorescence and western blot analysis.

Taken together these results highlight an exciting new paradigm in the DDR regulation, although many question remain how this Golgi DDR regulation functions in various cell types. Due to the exploratory nature of this study, most of the experiments were conducted using HeLa Kyoto cells, which might not be an ideal representation of the physiological state, and therefore to validate the relevance of these findings other model systems should be considered. In addition, the usage of DNA-damaging agents in this study, which often have side effects and usually result in more than just single-type DNA lesions, should be complemented by exploiting other DNA-damaging treatments, like UV and ionizing radiation, or CRISPR systems for more specific DNA lesion induction. Despite the limitations, the new findings in this work open up an exciting new niche, with a multitude of new avenues of research questions.

Proposed model

The results presented in this work reveal and confirm the presence of a complex relationship between the Golgi complex and DDR, identifying new interacting pathways and expanding on our current knowledge of DDR regulation and Golgi biology. The data presented in this work support the hypothesis that the Golgi complex serves as a hub for DNA damage response regulation. Here I propose a model where various DDR proteins are distributed throughout the Golgi in a DDR pathway-specific manner. In case of a DNA damage event, these proteins respond to specific DNA lesions through a shift in localisation either from the Golgi to the nucleus or from the nucleus to the Golgi, based on the type of DNA lesion present and their role in the specific DDR pathways. Furthermore, the Golgins form a matrix that serves as a scaffold for various DDR proteins to be anchored and localised to the Golgi membranes. The loss of this interaction can lead to consequences like genomic instability and impaired DDR signalling.

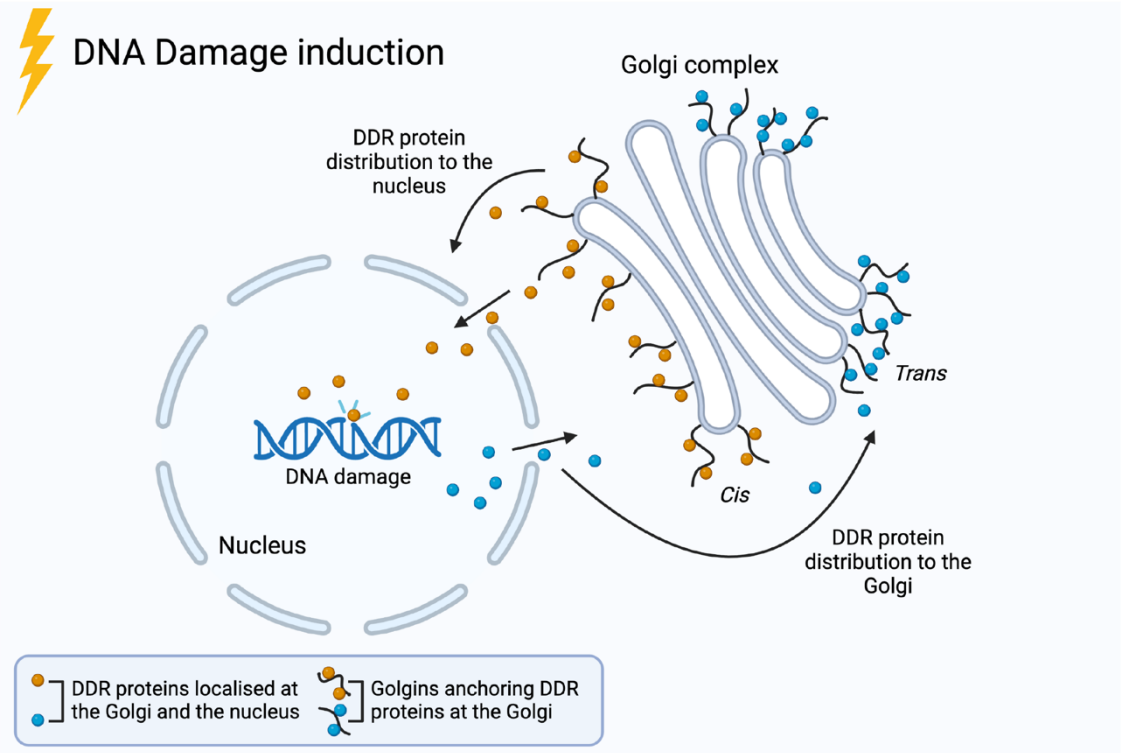

Figure 28. Proposed model of the Golgi as a hub for DDR regulation. DDR proteins are distributed throughout the Golgi and anchored to the Golgi membranes via Golgin family proteins. Upon specific DNA damage induction, required for DNA repair DDR proteins redistribute to the nucleus, while other, non-required for the specific repair proteins distribute to the Golgi.

Conclusions and perspectives

In conclusion, this work continues to build upon and further validates the presence of a novel pathway, where the Golgi plays a central role in the regulation of DNA damage response. In light of this, we set up collaborations with groups of Simone Köhler and Gautam Dey, to explore whether the function of Golgins in DDR is evolutionary preserved in other species, like c. elegans and different species of yeast. Furthermore, we are dissecting further the role of the Golgi and Golgins in DDR, by using complementary strategies together with immunofluorescence assays, biochemical assays and MS, in order to expand the knowledge and add more mechanistic details towards understanding these processes.

On a larger perspective, when taking into context the established role of the Golgi complex as a cellular hub for signalling, transport and post-translational modification (Jackson, 2009; Wilson *et al.*, 2011; Millarte and Farhan, 2012), the organelle presents itself as an ideal candidate for DNA damage response regulation. The Golgi has already been shown to be the link between nuclear and cytoplasmic processes for a number of essential pathways as already described in the context of cholesterol homeostasis (Brown and Goldstein, 1997; Bien and Espenshade, 2010) and inflammation among many others (Wilson *et al.*, 2011; Millarte and Farhan, 2012; Scharaw *et al.*, 2016). Additionally taking into consideration the proximity of the two organelles, the Golgi's cellular influence in numerous pathways and its unique compact architecture are just a few examples of why the Golgi plays such a role in DDR.

Finally, this work not only raises questions regarding Golgi's role in DDR but also leads to pondering what functions DDR have at the Golgi complex; are processes such as membrane trafficking, glycosylation, and cytoskeletal organisation occurring at this organelle being regulated by Golgi localising DDR proteins in response to DNA damage? These findings are a beginning of a new direction in the DNA damage repair field, shifting from a nuclear-centric to a more global picture of how DNA damage response is regulated, opening up possibilities for finding new therapeutic targets.

CHAPTER 4

Materials and methods

The materials used in this work are listed in tables 2-18.

Mammalian cell culture

Cell line	Source
Human HeLa Kyoto	Gift from Shuh Narumiya, Kyoto University, Japan
Human U2-O S	Pepperkok group, EMBL Heidelberg
Normal Human Lung Fibroblasts NHLF	Lonza

Table 2. Mammalian cell lines.

Reagent	Source	Identifier
DMEM (Dulbecco's Modified Eagle Medium) 1g/L D-glucose	Gibco	Cat#11880028
FCS (Fetal Calf Serum)	Gibco	Cat#10270
L-Glutamine	Sigma-Aldrich	Cat#G7513
Opti-MEM	Gibco	Cat#51958
Trypsin-EDTA 0.05%	Gibco	Cat#25300-054

Table 3. List of reagents used for mammalian cell culture.

Cell culture medium	Composition
FCS DMEM 2x	DMEM, 20% FCS (v/v), 1% L-Glutamine (v/v)
Freezing Medium	50% DMEM (v/v), 40% FCS (v/v), 10% DMSO (v/v)
Normal Culture Medium	DMEM, 10 % FCS (v/v), 1% L-Glutamine (v/v)
Serum Free DMEM	DMEM, 1% L-Glutamine (v/v)

Table 4. Composition of growth media used for mammalian cell culture.

Reagents

Reagent	Source	Identifier
Agarose	Sigma-Aldrich	Cat#A-9539
Agarose Low-melting point	Sigma-Aldrich	Cat#A9414
Ampicillin	Sigma-Aldrich	Cat#A-9393
Bovine Serum Albumin (BSA)	Sigma-Aldrich	Cat#A2153
Dimethyl sulfoxide (DMSO)	Sigma-Aldrich	Cat#D2438
DL-Dithiothreitol (DTT)	Sigma-Aldrich	Cat#D0632
EDTA-Free Protease Inhibitor Cocktail (PIC)	Roche	Cat#1836170001
Ethanol	Merck	Cat#1.00983
Ethylenediaminetetraacetic acid (Na_2EDTA)	Merck Millipore	Cat#324503
Glycerine	VWR	Cat#56-81-5
Glycine	Merck	Cat#1.04201
Hoechst 33342	Thermofisher Scientific	Cat#H21492
Kanamycin	Sigma-Aldrich	Cat#K-0254
Methanol	Merck	Cat#322415
Milk powder	Frema	-
Oligofectamine 2000 Transfection reagent	Thermofisher Scientific	Cat#12252011
Paraformaldehyde (PFA)	Thermofisher Scientific	Cat#50-980-491
Precision plus protein prestained standard marker	Bio-Rad	Cat#1610394
Sodium Chloride (NaCl)	Merck	Cat#1.06404
Sodium Dodecyl Sulfate (SDS) 20% Solution	Bio-Rad	Cat#1610418
Sodium Hydroxide (NaOH)	Merck	Cat#1.06498
SYBR Gold	Thermofisher Scientific	Cat#S11494
SYBR Safe	Thermofisher Scientific	Cat#S33102
Trichloroacetic acid (Tris-HCl)	Merck	Cat#1.0081
Triton X-100	Sigma-Aldrich	Cat#T8787
Trizma base	Sigma-Aldrich	Cat#T1503
Tween-20	Sigma-Aldrich	Cat#P7949

Table 5. List of reagents.

Drugs and inhibitors

Chemical	Source	Identifier
Camptothecin	Abcam	Cat#ab120115
Cycloheximide	Calbiochem	Cat#200-636-0
Doxorubicin	Abcam	Cat#ab120629
Hydrogen Peroxide H_2O_2	Sigma-Aldrich	Cat#H1009
Importazole	Sigma-Aldrich	Cat#SML0341
Nocodazole	Sigma-Aldrich	Cat#M1404
Potassium Bromide $KBrO_3$	Merck Millipore	Cat#104912

Table 6. List of drugs and inhibitors.

Buffers and solutions

Solution	Source	Composition
sPBS	Self-generated	2.7 mM KCl 1.4 mM KH_2PO_4 4.8 mM Na_2HPO_4 137 mM NaCl in ddH_2O, pH 7.4, autoclaved
1M HEPES (4-(2-hydroxyethyl-) piperazin-1-ethansultonic acid)	Media kitchen, EMBL	23.8% HEPES (w/v) in ddH_2O, pH 7.25, autoclaved
NuPAGE MOPS SDS running buffer (20X)	Thermofisher Scientific Cat#NP0001	Diluted to 1X buffer in ddH_2O
4% PFA fixation buffer	Self-generated	4% PFA in sPBS
Sample buffer (2X)	Self-generated	200 mM Tris-HCl 25% glycerol (v/v) 11.25% SDS (v/v) 325 mM DTT 0.0125% (w/v) bromphenol blue, pH 6.8
Sample buffer (5X)	Self-generated	200 mM Tris-HCl 25% glycerol (v/v) 11.25% SDS (v/v) 325 mM DTT 0.0125% bromphenol blue (w/v), pH 6.8
Sample buffer (2X) for MS-IP		65.8 mM Tris-HCl 26.3% Glycerol (v/v) 2.1% SDS (v/v) 325 mM DTT, pH 6.8
Phosphate Buffered Saline (PBS)	Media kitchen, EMBL	2.7 mM KCl 1.4 mM KH_2PO_4 4.8 mM Na_2HPO_4 137 mM NaCl in ddH_2O, pH 7.4, autoclaved
Triton X-100 permeabilization buffer	Self-generated	0.1% Triton X-100 (v/v) in sPBS
Western blot blocking buffer	Self-generated	0.1% Tween-20 (v/v) 5%. Milk powder (w/v) in PBS
Western blot transfer buffer (10X)	Self-generated	2.9% Glycin (w/v) 5.8% Trizma Base (w/v) 0.5% BSA (w/v) in ddH_2O
Western blot transfer buffer (1X) with SDS	Self-generated	10X Transfer buffer diluted to 1X in ddH_2O 20% Methanol (v/v) 0.1% SDS (v/v)

Western blot washing buffer (PBS-T)	Self-generated	0.1% Tween-20 (v/v) in PBS
IP lysis buffer	Self-generated	50 mM HEPES 130 mM NaCl, 1 mM DTT 1% NP-40 1X EDTA-free protease inhibitors in ddH_2O
RIPA lysis and extraction buffer	Thermofisher Scientific Cat#89900	-

Table 7. List of buffers and solutions.

Oligonucleotides

Gene	Sense siRNA sequence 5'-3'	Antisense siRNA sequence 5'-3'	siRNA ID	Source
CCAR1	GGAAAUCUGAAGACGAUAAtt	UUAUCGUCUUCAGAUUUCCta	s31410	Ambion
CCAR1	GGUCUAAACUUGAUCCAAAtt	UUUGGAUCAAGUUUAGACCaa	s31411	Ambion
CUX1	GCAUAAGGUUCAGAGCCUAtt	UAGGCUCUGAACCUUAUGCtc	s3769	Ambion
EFHD1	GGGUAAUGGUGGGUCUUAAtt	UUAAGACCCACCAUUACCCag	s37169	Ambion
ESCO2	CGUGUCCUGUCUGAACCAAtt	UUGGUUCAGACAGGACACGaa	s45967	Ambion
FAM214A	GCAUGACUCCAGUUCGGUUtt	AACCGAACUGGAGUCAUGCat	s32060	Ambion
FMN2	CAGUCAGACGAACUCGAAAtt	UUUCGAGUUCGUCUGACUGtg	s32270	Ambion
Giantin	GAAGCUUGAGGAACACGAAtt	UUCGUGUUCCUCAAGCUUCct	s5951	Ambion
Giantin	GGGAAUCCAUAGACGGAAAtt	UUUCCGUCUAUGGAUUCCCtt	s5952	Ambion
Giantin	GCAUAGUGGGUGACUAUCAtt	UGAUAGUCACCCACUAUGCgg	s5953	Ambion
GM130	GGUUCACAUUCAGACCAUAtt	UAUGGUCUGAAUGUGAACCtg	s5942	Ambion
GMAP210	GAACUGUCAAAUGCACGUAtt	UACGUGCAUUUGACAGUUCtt	s17811	Ambion
GMAP210	GAAAUUGGAAUGUAGUAAAtt	UUUACUACAUUCCAAUUUCaa	s17812	Ambion
GOLGA2B	GAGAGUACAUCGCACUGUAtt	UACAGUGCGAUGUACUCUCcc	s31034	Ambion
GOLGA4	CCUCUGAUAUGGAUAGCGAtt	UCGCUAUCCAUAUCAGAGGgt	s5949	Ambion
GOLGA6A	CAGCGGUGGUUACAGCAGAtt	UCUGCUGUAACCACCGCUGga	s50879	Ambion
GOLGA7	GCAUAUACCAUCUUCCUAUtt	AUAGGAAGAUGGUAUAUGCtg	s54837	Ambion
GOLGIN45	GAGUUCACCUGAUAAUCCAtt	UGGAUUAUCAGGUGAACUCtc	s16272	Ambion
GOLGIN45	CCACCUUACUUGCUACAAAtt	UUUGUAGCAAGUAAGGUGGtt	s16273	Ambion
GOLGIN45	GGAGUUAUAGAACCUAAUAtt	UAUUAGGUUCUAUAACUCCct	s16274	Ambion
LIG1	GGAUCCAUCUGGUUACAAUtt	AUUGUAACCAGAUGGAUCCag	s8174	Ambion
LIG1	GGUUUAUUCGAGUCCGUGAtt	UCACGACUCGAAUAAACCga	s8175	Ambion
LRIG2	GGAUCUGACUAUUCGCACUtt	AGUGCGAAUAGUCAGAUCCat	s19090	Ambion
LRRIQ3	GGAUAUGAAGCAAAAUGGAtt	UCCAUUUUGCUUCAUAUCCtc	s229429	Ambion
MSH6	GGCUGUAAACGAUACUGGAtt	UCCAGUAUCGUUUACAGCCct	s6286	Ambion
MSH6	GGGCUAUAAUGUAUGAAGAtt	UCUUCAUACAUUAUAGCCCtg	s534226	Ambion
NBN	GAUAAUUCUAAGUAUGGUAtt	UACCAUACUUAGAAUUAUCtt	s9292	Ambion
NEG9	UACGACCGGUCUAUCGUAGtt	CUACGAUAGACCGGUCGUAtt	s444246	Ambion
PFDN6	CGGUGCUAGUCAAACAGGAtt	UCCUGUUUGACUAGCACCGga	s20500	Ambion
POLQ	CCGCUUUUGGAGUCAGUAAtt	UUACUGACUCCAAAAGCGGta	s21059	Ambion
POLQ	CAACAACCCUUAUCGUAAAtt	UUUACGAUAAGGGUUGUUGtc	s21060	Ambion
RAD51C	GCAAAUUAUCAGAAGAGAAtt	UUCUCUUCUGAUAAUUUGCag	s11738	Ambion
RAD51C	GCAAAUUAUCAGAAGAGAAtt	UUCUCUUCUGAUAAUUUGCag	s11737	Ambion
SDCCAG8	GGAACGACUUAGCUGAAUAtt	UAUUCAGCUAAGUCGUUCCtc	s21235	Ambion
TOPORS	GGAAAGUAGCAGACCUAGAtt	UCUAGGUCUGCUACUUUCCct	s19911	Ambion
TOPORS	GAAAGAUCUUUGCGGAAAAtt	UUUUCCGCAAAGAUCUUUCat	s19912	Ambion
USP1	GGUUAAAGUCUGCAACUAAtt	UUAGUUGCAGACUUUAACCaa	s14724	Ambion

Table 8. List of siRNA oligonucleotides.

Antibodies

Protein	Host	Clone	Dilution	Source	Identifier
CCAR1	Rabbit	Polyclonal	1:500	Gift from Emma Lundberg, HPA Project	Cat#HPA007856
EFHD1	Rabbit	Polyclonal	1:200	Gift from Emma Lundberg, HPA Project	Cat#HPA049331
ESCO2	Rabbit	Polyclonal	1:200	Gift from Emma Lundberg, HPA Project	Cat#HPA053679
FAM214A	Rabbit	Polyclonal	1:200	Gift from Emma Lundberg, HPA Project	Cat#HPA066144
FMN2	Rabbit	Polyclonal	1:200	Gift from Emma Lundberg, HPA Project	Cat#HPA070474
LIG1	Rabbit	Polyclonal	1:200	Gift from Emma Lundberg, HPA Project	Cat#HPA041431
LRIG2	Rabbit	Polyclonal	1:200	Gift from Emma Lundberg, HPA Project	Cat#HPA015538
LRRIQ3	Rabbit	Polyclonal	1:200	Gift from Emma Lundberg, HPA Project	Cat#HPA030798
MSH6	Rabbit	Polyclonal	1:200	Gift from Emma Lundberg, HPA Project	Cat#HPA028446
NBN	Rabbit	Polyclonal	1:200	Gift from Emma Lundberg, HPA Project	Cat#HPA001429
PFDN6	Rabbit	Polyclonal	1:200	Gift from Emma Lundberg, HPA Project	Cat#HPA048123
POLQ	Rabbit	Polyclonal	1:200	Gift from Emma Lundberg, HPA Project	Cat#HPA053359
RAD51C	Rabbit	Polyclonal	1:200	Gift from Emma Lundberg, HPA Project	Cat#HPA061958
RAD51C	Rabbit	Polyclonal	1:500	Abcam	Cat#ab72063
SDCCAG8	Rabbit	Polyclonal	1:200	Gift from Emma Lundberg, HPA Project	Cat#HPA025721
TOPORS	Rabbit	Polyclonal	1:200	Gift from Emma Lundberg, HPA Project	Cat#HPA065661
USP1	Rabbit	Polyclonal	1:200	Gift from Emma Lundberg, HPA Project	Cat#HPA054332
USP1	Rabbit	Polyclonal	1:200	Proteintech	Cat#14346-1-AP
GM130	Mouse	Monoclonal	1:400	BD Biosciences	Cat#BD610822
TGN46	Sheep	Polyclonal	1:1000	Bio-Rad	Cat#AHP500GT
BRCA1	Mouse	Monoclonal	1:200	Abcam	Cat#ab16780
XRCC2	Mouse	Monoclonal	1:200	Santa Cruz	Cat#sc-56254
VSVG	Mouse	Monoclonal	1:100	Gift from Kai Simmons (MPI, Dresden)	-

Table 9. List of primary antibodies used in immunofluorescence experiments.

Protein/Label	Host	Clone	Dilution	Source	Identifier
AlexaFluor 405-Mouse	Goat	Polyclonal	1:200	Thermofisher Scientific	Cat# A1100
AlexaFluor 488-Rabbit	Goat	Polyclonal	1:400	Thermofisher Scientific	Cat#A11008
AlexaFluor 488-Mouse	Goat	Polyclonal	1:400	Thermofisher Scientific	Cat#A11001
AlexaFluor 568-Rabbit	Goat	Polyclonal	1:400	Thermofisher Scientific	Cat#A11011
AlexaFluor 568-Mouse	Goat	Polyclonal	1:400	Thermofisher Scientific	Cat#A11004
AlexaFluor 647-Mouse	Goat	Polyclonal	1:400	Thermofisher Scientific	Cat#A21236
AlexaFluor 647-Rabbit	Goat	Polyclonal	1:400	Thermofisher Scientific	Cat#A21245
AlexaFluor 647-Sheep	Donkey	Polyclonal	1:200	Thermofisher Scientific	Cat#A21448

Table 10. List of secondary antibodies used in immunofluorescence experiments.

Protein	Host	Clone	Dilution	Source	Identifier
CCAR1	Rabbit	Polyclonal	1:2000	Atlas Antibodies	Cat#HPA007856
CCAR1	Rabbit	Polyclonal	1:2000	Novus Biologicals	Cat#NB500-186
CCAR1	Mouse	Monoclonal	1:2000	Santa Cruz	Cat#SC-525629
CHK2	Rabbit	Polyclonal	1:2000	Thermofisher Scientific	Cat#PA5-17818
DNA-PKcs	Rabbit	Polyclonal	1:2000	Thermofisher Scientific	Cat#PA5-78130
GM130	Mouse	Monoclonal	1:2000	BD Biosciences	Cat#610822
GMAP-210	Rabbit	Polyclonal	1:2000	Santa Cruz	Cat#NB100-59836
GMAP-210	Mouse	Monoclonal	1:2000	BD Biosciences	Cat#611712
GOLGIN-45	Rabbit	Polyclonal	1:2000	Atlas Antibodies	Cat#HPA067113
GOLGIN-45	Mouse	Monoclonal	1:2000	Santa Cruz	Cat#sc-515193
GOLGIN97	Mouse	Monoclonal	1:2000	Molecular Probes	Cat#A21270
LAMINB1	Rabbit	Polyclonal	1:2000	Abcam	Cat#ab16048
LIG1	Mouse	Monoclonal	1:2000	Novus Biologicals	Cat#NB100-119
LIG1	Rabbit	Polyclonal	1:2000	Atlas Antibodies	Cat#HPA048071
NBN	Rabbit	Polyclonal	1:2000	Atlas Antibodies	Cat#HPA001429
p-ATM	Mouse	Monoclonal	1:2000	Thermofisher Scientific	Cat#MA1-2020
USP1	Rabbit	Polyclonal	1:2000	Proteintech	Cat#14346-1-AP
Vinculin	Rabbit	Monoclonal	1:2000	Abcam	Cat#ab219649
α-TUBULIN	Mouse	Monoclonal	1:10000	Neomarkers	Cat#MS581

Table 11. List of primary antibodies used in western blot experiments.

Protein/Label	Host	Clone	Dilution	Source	Identifier
HRP-anti-rabbit	Goat	Polyclonal	1:16000	Sigma	Cat#A0545
HRP-anti-mouse	Rabbit	Polyclonal	1:8000	Sigma	Cat#A9044
HRP-anti-sheep	Mouse	Polyclonal	1:8000	Sigma	Cat#A9452

Table 12. List of secondary antibodies used in western blot experiments.

Protein	Host	Clone	Dilution	Source	Identifier
CCAR1	Mouse	Monoclonal	1:600	Santa Cruz	Cat#SC-525629
CUX1	Rabbit	Polyclonal	1:600	Proteintech	Cat#11733-1-AP
ESCO2	Rabbit	Polyclonal	1:600	Atlas Antibodies	Cat#HPA053679
GM130	Mouse	Monoclonal	1:600	BD Transduction Laboratories	Cat#BD610822
GMAP-210	Mouse	Monoclonal	1:600	BD Transduction Laboratories	Cat#611712
GOLGA7	Mouse	Monoclonal	1:600	Novus Biologicals	Cat#H00051125-M01
GOLGIN-245	Mouse	Monoclonal	1:600	BD Transduction Laboratories	Cat#BD611280
GOLGIN-45	Mouse	Monoclonal	1:600	Santa Cruz	Cat#sc-515193
GOLGIN97	Rabbit	Polyclonal	1:600	Abcam	Cat#ab84340
LIG1	Mouse	Monoclonal	1:600	Novus Biologicals	Cat#NB100-119
MSH6	Rabbit	Polyclonal	1:600	Atlas Antibodies	Cat#HPA028446
NBN	Rabbit	Polyclonal	1:600	Atlas Antibodies	Cat#HPA001429
SDCCAG8	Rabbit	Polyclonal	1:600	Abcam	Cat#ab228891
USP1	Rabbit	Polyclonal	1:600	Proteintech	Cat#14346-1-AP

Table 13. List of primary antibodies used in MS-IP experiments.

Enzymes

Enzyme	Source	Identifier
Benzonase 25 U/µL	Novagen	Cat#70746
Proteinase K	Thermofisher Scientific	Cat#EO0491

Table 14. List of Enzymes.

Kits

Kit	Source	Identifier
Subcellular Protein Fractionation Kit for Cultured cells	Thermofisher Scientific	Cat#78840
Velocity DNA Polymerase	Meridian Bioscience	Cat#BIO-21098

Table 15. List of kits.

Equipment

Equipment	Source
50 mL Reagent Reservoir	Corning Cat#4870
Cell culture dish 10 cm	Thermofisher Scientific Cat#363401
Cell culture dish 15 cm	Thermofisher Scientific Cat#168381
Cell culture plate 24-well	Thermofisher Scientific Cat#142475
Cell culture plate 6-well	Thermofisher Scientific Cat#140675
Cell culture plate 96-well	Thermofisher Scientific Cat#167008
Cell scraper	Corning Cat#3010
Cool Cell freezing container	Corning Cat#CLS432004
Cryotubes	Thermofisher Scientific Cat#363401
GelBond films for agarose gels	Lonza Cat#53740
Glass bottom imaging plate 96-well	Zell-Kontakt Cat#5241
Glass Coverslips 11 mm diameter	Th. Geyer Cat#CB00120RA1
Immobilon PVDF Membrane	Merck Millipore Cat#IPVH00010
Microscope Cover Glasses 24 x 32 mm	WWR Cat#631-0691
NuPAGE 4-12% Bis-Tris, 1.0 mm x 10 well Protein Gel	Thermofisher Scientific Cat#NP0321
NuPAGE 4-12% Bis-Tris, 1.0 mm x 12 well Protein Gel	Thermofisher Scientific Cat#NP0322
NuPAGE 4-12% Bis-Tris, 1.5 mm x 10 well Protein Gel	Thermofisher Scientific Cat#NP0335
Object slides with frosted end	Fisher Cat#1156-2203
Protein-G Agarose	Roche Cat#11719416001
Whatman paper	Whatman Cat#3030817

Table 16. List of laboratory equipment.

Laboratory machines

Machine	Source
Azure 280 Western blot imaging system	Azure Biosystems
Centrifuge 5408 R	Eppendorf
Centrifuge 5417 R	Eppendorf
Dry Block heating system 7E9733	Grant
Electrophoresis chamber	EMBL Heidelberg workshop
Electrophoresis chamber	EMBL Workshop
Magnetic stirring hotplate MR3001 K	Heidolph
Mini centrifuge	Carl Roth
Mini Trans-blot Cell Blotting system	Bio-Rad
Mini Trans-Blot Cell system	Bio-Rad
Nanodrop 8000 Spectrophotometer	Peqlab
neoLab-Rotator 2-1175	Sigma
Protein Gel Electrophoresis XCell Sure Lock System	Thermofisher Scientific
Roller mixer RS-TS05	Phoenix Instrument
Rotary shake	neoLab
Scale	VWR
Scale SBA 51	Scaltec
ThermoMixer C	Eppendorf
Tissue culture incubator	Binder
Water bath	GFLR

Table 17. List of laboratory machines.

Microscopes

Microscope	Source
Automated widefield screening microscope Scan^R	Olympus
Automated widefield screening microscope Nikon Ti-E	Nikon
Confocal laser scanning microscope FV3000	Olympus

Table 18. List of microscopes.

Software

Software	Source
Adobe Acrobat	Adobe Systems Incorporated, San Jose, USA
Adobe Illustrator 2023	Adobe Systems Incorporated, San Jose, USA
Adobe Photoshop 2023	Adobe Systems Incorporated, San Jose, USA
CellProfiler	Broad Institute, Cambridge, USA
Cytoscape	Institute of Systems Biology, Seattle, USA
Fiji	Johannes Schindelin, Max Planck Institute of Molecular Cell Biology and Genetics, Dresden, Germany and others
GraphPad Prism 9	Dotmatics, Boston, Massachusetts
Mendeley Desktop	Elsevier, Amsterdam, Netherlands
Microsoft Office 2022	Microsoft Corporation, Redmond, USA
SnapGene	Dotmatics, Boston, Massachusetts

Table 19. List of software

Webtools

Usage	Source
Creating schemes	BioRender: https://www.biorender.com
Gene Ontology (GO) analysis	UniProt database: https://www.uniprot.org
Prediction of NLS, NES motifs	ELM database: http://elm.eu.org
Protein-protein interaction networks	STRING database: https://string-db.org/

Table 20. List of webtools.

Cell biology

Tissue culture

HeLa Kyoto, U2-OS and NHLF cells were cultured in 10 cm^2 (Nunc) dishes in 1g/l DMEM growth medium supplemented with 10% FCS and 1% L-Glutamine at 37ºC and 5% CO_2 in a humidified incubator. Cells were regularly passaged 3 times a week (or when required) until they reached passage 18 and then discarded. For passaging, the growth medium was removed from the cell culture dish, cells were washed with 1 ml 0.5% Trypsin-EDTA solution, then incubated with 1 ml 0.5% Trypsin-EDTA solution for 5 minutes at 37ºC till they get detached from the dish. To stop the enzymatic reaction, cells were suspended with 9 ml of fresh growth medium DMEM and

dispensed into new 10 cm dishes. All cell culture was done in the laminar flow hood that was sterilised before use.

Plating cells

Cells were plated at a specific confluence depending on the format of the cell culture dish and the length of the experiment. To achieve this, after trypsinisation (described above) cells in suspension were counted using a hemocytometer and plated at the confluence listed below (**Table 21.**)

Seeding cell number/well	**Plate format**	
	24-Well plate	96-Well plate
Next day use	30000 cells/well	6000 cells/well
72-hour experiment	7500 cells/well	1500 cells/well

Table 21. Cell numbers for plating in alternative plate formats.

Cell freezing

In order to keep the stocks for future use a cell freezing procedure was performed. Cells were cultured in 10 cm^2 up to 80% confluency, washed with 1 ml 0.5% Trypsin-EDTA solution and incubated with 1 ml 0.5% Trypsin-EDTA solution at 37ºC for 5 min. Trypsin activity was neutralised by resuspending cells with 9 ml DMEM medium. The Cell suspension was centrifuged (5804R Eppendorf) at 1000 rpm for 5 min. The supernatant was aspirated and the cell pellet was resuspended in 5 ml cell freezing medium and aliquoted into 1 ml cryotubes. Cryotubes were placed into a cell-freezing container at -80ºC for 24 hours and then transferred to liquid nitrogen tanks (-160ºC) for long-term storage.

Drug treatments

Cells were treated 24 hours after seeding (for cell numbers see **Table 21**). For Hydrogen Peroxide (H_2O_2) experiments cells were treated for 20 minutes at a concentration of 5 mM, and then the cell growth medium with the drug was removed and replaced with fresh cell growth medium for 30 minutes of recovery. For doxorubicin and $KBrO_3$ experiments cells were treated for 3 hours at the concentration

of 40 µM and 5 mM, respectively. For treatments with camptothecin cells were treated for 16 hours at a concentration of 0.1 µM. For importin-ß inhibitor experiments, cells were pre-treated with importin-ß inhibitor importazole at a concentration of 20 µM for 30 minutes before treatment with doxorubicin. To induce disruption of the Golgi ribbon cells were treated with microtubule depolymerization agent, Nocodazole for 3 hours at a concentration of 33 µM.

siRNA transfections

The day prior to transfection, HeLa Kyoto cells were plated into cell culture plates at the numbers listed in **Table 21**., such that they have a confluency of 40-50% the following day. Reaction volumes for alternative plate formats are listed below (**Table 22.**). For experiments performed in 96 well-plates, 0.04 µL of a 30 µM siRNA stock was added to 9 µL OptiMEM; at the same time in a separated tube, 0.1 µL of Oligofectamine (Life Technologies) was added to 0.9 µL of OptiMEM. Both solutions were mixed by pipetting, incubated for 7 minutes at room temperature and then combined. The final transfection mix was incubated for 20 min at room temperature. The growth medium was removed from the cells and exchanged with 40 µL of Serum Free DMEM. After the incubation time, siRNA transfection mixtures were dropwise added to the cells and incubated for 4 hours at 37ºC and 5% CO_2. After incubation time, Serum Free DMEM was complemented with 50 µL DMEM containing 20% FCS and 1% L-Glutamine. Cells were incubated for 72 hours at 37ºC and 5% CO_2.

24-well plate	0.16 µL siRNA + 45 µL OptiMEM 0.5 µL Oligofectamine + 4.5 µL OptiMEM	200 µL Serum Free DMEM 250 µL 2x FCS DMEM
96-well plate	0.04 µL siRNA + 9 µL OptiMEM 0.1 µL Oligofectamine + 0.9 µL OptiMEM	40 µL Serum Free DMEM 50 µL 2x FCS DMEM

Table 22. Reaction volumes for alternative plate formats.

Immunofluorescence assay

To visualise proteins of interest immunofluorescent staining was performed. For this, cells were seeded in 96-well plates with glass bottom (Zell-Kontakt) and treated with selected agents. Then, the growth medium was aspirated and cells were fixed with 4% PFA fixation buffer for 20 minutes. Fixation was performed at room temperature in the

fume hood. PFA fixed cells were subsequently washed three times (5 minutes each) with sPBS buffer at room temperature. After this, cells were either stored at 4 ºC or it was directly proceeded with the immunostaining procedure. For this, cells were permeabilized with 0.1 % Triton X-100 for 15 minutes at room temperature. Then cells were incubated with the primary antibodies (for dilutions see **Table 9**.) in sPBS buffer at 4 ºC overnight. The next day, the primary antibodies solution was removed and followed by three washes with sPBS, 5 minutes each; then incubated with fluorescent dye-conjugated secondary antibodies in sPBS buffer for 1 hour at room temperature. Afterwards, cells were washed three times with sPBS for 5 minutes each, the cell nuclei were stained with Hoechst or Doxorubicin solution (dilution 1:2000) for 15 minutes at room temperature, followed by three washes with sPBS. Ready samples were immediately used for imaging or stored at 4 ºC.

VSV-G assay

To test whether depletion DNA damage response proteins that localise to the Golgi impact transport from ER to the Golgi complex the VSVG assay was performed (Wehland et al., 1982). This method is based on the properties and trafficking of ts045 vesicular stomatitis virus G protein is fused at the cytoplasmic tail with YFP (VSVG-ts045-YFP) as a reporter. This protein is misfolded and retained at the Endoplasmic Reticulum (ER) at the temperature of 40 ºC, but at the temperature of 32 ºC, it correctly folds and moves from the ER to the Golgi complex before being transported to the plasma membrane. First, HeLa Kyoto cells were seeded in 96-well plates for a 72-hour experiment (for cell numbers see **Table 21**.) followed by the 72-hour siRNA transfection (**Table 22**). After 48 hours cells were infected with adenovirus expressing VSVG-ts045-YFP for 1 hour at 37 ºC (dilution of the virus 1:200) in 50 µL DMEM supplemented with 10% FCS. Then cells were washed once with DMEM 10% FCS medium and transferred to 39.5 ºC for 16 hours with 100 µL of DMEM. The release of VSVG was performed by moving the cells to 32 ºC, adding DMEM containing 25 µg/mL cycloheximide and 25 mM HEPES for 60 minutes. After incubation, the medium was removed and cells were washed once with PBS followed by fixation with 4% PFA for 15 minutes. Cells were then washed three times with PBS and incubated with the anti-VSVG antibody for 60 minutes at room temperature. Next, cells were washed three times with PBS and incubated with anti-mouse-A647 and nuclear stain Hoechst

(dilution 1:2000). Finally, samples were washed three times with PBS and imaged with a wide-field automatic microscope Scan^R (Olympus) and quantified as previously described (Simpson *et al.*, 2012).

Microscopy

Wide-field microscopy

Imaging of high-throughput experiments was done using an automated wide-field screening microscope Scan^R (Olympus). For VSV-G assay experiments, 16 fields of view per well were acquired sequentially with 20x UPlanApo NA 0.7 Air Ph2 objective (Olympus). Dapi, eGFP and mCherry channels were acquired per field of view.

Confocal microscopy

For visualisation of fixed and immunostained samples confocal microscope, FV3000 (Olympus) was used. Images were acquired in Z-stacks that would cover the entire cell thickness. The stack thickness was kept constant between the samples and the number of stacks was adjusted depending on the sample. Objectives and filters used in the experiments are listed in the table below.

Microscope	Source	Objective	Detection lasers
FV3000	Olympus	UPLSAPO 20X / NA 0.75 / air WD 0.6mm UPLSAPO40X / NA 0.95 / air WD 0.18mm UPLSAPO 60X S / NA 1,3 / Silicon WD 0.3mm	405 nm, 488 nm, 561 nm, 640 nm.

Table 23. Used confocal microscope objectives and imaging settings.

Biochemistry

Cell lysis

HeLa Kyoto cells were seeded in 24-well dishes followed by siRNA transfection or drug treatment assays. After treatment was finished, cells were placed on ice to prevent protein degradation. The cell growth medium was aspirated and cells were washed once by adding 0.5 mL ice-cold PBS. Cells were lysed by adding 50 µL of ice-cold RIPA buffer (Thermofisher Scientific) supplemented with a final concentration of 1X PIC solution and 40 mM DTT. Samples were incubated on ice for 5 minutes, swirling the plate occasionally for uniform spreading of the lysis buffer. Then, the cell lysis was completed using a cell scrapper and the sample was transferred to a microcentrifuge tube. Samples were centrifuged at 14000 rpm for 15 minutes to collect cell debris. The supernatant containing proteins was transferred to a new tube and mixed with 5X Sample buffer and incubated for 5 minutes at 95 ºC (Thermomixer, Eppendorf) to ensure complete protein denaturation. Next, it was ensured that the sample does not have remaining DNA and RNA molecules left, which could interfere with the following western blot analysis. For this, 0.5 µL endonuclease Benzonase was added to the sample, together with 0.5 µL of 0.5 M $MgCl_2$, where magnesium ions served to ensure Benzonase enzymatic activity. The reaction mix was incubated for 10 min at room temperature. After incubation sample was directly used for western blot analysis, described below or stored at -80ºC for further use.

Subcellular fractionation

To validate the localisation of proteins that were observed by immunofluorescence, subcellular protein fractionation of cultured cells was performed using a subcellular fractionation kit (Thermofisher Scientific) following the manufacturer's instructions. For this, HeLa Kyoto cells were grown in a 10 cm^2 plate to the confluence of 80 % and then treated with selected concentrations of DNA-damaging agents. After treatment was finished, cells were trypsinised as previously described and harvested by centrifugation at 1000 rpm for 5 minutes. All of the centrifugations from this step were performed at a microcentrifuge pre-cooled to 4 ºC. After the centrifugation, the medium was aspirated and the resulting cell pellet was washed by suspending it with ice-cold

PBS, transferring it to a 1.5 mL microcentrifuge tube and centrifuging at 1000 rpm for 5 minutes, the supernatant was carefully removed and discarded. Then the cell pellet was suspended in 500 µL ice-cold CEB buffer (Thermofisher Scientific) containing protease inhibitors and incubated for 10 minutes at 4 ºC with gentle mixing, followed by centrifugation at 1000 rpm for 5 minutes. The supernatant (cytoplasmic extract) was immediately transferred to a clean pre-chilled tube on ice and 500 µL of MEB buffer (Thermofisher Scientific) containing protease inhibitors was added to the pellet by pipetting. The tube was then vortexed for 5 seconds on the highest setting and incubated at 4 ºC for 10 minutes with gentle mixing, followed by centrifugation at 3000 rpm for 5 minutes. The supernatant containing membrane extract was transferred to a clean pre-chilled microcentrifuge tube. Next, 250 µL of ice-cold NEB buffer (Thermofisher Scientific) containing protease inhibitors was added to the pellet, mixed by pipetting and vortexed for 15 seconds on the highest setting, then incubated for 30 minutes at 4 ºC with gentle mixing. After incubation, the sample was centrifuged at 5000 rpm for 5 minutes and the supernatant containing soluble nuclear fraction was transferred to a clean pre-chilled tube on ice. In the last fractionation step, 250 µL NEB buffer supplemented with 12.5 µL of 100 mM $CaCl_2$ and 7.5 µL Micrococcal Nuclease was added. The sample was mixed by pipetting and vortexed for 15 seconds at the highest speed, followed by 15 minutes of incubation at room temperature. After incubation, the sample was vortexed once again on the highest setting for 15 seconds and centrifuged at 14000 rpm (highest setting of microcentrifuge) for 5 minutes; the supernatant containing chromatin-found nuclear fraction was added to the soluble nuclear fraction. Samples were either directly used for western blot analysis or placed at -80 ºC for long-term storage and further usage.

Immunoprecipitation

To perform Immunoprecipitation (IP) of selected proteins HeLa Kyoto cells were seeded in a 10 cm^2 dish such that they have 90% confluency on the day of cell lysis. For cell lysis, plates with cells were kept on ice to prevent protein degradation, the cell growth medium was removed and cells were washed twice with 2 mL ice-cold PBS, followed by the addition of 400 µL of ice-cold lysis buffer containing protease inhibitors. Cells were incubated for 5 min, scraped off the dish and transferred to 1.5 mL Eppendorf tubes. The cell suspension was centrifuged at 6000 rpm for 6 min, at 4 ºC.

After centrifugation, the supernatant was transferred to new 1.5 mL tubes. For the following steps, 20 µL of the whole cell lysate was transferred to a separate tube and was used later on as one of the controls in the experiment. The rest of the cell extract was split into 2 tubes, one of those incubated overnight with 1 µL of the antibody against the protein of interest, the second with the whole lysate, which will be later used as a control for G-coupled agarose beads' specificity. Both tubes were incubated on a rotating wheel overnight at 4 ºC. The following day, 25 µL of G-coupled agarose beads were prepared for each IP sample by pipetting double the amount of the slurry and washing twice with ice-cold water and once with lysis buffer, each step followed by centrifugation at 100 rpm for 5 minutes. To precipitate the proteins, 25 µL of prepared beads were added to the supernatant with antibody, as well as to the control cell extract sample. Samples with beads were incubated for 4 hours at 4 ºC on a rotating wheel. After incubation, samples were centrifugated at 1000 rpm for 5 minutes at 4ºC to remove the supernatant. Agarose beads with bound proteins were washed 3 times with lysis buffer, each step followed by centrifugation at 1000 rpm for 5 minutes, at 4ºC. The sample was mixed with 25 µL of 2x Sample Buffer and incubated for 5 minutes at 95 ºC (Thermomixer, Eppendorf) to ensure complete protein denaturation. In the last sample preparation step, it was ensured that the sample does not have any DNA and RNA molecules left, that could interfere with the following western blot analysis. To achieve this, 0.5 µL endonuclease Benzonase was added to the sample, together with 0.5 µL of 0.5 M $MgCl_2$, where magnesium ions served to ensure Benzonase enzymatic activity. The reaction mix was incubated for 10 min at room temperature. Samples were then directly used for western blot analysis or stored at -80 ºC until further usage.

Western blot

Protein samples prepared as explained in the previous sections were used for Western blot analysis. For this, protein samples were incubated at 95 °C for 5 minutes (Thermomixer, Eppendorf) followed by SDS-PAGE analysis, performed on pre-cast 4%-12% Bis-Tris mini protein gel (Thermofisher Scientific), loading 20 µL of the sample per well. 12 µL of Precision Plus Protein Dual Color Standard marker (Bio-Rad) was additionally loaded to a well and used to determine the molecular weight of

separated proteins. SDS-PAGE gels were run using NuPAGE™ MOPS running buffer (Life Technologies) at 90 V for 1 hour and 30 minutes.

After proteins were separated by size to detect them using specific antibodies, they were then transferred from SDS-PAGE Gel on a PVDF membrane (pore size 0.45 µM (Merck, Millipore). For this, the PVDF membrane was cut to the size of the pre-cast protein gel followed by activation via incubation in methanol for 5 minutes and washing in Transfer buffer (see materials). Sandwiches for transfer were stacked as follows – sponge, two chromatographic papers (Whatman) soaked in cold transfer buffer; SDS-PAGE gel with separated protein samples; PVDF activated membrane; two chromatographic papers (Whatman) soaked in cold transfer buffer; sponge. The sandwich was placed into a western blot cassette and placed in a Mini-Protean II cell gel system (Bio-Rad) filled up to the top with Transfer buffer (membrane in the direction of the detection anode), additionally placing ice pack and a magnetic stirrer for mixing the buffer during the transfer. This way it was ensured that negatively charged proteins would be transferred from the SDS-PAGE gel to the PVDF membrane. The transfer chamber was placed on a magnetic stirring plate (Heidolph) and the transfer was performed at 100 V for 1,5 hours at 4 ºC. After the run, the membrane was washed once in PBS-T buffer and incubated in blocking buffer for 1 hour at room temperature. This step was performed to prevent nonspecific antibody binding by blocking free binding sides on the membrane. The blocking step was followed by staining with primary antibodies diluted in blocking buffer (see dilutions **Table 11.**) at 4 ºC overnight. The following day membrane was washed three times with PBS-T buffer for 10 minutes to remove the unbound antibody. The membrane was incubated with a secondary HRP-coupled antibody solution in a blocking buffer for 1 hour at room temperature. After incubation, the membrane was washed three times for 10 minutes with PBS-T washing buffer and three times for 10 minutes with PBS buffer. For protein visualisation, the membrane was incubated for 1 min with chemiluminescence substrate (Pierce™ ECL Plus Western Blotting Substrate, Thermofisher Scientific) following the manufacturer's instructions and immediately visualised on Azure 280 (Biozym) chemiluminescence imaging system. Images with protein bands were analysed and quantified using ImageJ software. The intensity of bands of protein of interest was measured and normalised to the intensity of control protein α-tubulin bands on the same gel. In cell fractionation experiments, the intensity of protein bands

from each fraction was normalised to the control protein band for each fraction – nuclear fraction – Lamin B1, membrane-Golgi fraction – GM130, cytoplasmic fraction - α-tubulin.

Mass spectrometry

Subcellular fractionation samples for MS analysis were prepared as described in the subcellular fractionation section. MS-IP samples were prepared as described in the IP section, skipping the last step of Benzonase digestion. Samples were processed in the MS facility, EMBL Heidelberg by Per Haberkant. The initial analysis of MS experiments was performed by Frank Stein.

Comet assay

To measure DNA fragmentation in individual cells a gel electrophoresis method called the comet assay was carried out. This method was performed as previously described (Vodenkova et al. 2020). All buffers used in the comet assay are listed in **Table 24**. For this, cells were seeded in 24-well plates and collected by trypsinisation, after siRNA transfection and/or drug treatment assay was finished. Cells were centrifuged at 5000 rpm for 4 minutes at 4 ºC. The resulting cell pellet was washed twice with PBS followed by centrifugation at 5000 rpm at 4 ºC. The supernatant was removed and the cell pellet was suspended in PBS (20-25 x 10^4 cells/ml). The cell suspension was mixed with 2 % low melting point agarose (pre-warmed to 42 ºC) at the ratio 1:1; 40 µL of the mix was pipetted on pre-cut 75 x 25 mm Gel Bond Film (Lonza) coated by merging them into 1 % normal melting point agarose and drying at 42 ºC for 2 hours. Immediately after pipetting the cell sample on the Gel Bond Film, a 24 x 32 mm glass coverslip was placed on top, distributing the agarose drop to form a thin layer of agarose gel between the two surfaces. Prepared slides were incubated for 15 minutes at room temperature, then placed at 4 ºC for another 20 minutes. After incubation, the coverslip was removed and slides were immersed into a Lysis buffer (**Table 24.**) and incubated overnight at 4 ºC for cell lysis to be complete.

The following day, the Lysis Buffer was removed and slides were washed by submerging them in ice-cold water for 30 minutes, then placed in an electrophoresis

chamber filled with Alkaline Electrophoresis Buffer, incubated for 20 minutes followed by electrophoresis at 0.5 V/cm for 1 hour. After the run was complete, slides were neutralised with a Neutralisation buffer for 20 minutes and washed with ice-cold water for 1-2 minutes. Next, slides were stained with Sybr Gold dye solution (dilution 1:20000) in ddH_2O for 20 minutes at room temperature, followed by three washed for 60 minutes with generous amounts of water. Finally, the slides were dried on a heating block at 42 ºC until completely dry. The slides with comets were imaged with an automated Olympus Scan^R screening microscope. Comets were analysed using OpenComet Plugin on ImageJ (Gyori et al., 2014).

Buffer	Composition	Source
Lysis Buffer (pH 10)	100 mM Na_2EDTA, 2.5 M NaCl, 10 mM Tris-HCl, 1% Triton-X 100 (v/v)	Self-generated
Alkaline Electrophoresis Buffer (pH 13)	300 mM NaOH, 1mM Na_2EDTA	Self-generated
Neutralisation Buffer	0.4 M Tris-HCl	Self-generated

Table 24. Buffers used in the comet assay.

Image analysis using Image J and cell profiler

Image analysis was performed using Fiji and Cell Profiler software and designed pipelines for specific experiments, developed by George Galea (Pepperkok group, EMBL Heidelberg). The used pipeline example and the detailed parameters are listed in the **Appendix**. Briefly, as a first step z-projections of acquired confocal images of individual channels were saved as separate images. The images were then loaded into the Cell Profiler pipeline (*Images*). In the first module of the pipeline, meaningful names for each channel were assigned (*NamesAndTypes*). Next, cells were segmented based on the size and shape of the nucleus, and detected using a threshold for the nuclear fluorescence intensity (Hoechst or DOX) (*IdentifyPrimaryObjects*). Next, the outlines of the whole cell and cell area were defined based on the position of the Golgi (Golgi marker channel) and the nucleus (nuclear stain channel), through digital dilation of the nucleus by the given diameter (*IdentifySecondaryObjects*). Then, within the defined cell area, the nuclei (nuclear stain), the Golgi (Golgi marker) and antibody staining against the protein of interest were masked (*MaskImage*) and then identified based on size and shape, detected using a threshold (*IdentifyPrimaryObjects*). Since the proteins of interest are dual-

localised and in some images the cell nucleus and the Golgi overlap, to get more accurate measurements, the nucleus and the Golgi were segmented separately, removing cells with organelles overlapping. For this, the masked Golgi was removed from the masked image of an antibody of interest, creating a masked image with just the nuclei without the Golgi. Then, the nuclei were removed from the masked image of the antibody of interest, creating a mask with just Golgi, without the nuclei (*MaskImage*). The intensity measurements were then taken for just Golgi intensity in the masked image for Golgi without nuclei and vice versa (*MeasureObjectIntensity*). The intensity measurements were exported from the pipeline as a .csv spreadsheet, followed by further analysis, calculating intensity changes in control and treated cells. Additionally, the images of segmented objects were exported as .tiff files (*SaveImages*), visualising segmented objects with an overlay of nuclear and Golgi markers, as well as the protein of interest (*OverlayOutlines*) as well as a number for identification for each cell (*DisplayDataOnImage*).

Statistical analysis

All experiments were repeated at least three times if not otherwise stated. All statistical analysis was performed using GraphPad Prism 9 software. For data fitting normal distribution, pairwise comparison was performed using a two-tailed t-test and for multiple comparisons, one-way ANOVA analysis was applied. Statistical significance in data not fitting normal distribution was analysed using the Mann-Whitney test where $P < 0.05$ was considered statistically significant.

References

Abdel Rahman, A. M., Ryczko, M., Nakano, M., Pawling, J., Rodrigues, T., Johswich, A., Taniguchi, N., Dennis, J. W. (2015). Golgi N-glycan branching N-acetylglucosaminyltransferases I, V and VI promote nutrient uptake and metabolism. *Glycobiology*, *25*(2), 225–240. https://doi.org/10.1093/glycob/cwu105

Adamson, B., Smogorzewska, A., Sigoillot, F. D., King, R. W., Elledge, S. J. (2012). A genome-wide homologous recombination screen identifies the RNA-binding protein RBMX as a component of the DNA-damage response. *Nature cell biology*, *14*(3), 318–328. https://doi.org/10.1038/ncb2426

Airik, R., Schueler, M., Airik, M., Cho, J., Ulanowicz, K. A., Porath, J. D., Hurd, T. W., Bekker-Jensen, S., Schrøder, J. M., Andersen, J. S., Hildebrandt, F. (2016). SDCCAG8 Interacts with RAB Effector Proteins RABEP2 and ERC1 and Is Required for Hedgehog Signaling. *PloS one*, *11*(5), e0156081. https://doi.org/10.1371/journal.pone.0156081

Balakrishnan, L., Brandt, P. D., Lindsey-Boltz, L. A., Sancar, A., Bambara, R. A. (2009). Long patch base excision repair proceeds via coordinated stimulation of the multienzyme DNA repair complex. *The Journal of biological chemistry*, *284*(22), 15158–15172. https://doi.org/10.1074/jbc.M109.000505

Banani, S. F., Lee, H. O., Hyman, A. A., Rosen, M. K. (2017). Biomolecular condensates: organizers of cellular biochemistry. *Nature reviews. Molecular cell biology*, *18*(5), 285–298. https://doi.org/10.1038/nrm.2017.7

Barr, F. A., Short, B. (2003). Golgins in the structure and dynamics of the Golgi apparatus. *Current opinion in cell biology*, *15*(4), 405–413. https://doi.org/10.1016/s0955-0674(03)00054-1

Barr, F. A. and Warren, G. (1996) 'Disassembly and reassembly of the Golgi apparatus', in *Seminars in Cell & Developmental Biology*. Elsevier, pp. 505–510.

Bartz, F., Kern, L., Erz, D., Zhu, M., Gilbert, D., Meinhof, T., Wirkner, U., Erfle, H., Muckenthaler, M., Pepperkok, R., Runz, H. (2009). Identification of cholesterol-regulating genes by targeted RNAi screening. *Cell metabolism*, *10*(1), 63–75. https://doi.org/10.1016/j.cmet.2009.05.009

Beznoussenko, G. V., Parashuraman, S., Rizzo, R., Polishchuk, R., Martella, O., Di Giandomenico, D., Fusella, A., Spaar, A., Sallese, M., Capestrano, M. G., Pavelka, M., Vos, M. R., Rikers, Y. G., Helms, V., Mironov, A. A., Luini, A. (2014). Transport of soluble proteins through the Golgi occurs by diffusion via continuities across cisternae. *eLife*, *3*, e02009. https://doi.org/10.7554/eLife.02009

Bien, C. M., Espenshade, P. J. (2010). Sterol regulatory element binding proteins in fungi: hypoxic transcription factors linked to pathogenesis. *Eukaryotic cell*, *9*(3), 352–359. https://doi.org/10.1128/EC.00358-09

Bock, J. B., Matern, H. T., Peden, A. A., Scheller, R. H. (2001). A genomic perspective on membrane compartment organization. *Nature*, *409*(6822), 839–841. https://doi.org/10.1038/35057024

Bohr V. A. (2002). Repair of oxidative DNA damage in nuclear and mitochondrial DNA, and some changes with aging in mammalian cells. *Free radical biology & medicine*, *32*(9), 804–812. https://doi.org/10.1016/s0891-5849(02)00787-6

Boncompain, G., Perez, F. (2013). The many routes of Golgi-dependent trafficking. *Histochemistry and cell biology*, *140*(3), 251–260. https://doi.org/10.1007/s00418-013-1124-7

Borghini, A., Roursgaard, M., Andreassi, M. G., Kermanizadeh, A., Møller, P. (2017). Repair activity of oxidatively damaged DNA and telomere length in human lung epithelial cells after exposure to multi-walled carbon nanotubes. *Mutagenesis*, *32*(1), 173–180. https://doi.org/10.1093/mutage/gew036

Borszéková Pulzová, L., Ward, T. A., Chovanec, M. (2020). XPA: DNA Repair Protein of Significant Clinical Importance. *International journal of molecular sciences*, *21*(6), 2182. https://doi.org/10.3390/ijms21062182

Brown, M. S., Goldstein, J. L. (1997). The SREBP pathway: regulation of cholesterol metabolism by proteolysis of a membrane-bound transcription factor. *Cell*, *89*(3), 331–340. https://doi.org/10.1016/s0092-8674(00)80213-5

Brown, M. S., Goldstein, J. L. (1997). The SREBP pathway: regulation of cholesterol metabolism by proteolysis of a membrane-bound transcription factor. *Cell*, *89*(3), 331–340. https://doi.org/10.1016/s0092-8674(00)80213-5

Burgess, J. T., Rose, M., Boucher, D., Plowman, J., Molloy, C., Fisher, M., O'Leary, C., Richard, D. J., O'Byrne, K. J., Bolderson, E. (2020). The Therapeutic Potential of DNA Damage Repair Pathways and Genomic Stability in Lung Cancer. *Frontiers in oncology*, *10*, 1256. https://doi.org/10.3389/fonc.2020.01256

Buschman, M. D., Rahajeng, J., Field, S. J. (2015). GOLPH3 links the Golgi, DNA damage, and cancer. *Cancer research*, *75*(4), 624–627. https://doi.org/10.1158/0008-5472.CAN-14-3081

Carusillo, A., Mussolino, C. (2020). DNA Damage: From Threat to Treatment. *Cells*, *9*(7), 1665. https://doi.org/10.3390/cells9071665

Cautain, B., Hill, R., de Pedro, N., Link, W. (2015). Components and regulation of nuclear transport processes. *The FEBS journal*, *282*(3), 445–462. https://doi.org/10.1111/febs.13163

Ceccaldi, R., Liu, J. C., Amunugama, R., Hajdu, I., Primack, B., Petalcorin, M. I., O'Connor, K. W., Konstantinopoulos, P. A., Elledge, S. J., Boulton, S. J., Yusufzai, T., D'Andrea, A. D. (2015). Homologous-recombination-deficient tumours are dependent on Polθ-mediated repair. *Nature*, *518*(7538), 258–262. https://doi.org/10.1038/nature14184

Chang, H. H. Y., Pannunzio, N. R., Adachi, N., Lieber, M. R. (2017). Non-homologous DNA end joining and alternative pathways to double-strand break repair. *Nature reviews. Molecular cell biology*, *18*(8), 495–506. https://doi.org/10.1038/nrm.2017.48

Chang, H. H., Lieber, M. R. (2016). Structure-Specific nuclease activities of Artemis and the Artemis: DNA-PKcs complex. *Nucleic acids research*, *44*(11), 4991–4997. https://doi.org/10.1093/nar/gkw456

Chapman, J. R., Taylor, M. R., Boulton, S. J. (2012). Playing the end game: DNA double-strand break repair pathway choice. *Molecular cell*, *47*(4), 497–510. https://doi.org/10.1016/j.molcel.2012.07.029

Chatterjee, N., Walker, G. C. (2017). Mechanisms of DNA damage, repair, and mutagenesis. *Environmental and molecular mutagenesis*, *58*(5), 235–263. https://doi.org/10.1002/em.22087

Chen, X., Ballin, J. D., Della-Maria, J., Tsai, M. S., White, E. J., Tomkinson, A. E., Wilson, G. M. (2009). Distinct kinetics of human DNA ligases I, IIIalpha, IIIbeta, and IV reveal direct DNA sensing ability and differential physiological functions in DNA repair. *DNA repair*, *8*(8), 961–968. https://doi.org/10.1016/j.dnarep.2009.06.002

Cheung, P. Y., Limouse, C., Mabuchi, H., Pfeffer, S. R. (2015). Protein flexibility is required for vesicle tethering at the Golgi. *eLife*, *4*, e12790. https://doi.org/10.7554/eLife.12790

Christie, M., Chang, C. W., Róna, G., Smith, K. M., Stewart, A. G., Takeda, A. A., Fontes, M. R., Stewart, M., Vértessy, B. G., Forwood, J. K., Kobe, B. (2016). Structural Biology and Regulation of Protein Import into the Nucleus. *Journal of molecular biology*, *428*(10 Pt A), 2060–2090. https://doi.org/10.1016/j.jmb.2015.10.023

Ciccia, A., Elledge, S. J. (2010). The DNA damage response: making it safe to play with knives. *Molecular cell*, *40*(2), 179–204. https://doi.org/10.1016/j.molcel.2010.09.019

Collis, S. J., Boulton, S. J. (2007). Emerging links between the biological clock and the DNA damage response. *Chromosoma*, *116*(4), 331–339. https://doi.org/10.1007/s00412-007-0108-6

Czajkowski, D., Szmyd, R., Gee, H. E. (2022). Impact of DNA damage response defects in cancer cells on response to immunotherapy and radiotherapy. *Journal of medical imaging and radiation oncology*, *66*(4), 546–559. https://doi.org/10.1111/1754-9485.13413

David, S. S., O'Shea, V. L., Kundu, S. (2007). Base-excision repair of oxidative DNA damage. *Nature*, *447*(7147), 941–950. https://doi.org/10.1038/nature05978

Dejgaard, S. Y., Murshid, A., Dee, K. M., Presley, J. F. (2007). Confocal microscopy-based linescan methodologies for intra-Golgi localization of proteins. *The journal of histochemistry and cytochemistry: official journal of the Histochemistry Society*, *55*(7), 709–719. https://doi.org/10.1369/jhc.6A7090.2007

Deriano, L., Roth, D. B. (2013). Modernizing the nonhomologous end-joining repertoire: alternative and classical NHEJ share the stage. *Annual review of genetics*, *47*, 433–455. https://doi.org/10.1146/annurev-genet-110711-155540

Dirksen, M. L., Blakely, W. F., Holwitt, E., Dizdaroglu, M. (1988). Effect of DNA conformation on the hydroxyl radical-induced formation of 8,5'-cyclopurine 2'-deoxyribonucleoside residues in DNA. *International journal of radiation biology*, *54*(2), 195–204. https://doi.org/10.1080/09553008814551631

Egea, G., Serra-Peinado, C., Gavilán, M. P. and Rios, R. M. (2015) 'Cytoskeleton and Golgi-apparatus interactions: a two-way road of function and structure', in.

Fadda, A., Butt, F., Tomei, S., Deola, S., Lo, B., Robay, A., Al-Shakaki, A., Al-Hajri, N., Crystal, R., Kambouris, M., Wang, E., Marincola, F. M., Fakhro, K. A., Cugno, C. (2016). Two hits in one: whole genome sequencing unveils LIG4 syndrome and urofacial syndrome in a case report of a child with complex phenotype. *BMC medical genetics*, *17*(1), 84. https://doi.org/10.1186/s12881-016-0346-7

Farber-Katz, S. E., Dippold, H. C., Buschman, M. D., Peterman, M. C., Xing, M., Noakes, C. J., Tat, J., Ng, M. M., Rahajeng, J., Cowan, D. M., Fuchs, G. J., Zhou, H., Field, S. J. (2014). DNA damage triggers Golgi dispersal via DNA-PK and GOLPH3. *Cell*, *156*(3), 413–427. https://doi.org/10.1016/j.cell.2013.12.023

Fousteri, M., Mullenders, L. H. (2008). Transcription-coupled nucleotide excision repair in mammalian cells: molecular mechanisms and biological effects. *Cell research*, *18*(1), 73–84. https://doi.org/10.1038/cr.2008.6

Frit, P., Barboule, N., Yuan, Y., Gomez, D., Calsou, P. (2014). Alternative end-joining pathway(s): bricolage at DNA breaks. *DNA repair*, *17*, 81–97. https://doi.org/10.1016/j.dnarep.2014.02.007

Galea, G., Kuodyte, K., Khan, M.M., Thul, P., Neumann, B., Lundberg, E. Pepperkok, R. (2022) 'The Golgi complex is a regulatory hub for homologous recombination-mediated DNA repair', *bioRxiv*, p. 2022.10.17.512236. https://doi.org/10.1101/2022.10.17.512236

Gillingham A. K. (2018). At the ends of their tethers! How coiled-coil proteins capture vesicles at the Golgi. *Biochemical Society transactions*, *46*(1), 43–50. https://doi.org/10.1042/BST20170188

Gillingham, A. K., Munro, S. (2016). Finding the Golgi: Golgin Coiled-Coil Proteins Show the Way. *Trends in cell biology*, *26*(6), 399–408. https://doi.org/10.1016/j.tcb.2016.02.005

Glick B. S. (2002). Can the Golgi form de novo? *Nature reviews. Molecular cell biology*, *3*(8), 615–619. https://doi.org/10.1038/nrm877

Goud, B., Gleeson, P. A. (2010). TGN golgins, Rabs and cytoskeleton: regulating the Golgi trafficking highways. *Trends in cell biology*, *20*(6), 329–336. https://doi.org/10.1016/j.tcb.2010.02.006

Griffiths, G., Simons, K. (1986). The trans Golgi network: sorting at the exit site of the Golgi complex. *Science (New York, N.Y.)*, *234*(4775), 438–443. https://doi.org/10.1126/science.2945253

Grollman, A. P., Moriya, M. (1993). Mutagenesis by 8-oxoguanine: an enemy within. *Trends in genetics: TIG*, *9*(7), 246–249. https://doi.org/10.1016/0168-9525(93)90089-z

Harel, A., Forbes, D. J. (2004). Importin beta: conducting a much larger cellular symphony. *Molecular cell*, *16*(3), 319–330. https://doi.org/10.1016/j.molcel.2004.10.026

Harper, J. W., Elledge, S. J. (2007). The DNA damage response: ten years after. *Molecular cell*, *28*(5), 739–745. https://doi.org/10.1016/j.molcel.2007.11.015

Hartlerode, A. J., Scully, R. (2009). Mechanisms of double-strand break repair in somatic mammalian cells. *The Biochemical journal*, *423*(2), 157–168. https://doi.org/10.1042/BJ20090942

Hegde, M. L., Hazra, T. K., Mitra, S. (2008). Early steps in the DNA base excision/single-strand interruption repair pathway in mammalian cells. *Cell research*, *18*(1), 27–47. https://doi.org/10.1038/cr.2008.8

Hirschberg, K., Miller, C. M., Ellenberg, J., Presley, J. F., Siggia, E. D., Phair, R. D., Lippincott-Schwartz, J. (1998). Kinetic analysis of secretory protein traffic and characterization of golgi to plasma membrane transport intermediates in living

cells. *The Journal of cell biology*, *143*(6), 1485–1503. https://doi.org/10.1083/jcb.143.6.1485

Hoeijmakers J. H. (2009). DNA damage, aging, and cancer. *The New England journal of medicine*, *361*(15), 1475–1485. https://doi.org/10.1056/NEJMra0804615

Hoeijmakers J. H. (2001). Genome maintenance mechanisms for preventing cancer. *Nature*, *411*(6835), 366–374. https://doi.org/10.1038/35077232

Hoelz, A., Debler, E. W., Blobel, G. (2011). The structure of the nuclear pore complex. *Annual review of biochemistry*, *80*, 613–643. https://doi.org/10.1146/annurev-biochem-060109-151030

Hsu, R. M., Zhong, C. Y., Wang, C. L., Liao, W. C., Yang, C., Lin, S. Y., Lin, J. W., Cheng, H. Y., Li, P. Y., Yu, C. J. (2018). Golgi tethering factor golgin-97 suppresses breast cancer cell invasiveness by modulating NF-κB activity. *Cell communication and signaling : CCS*, *16*(1), 19. https://doi.org/10.1186/s12964-018-0230-5

Hu, L. Y., Chang, C. C., Huang, Y. S., Chou, W. C., Lin, Y. M., Ho, C. C., Chen, W. T., Shih, H. M., Hsiung, C. N., Wu, P. E., Shen, C. Y. (2018). SUMOylation of XRCC1 activated by poly (ADP-ribosyl)ation regulates DNA repair. *Human molecular genetics*, *27*(13), 2306–2317. https://doi.org/10.1093/hmg/ddy135

Hu, L.Y., Chang, C.C., Huang, Y.S., Chou, W.C., Lin, Y.M., Ho, C.C., Chen, W.T., Shih, H.M., Hsiung, C.N., Wu, P.E. and Shen, C.Y. (2018b) 'SUMOylation of XRCC1 activated by poly (ADP-ribosyl)ation regulates DNA repair', *Human Molecular Genetics*. doi: 10.1093/hmg/ddy135.

Hu, L. Y., Chang, C. C., Huang, Y. S., Chou, W. C., Lin, Y. M., Ho, C. C., Chen, W. T., Shih, H. M., Hsiung, C. N., Wu, P. E., Shen, C. Y. (2018). SUMOylation of XRCC1 activated by poly (ADP-ribosyl)ation regulates DNA repair. *Human molecular genetics*, *27*(13), 2306–2317. https://doi.org/10.1093/hmg/ddy135

Hutten, S., Kehlenbach, R. H. (2007). CRM1-mediated nuclear export: to the pore and beyond. *Trends in cell biology*, *17*(4), 193–201. https://doi.org/10.1016/j.tcb.2007.02.003

Iliakis, G., Wang, H., Perrault, A. R., Boecker, W., Rosidi, B., Windhofer, F., Wu, W., Guan, J., Terzoudi, G., Pantelias, G. (2004). Mechanisms of DNA double

strand break repair and chromosome aberration formation. *Cytogenetic and genome research*, *104*(1-4), 14–20. https://doi.org/10.1159/000077461

Iliakis, G., Murmann, T., Soni, A. (2015). Alternative end-joining repair pathways are the ultimate backup for abrogated classical non-homologous end-joining and homologous recombination repair: Implications for the formation of chromosome translocations. *Mutation research. Genetic toxicology and environmental mutagenesis*, *793*, 166–175. https://doi.org/10.1016/j.mrgentox.2015.07.001

Ishida, R., Yamamoto, A., Nakayama, K., Sohda, M., Misumi, Y., Yasunaga, T., Nakamura, N. (2015). GM130 is a parallel tetramer with a flexible rod-like structure and N-terminally open (Y-shaped) and closed (I-shaped) conformations. *The FEBS journal*, *282*(11), 2232–2244. https://doi.org/10.1111/febs.13271

Ismail, I. H., Gagné, J. P., Genois, M. M., Strickfaden, H., McDonald, D., Xu, Z., Poirier, G. G., Masson, J. Y., Hendzel, M. J. (2015). The RNF138 E3 ligase displaces Ku to promote DNA end resection and regulate DNA repair pathway choice. *Nature cell biology*, *17*(11), 1446–1457. https://doi.org/10.1038/ncb3259

Iyama, T., Wilson, D. M., 3rd (2013). DNA repair mechanisms in dividing and non-dividing cells. *DNA repair*, *12*(8), 620–636. https://doi.org/10.1016/j.dnarep.2013.04.015

Jackson C. L. (2009). Mechanisms of transport through the Golgi complex. *Journal of cell science*, *122*(Pt 4), 443–452. https://doi.org/10.1242/jcs.032581

Jackson, S. P., Bartek, J. (2009). The DNA-damage response in human biology and disease. *Nature*, *461*(7267), 1071–1078. https://doi.org/10.1038/nature08467

Jamieson J. D. (1998). The Golgi complex: perspectives and prospectives. *Biochimica et biophysica acta*, *1404*(1-2), 3–7. https://doi.org/10.1016/s0167-4889(98)00043-3

Jazayeri, A., Falck, J., Lukas, C., Bartek, J., Smith, G. C., Lukas, J., Jackson, S. P. (2006). ATM- and cell cycle-dependent regulation of ATR in response to DNA double-strand breaks. *Nature cell biology*, *8*(1), 37–45. https://doi.org/10.1038/ncb1337

Jevitt, A. M., Rankin, B. D., Chen, J., Rankin, S. (2023). The cohesin modifier ESCO2 is stable during DNA replication. *Chromosome research: an international journal on the molecular, supramolecular and evolutionary aspects of chromosome biology*, *31*(1), 6. https://doi.org/10.1007/s10577-023-09711-1

Jiricny J. (2006). The multifaceted mismatch-repair system. *Nature reviews. Molecular cell biology*, *7*(5), 335–346. https://doi.org/10.1038/nrm1907

Kawanishi, S., Murata, M. (2006). Mechanism of DNA damage induced by bromate differs from general types of oxidative stress. *Toxicology*, *221*(2-3), 172–178. https://doi.org/10.1016/j.tox.2006.01.002

Kent, T., Chandramouly, G., McDevitt, S. M., Ozdemir, A. Y., Pomerantz, R. T. (2015). Mechanism of microhomology-mediated end-joining promoted by human DNA polymerase θ. *Nature structural & molecular biology*, *22*(3), 230–237. https://doi.org/10.1038/nsmb.2961

Kim, J. H., Yang, C. K., Heo, K., Roeder, R. G., An, W., Stallcup, M. R. (2008). CCAR1, a key regulator of mediator complex recruitment to nuclear receptor transcription complexes. *Molecular cell*, *31*(4), 510–519. https://doi.org/10.1016/j.molcel.2008.08.001

Klumperman J. (2011). Architecture of the mammalian Golgi. *Cold Spring Harbor perspectives in biology*, *3*(7), a005181. https://doi.org/10.1101/cshperspect.a005181

Ko, P. J., Woodrow, C., Dubreuil, M. M., Martin, B. R., Skouta, R., Bassik, M. C., Dixon, S. J. (2019). A ZDHHC5-GOLGA7 Protein Acyltransferase Complex Promotes Nonapoptotic Cell Death. *Cell chemical biology*, *26*(12), 1716–1724.e9. https://doi.org/10.1016/j.chembiol.2019.09.014

Kooy, J., Toh, B. H., Pettitt, J. M., Erlich, R., Gleeson, P. A. (1992). Human autoantibodies as reagents to conserved Golgi components. Characterization of a peripheral, 230-kDa compartment-specific Golgi protein. *The Journal of biological chemistry*, *267*(28), 20255–20263.

Krishnan, M., Senagolage, M. D., Baeten, J. T., Wolfgeher, D. J., Khan, S., Kron, S. J., McNerney, M. E. (2022). Genomic studies controvert the existence of the

CUX1 p75 isoform. *Scientific reports*, *12*(1), 151. https://doi.org/10.1038/s41598-021-03930-4

Krokan, H. E., Bjørås, M. (2013). Base excision repair. *Cold Spring Harbor perspectives in biology*, *5*(4), a012583. https://doi.org/10.1101/cshperspect.a012583

Kulkarni, A., Wilson, D. M., 3rd (2008). The involvement of DNA-damage and -repair defects in neurological dysfunction. *American journal of human genetics*, *82*(3), 539–566. https://doi.org/10.1016/j.ajhg.2008.01.009

Kumar, M., Michael, S., Alvarado-Valverde, J., Mészáros, B., Sámano-Sánchez, H., Zeke, A., Dobson, L., Lazar, T., Örd, M., Nagpal, A., Farahi, N., Käser, M., Kraleti, R., Davey, N. E., Pancsa, R., Chemes, L. B., Gibson, T. J. (2022). The Eukaryotic Linear Motif resource: 2022 release. *Nucleic acids research*, *50*(D1), D497–D508. https://doi.org/10.1093/nar/gkab975

Kunkel, T. A., Erie, D. A. (2005). DNA mismatch repair. *Annual review of biochemistry*, *74*,681–710. https://doi.org/10.1146/annurev.biochem.74.082803.133243

Lamb, C. A., Yoshimori, T., Tooze, S. A. (2013). The autophagosome: origins unknown, biogenesis complex. *Nature reviews. Molecular cell biology*, *14*(12), 759–774. https://doi.org/10.1038/nrm3696

Lan, Y., Zhang, N., Liu, H., Xu, J., Jiang, R. (2016). Golgb1 regulates protein glycosylation and is crucial for mammalian palate development. *Development (Cambridge, England)*, *143*(13), 2344–2355. https://doi.org/10.1242/dev.134577

Lee, E. C. Y., Kok, J. S. T., Teh, B. T., Lim, K. S. (2022). Interplay between the DNA Damage Response and Immunotherapy Response in Cancer. *International journal of molecular sciences*, *23*(21), 13356. https://doi.org/10.3390/ijms232113356

Li G. M. (2008). Mechanisms and functions of DNA mismatch repair. *Cell research*, *18*(1), 85–98. https://doi.org/10.1038/cr.2007.115

Lieber M. R. (2010). The mechanism of double-strand DNA break repair by the nonhomologous DNA end-joining pathway. *Annual review of biochemistry*, *79*, 181–211. https://doi.org/10.1146/annurev.biochem.052308.093131

Lindahl T. (1993). Instability and decay of the primary structure of DNA. *Nature*, *362*(6422), 709–715. https://doi.org/10.1038/362709a0

Lowe M. (2011). Structural organization of the Golgi apparatus. *Current opinion in cell biology*, *23*(1), 85–93. https://doi.org/10.1016/j.ceb.2010.10.004

Lowe M. (2019). The Physiological Functions of the Golgin Vesicle Tethering Proteins. *Frontiers in cell and developmental biology*, *7*, 94. https://doi.org/10.3389/fcell.2019.00094

Lu, J., Wu, T., Zhang, B., Liu, S., Song, W., Qiao, J., Ruan, H. (2021). Types of nuclear localization signals and mechanisms of protein import into the nucleus. *Cell communication and signaling: CCS*, *19*(1), 60. https://doi.org/10.1186/s12964-021-00741-y

Ma, Y., Lu, H., Tippin, B., Goodman, M. F., Shimazaki, N., Koiwai, O., Hsieh, C. L., Schwarz, K., Lieber, M. R. (2004). A biochemically defined system for mammalian nonhomologous DNA end joining. *Molecular cell*, *16*(5), 701–713. https://doi.org/10.1016/j.molcel.2004.11.017

Maffucci, P., Chavez, J., Jurkiw, T. J., O'Brien, P. J., Abbott, J. K., Reynolds, P. R., Worth, A., Notarangelo, L. D., Felgentreff, K., Cortes, P., Boisson, B., Radigan, L., Cobat, A., Dinakar, C., Ehlayel, M., Ben-Omran, T., Gelfand, E. W., Casanova, J. L., Cunningham-Rundles, C. (2018). Biallelic mutations in DNA ligase 1 underlie a spectrum of immune deficiencies. *The Journal of clinical investigation*, *128*(12), 5489–5504. https://doi.org/10.1172/JCI99629

Makhoul, C., Gosavi, P., Gleeson, P. A. (2019). Golgi Dynamics: The Morphology of the Mammalian Golgi Apparatus in Health and Disease. *Frontiers in cell and developmental biology*, *7*, 112. https://doi.org/10.3389/fcell.2019.00112

Maréchal, A., Zou, L. (2013). DNA damage sensing by the ATM and ATR kinases. *Cold Spring Harbor perspectives in biology*, *5*(9), a012716. https://doi.org/10.1101/cshperspect.a012716

Matsuoka, S., Ballif, B. A., Smogorzewska, A., McDonald, E. R., 3rd, Hurov, K. E., Luo, J., Bakalarski, C. E., Zhao, Z., Solimini, N., Lerenthal, Y., Shiloh, Y., Gygi, S. P., Elledge, S. J. (2007). ATM and ATR substrate analysis reveals extensive protein networks responsive to DNA damage. *Science (New York, N.Y.)*, *316*(5828), 1160–1166. https://doi.org/10.1126/science.1140321

De Matteis, M. A., Luini, A. (2008). Exiting the Golgi complex. *Nature reviews. Molecular cell biology*, *9*(4), 273–284. https://doi.org/10.1038/nrm2378

Mellman, I., Simons, K. (1992). The Golgi complex: in vitro veritas?. *Cell*, *68*(5), 829–840. https://doi.org/10.1016/0092-8674(92)90027-a

Millarte, V., Farhan, H. (2012). The Golgi in cell migration: regulation by signal transduction and its implications for cancer cell metastasis. *TheScientificWorldJournal*, *2012*, 498278. https://doi.org/10.1100/2012/498278

Møller, P., Jantzen, K., Løhr, M., Andersen, M. H., Jensen, D. M., Roursgaard, M., Danielsen, P. H., Jensen, A., Loft, S. (2018). Searching for assay controls for the Fpg- and hOGG1-modified comet assay. *Mutagenesis*, *33*(1), 9–19. https://doi.org/10.1093/mutage/gex015

Møller P. (2018). The comet assay: ready for 30 more years. *Mutagenesis*, *33*(1), 1–7. https://doi.org/10.1093/mutage/gex046

Monis, W. J., Faundez, V., Pazour, G. J. (2017). BLOC-1 is required for selective membrane protein trafficking from endosomes to primary cilia. *The Journal of cell biology*, *216*(7), 2131–2150. https://doi.org/10.1083/jcb.201611138

Munro S. (2011). The golgin coiled-coil proteins of the Golgi apparatus. *Cold Spring Harbor perspectives in biology*, *3*(6), a005256. https://doi.org/10.1101/cshperspect.a005256

Murai, J., Yang, K., Dejsuphong, D., Hirota, K., Takeda, S., D'Andrea, A. D. (2011). The USP1/UAF1 complex promotes double-strand break repair through homologous recombination. *Molecular and cellular biology*, *31*(12), 2462–2469. https://doi.org/10.1128/MCB.05058-11

Musacchio A. (2022). On the role of phase separation in the biogenesis of membraneless compartments. *The EMBO journal*, *41*(5), e109952. https://doi.org/10.15252/embj.2021109952

Muschalik, N., Munro, S. (2018). Golgins. *Current biology: CB*, *28*(8), R374–R376. https://doi.org/10.1016/j.cub.2018.01.006

Muthu, M., Somagoni, J., Cheriyan, V. T., Munie, S., Levi, E., Ashour, A. E., Yassin, A. E., Alafeefy, A. M., Sochacki, P., Polin, L. A., Reddy, K. B., Larsen, S. D.,

Singh, M., Rishi, A. K. (2015). Identification and Testing of Novel CARP-1 Functional Mimetic Compounds as Inhibitors of Non-Small Cell Lung and Triple Negative Breast Cancers. *Journal of biomedical nanotechnology*, *11*(9), 1608–1627. https://doi.org/10.1166/jbn.2015.2099

Neumann, N., Lundin, D., Poole, A. M. (2010). Comparative genomic evidence for a complete nuclear pore complex in the last eukaryotic common ancestor. *PloS one*, *5*(10), e13241. https://doi.org/10.1371/journal.pone.0013241

Nijman, S. M., Huang, T. T., Dirac, A. M., Brummelkamp, T. R., Kerkhoven, R. M., D'Andrea, A. D., Bernards, R. (2005). The deubiquitinating enzyme USP1 regulates the Fanconi anemia pathway. *Molecular cell*, *17*(3), 331–339. https://doi.org/10.1016/j.molcel.2005.01.008

O'Regan, P., Wilson, C., Townsend, S., Thacker, J. (2001). XRCC2 is a nuclear RAD51-like protein required for damage-dependent RAD51 focus formation without the need for ATP binding. *The Journal of biological chemistry*, *276*(25), 22148–22153. https://doi.org/10.1074/jbc.M102396200

Paulsen, R. D., Soni, D. V., Wollman, R., Hahn, A. T., Yee, M. C., Guan, A., Hesley, J. A., Miller, S. C., Cromwell, E. F., Solow-Cordero, D. E., Meyer, T., Cimprich, K. A. (2009). A genome-wide siRNA screen reveals diverse cellular processes and pathways that mediate genome stability. *Molecular cell*, *35*(2), 228–239. https://doi.org/10.1016/j.molcel.2009.06.021

Pećina-Šlaus, N., Kafka, A., Salamon, I., Bukovac, A. (2020). Mismatch Repair Pathway, Genome Stability and Cancer. *Frontiers in molecular biosciences*, *7*, 122. https://doi.org/10.3389/fmolb.2020.00122

Pommier, Y., Leo, E., Zhang, H., Marchand, C. (2010). DNA topoisomerases and their poisoning by anticancer and antibacterial drugs. *Chemistry & biology*, *17*(5), 421–433. https://doi.org/10.1016/j.chembiol.2010.04.012

Qiu, S., Huang, J. (2021). MRN complex is an essential effector of DNA damage repair. *Journal of Zhejiang University. Science. B*, *22*(1), 31–37. https://doi.org/10.1631/jzus.B2000289

Rabouille, C., Kondylis, V. (2007). Golgi ribbon unlinking: an organelle-based G2/M checkpoint. *Cell cycle (Georgetown, Tex.)*, *6*(22), 2723–2729. https://doi.org/10.4161/cc.6.22.4896

Rass, U., Ahel, I., West, S. C. (2007). Defective DNA repair and neurodegenerative disease. *Cell*, *130*(6), 991–1004. https://doi.org/10.1016/j.cell.2007.08.043

Rebane, A. A., Ziltener, P., LaMonica, L. C., Bauer, A. H., Zheng, H., López-Montero, I., Pincet, F., Rothman, J. E., Ernst, A. M. (2020). Liquid-liquid phase separation of the Golgi matrix protein GM130. *FEBS letters*, *594*(7), 1132–1144. https://doi.org/10.1002/1873-3468.13715

Reginato, G., Cejka, P. (2020). The MRE11 complex: A versatile toolkit for the repair of broken DNA. *DNA repair*, *91-92*, 102869. https://doi.org/10.1016/j.dnarep.2020.102869

Rein, H. L., Bernstein, K. A., Baldock, R. A. (2021). RAD51 paralog function in replicative DNA damage and tolerance. *Current opinion in genetics & development*, *71*, 86–91. https://doi.org/10.1016/j.gde.2021.06.010

Rishi, A. K., Zhang, L., Boyanapalli, M., Wali, A., Mohammad, R. M., Yu, Y., Fontana, J. A., Hatfield, J. S., Dawson, M. I., Majumdar, A. P., Reichert, U. (2003). Identification and characterization of a cell cycle and apoptosis regulatory protein-1 as a novel mediator of apoptosis signaling by retinoid CD437. *The Journal of biological chemistry*, *278*(35), 33422–33435. https://doi.org/10.1074/jbc.M303173200

Rivero, S., Cardenas, J., Bornens, M., Rios, R. M. (2009). Microtubule nucleation at the cis-side of the Golgi apparatus requires AKAP450 and GM130. *The EMBO journal*, *28*(8), 1016–1028. https://doi.org/10.1038/emboj.2009.47

Rizzo, R., Parashuraman, S., Mirabelli, P., Puri, C., Lucocq, J., Luini, A. (2013). The dynamics of engineered resident proteins in the mammalian Golgi complex relies on cisternal maturation. *The Journal of cell biology*, *201*(7), 1027–1036. https://doi.org/10.1083/jcb.201211147

Sallmyr, A., Tomkinson, A. E. (2018). Repair of DNA double-strand breaks by mammalian alternative end-joining pathways. *The Journal of biological chemistry*, *293*(27), 10536–10546. https://doi.org/10.1074/jbc.TM117.000375

Sancar, A., Lindsey-Boltz, L. A., Kang, T. H., Reardon, J. T., Lee, J. H., Ozturk, N. (2010). Circadian clock control of the cellular response to DNA damage. *FEBS letters*, *584*(12), 2618–2625. https://doi.org/10.1016/j.febslet.2010.03.017

Sasaki, K., Yoshida, H. (2015). Organelle autoregulation-stress responses in the ER, Golgi, mitochondria and lysosome. *Journal of biochemistry*, *157*(4), 185–195. https://doi.org/10.1093/jb/mvv010

Scharaw, S., Iskar, M., Ori, A., Boncompain, G., Laketa, V., Poser, I., Lundberg, E., Perez, F., Beck, M., Bork, P., Pepperkok, R. (2016). The endosomal transcriptional regulator RNF11 integrates degradation and transport of EGFR. *The Journal of cell biology*, *215*(4), 543–558. https://doi.org/10.1083/jcb.201601090

Schärer O. D. (2013). Nucleotide excision repair in eukaryotes. *Cold Spring Harbor perspectives in biology*, *5*(10), a012609. https://doi.org/10.1101/cshperspect.a012609

Schumacher, B., Garinis, G. A., & Hoeijmakers, J. H. (2008). Age to survive: DNA damage and aging. *Trends in genetics: TIG*, *24*(2), 77–85. https://doi.org/10.1016/j.tig.2007.11.004

Scott, K. L., Kabbarah, O., Liang, M. C., Ivanova, E., Anagnostou, V., Wu, J., Dhakal, S., Wu, M., Chen, S., Feinberg, T., Huang, J., Saci, A., Widlund, H. R., Fisher, D. E., Xiao, Y., Rimm, D. L., Protopopov, A., Wong, K. K., Chin, L. (2009). GOLPH3 modulates mTOR signalling and rapamycin sensitivity in cancer. *Nature*, *459*(7250), 1085–1090. https://doi.org/10.1038/nature08109

Scully, R., Chen, J., Ochs, R. L., Keegan, K., Hoekstra, M., Feunteun, J., Livingston, D. M. (1997). Dynamic changes of BRCA1 subnuclear location and phosphorylation state are initiated by DNA damage. *Cell*, *90*(3), 425–435. https://doi.org/10.1016/s0092-8674(00)80503-6

Scully, R., Panday, A., Elango, R., Willis, N. A. (2019). DNA double-strand break repair-pathway choice in somatic mammalian cells. *Nature reviews. Molecular cell biology*, *20*(11), 698–714. https://doi.org/10.1038/s41580-019-0152-0

Sekhar, S. C., Venkatesh, J., Cheriyan, V. T., Muthu, M., Levi, E., Assad, H., Meister, P., Undyala, V. V., Gauld, J. W., Rishi, A. K. (2019). A H2AX^{-}CARP-1

Interaction Regulates Apoptosis Signaling Following DNA Damage. *Cancers*, *11*(2), 221. https://doi.org/10.3390/cancers11020221

Sengupta, D., Linstedt, A. D. (2011). Control of organelle size: the Golgi complex. *Annual review of cell and developmental biology*, *27*, 57–77. https://doi.org/10.1146/annurev-cellbio-100109-104003

Seo, W. Y., Jeong, B. C., Yu, E. J., Kim, H. J., Kim, S. H., Lim, J. E., Kwon, G. Y., Lee, H. M., Kim, J. H. (2013). CCAR1 promotes chromatin loading of androgen receptor (AR) transcription complex by stabilizing the association between AR and GATA2. *Nucleic acids research*, *41*(18), 8526–8536. https://doi.org/10.1093/nar/gkt644

Shamseldin, H. E., Bennett, A. H., Alfadhel, M., Gupta, V., Alkuraya, F. S. (2016). GOLGA2, encoding a master regulator of golgi apparatus, is mutated in a patient with a neuromuscular disorder. *Human genetics*, *135*(2), 245–251. https://doi.org/10.1007/s00439-015-1632-8

Shin, J. J. H., Gillingham, A. K., Begum, F., Chadwick, J., Munro, S. (2017). TBC1D23 is a bridging factor for endosomal vesicle capture by golgins at the trans-Golgi. *Nature cell biology*, *19*(12), 1424–1432. https://doi.org/10.1038/ncb3627

Shin, J. J. H., Crook, O. M., Borgeaud, A. C., Cattin-Ortolá, J., Peak-Chew, S. Y., Breckels, L. M., Gillingham, A. K., Chadwick, J., Lilley, K. S., Munro, S. (2020). Spatial proteomics defines the content of trafficking vesicles captured by golgin tethers. *Nature communications*, *11*(1), 5987. https://doi.org/10.1038/s41467-020-19840-4

Simpson, J. C., Joggerst, B., Laketa, V., Verissimo, F., Cetin, C., Erfle, H., Bexiga, M. G., Singan, V. R., Hériché, J. K., Neumann, B., Mateos, A., Blake, J., Bechtel, S., Benes, V., Wiemann, S., Ellenberg, J., Pepperkok, R. (2012). Genome-wide RNAi screening identifies human proteins with a regulatory function in the early secretory pathway. *Nature cell biology*, *14*(7), 764–774. https://doi.org/10.1038/ncb2510

Simsek, D., Jasin, M. (2010). Alternative end-joining is suppressed by the canonical NHEJ component Xrcc4-ligase IV during chromosomal translocation formation. *Nature structural & molecular biology*, *17*(4), 410–416. https://doi.org/10.1038/nsmb.1773

Smits, P., Bolton, A. D., Funari, V., Hong, M., Boyden, E. D., Lu, L., Manning, D. K., Dwyer, N. D., Moran, J. L., Prysak, M., Merriman, B., Nelson, S. F., Bonafé, L., Superti-Furga, A., Ikegawa, S., Krakow, D., Cohn, D. H., Kirchhausen, T., Warman, M. L., Beier, D. R. (2010). Lethal skeletal dysplasia in mice and humans lacking the golgin GMAP-210. *The New England journal of medicine*, *362*(3), 206–216. https://doi.org/10.1056/NEJMoa0900158

Soderholm, J. F., Bird, S. L., Kalab, P., Sampathkumar, Y., Hasegawa, K., Uehara-Bingen, M., Weis, K., Heald, R. (2011). Importazole, a small molecule inhibitor of the transport receptor importin-β. *ACS chemical biology*, *6*(7), 700–708. https://doi.org/10.1021/cb2000296

Spano, D., Colanzi, A. (2022). Golgi Complex: A Signaling Hub in Cancer. *Cells*, *11*(13), 1990. https://doi.org/10.3390/cells11131990

Stewart M. (2022). Function of the Nuclear Transport Machinery in Maintaining the Distinctive Compositions of the Nucleus and Cytoplasm. *International journal of molecular sciences*, *23*(5), 2578. https://doi.org/10.3390/ijms23052578

Stingele, J., Bellelli, R., Boulton, S. J. (2017). Mechanisms of DNA-protein crosslink repair. *Nature reviews. Molecular cell biology*, *18*(9), 563–573. https://doi.org/10.1038/nrm.2017.56

Strambio-De-Castillia, C., Niepel, M., Rout, M. P. (2010). The nuclear pore complex: bridging nuclear transport and gene regulation. *Nature reviews. Molecular cell biology*, *11*(7), 490–501. https://doi.org/10.1038/nrm2928

Sun, L. P., Li, L., Goldstein, J. L., Brown, M. S. (2005). Insig required for sterol-mediated inhibition of Scap/SREBP binding to COPII proteins in vitro. *The Journal of biological chemistry*, *280*(28), 26483–26490. https://doi.org/10.1074/jbc.M504041200

Svilar, D., Goellner, E. M., Almeida, K. H., Sobol, R. W. (2011). Base excision repair and lesion-dependent subpathways for repair of oxidative DNA damage. *Antioxidants & redox signaling*, *14*(12), 2491–2507. https://doi.org/10.1089/ars.2010.3466

Symington, L. S., Gautier, J. (2011). Double-strand break end resection and repair pathway choice. *Annual review of genetics*, *45*, 247–271. https://doi.org/10.1146/annurev-genet-110410-132435

Tahmaz, I., Shahmoradi Ghahe, S., Topf, U. (2022). Prefoldin Function in Cellular Protein Homeostasis and Human Diseases. *Frontiers in cell and developmental biology*, *9*, 816214. https://doi.org/10.3389/fcell.2021.816214

Tewey, K. M., Rowe, T. C., Yang, L., Halligan, B. D., Liu, L. F. (1984). Adriamycin-induced DNA damage mediated by mammalian DNA topoisomerase II. *Science (New York, N.Y.)*, *226*(4673), 466–468. https://doi.org/10.1126/science.6093249

Timney, B. L., Raveh, B., Mironska, R., Trivedi, J. M., Kim, S. J., Russel, D., Wente, S. R., Sali, A., Rout, M. P. (2016). Simple rules for passive diffusion through the nuclear pore complex. *The Journal of cell biology*, *215*(1), 57–76. https://doi.org/10.1083/jcb.201601004

Vodenkova, S., Azqueta, A., Collins, A., Dusinska, M., Gaivão, I., Møller, P., Opattova, A., Vodicka, P., Godschalk, R. W. L., Langie, S. A. S. (2020). An optimized comet-based in vitro DNA repair assay to assess base and nucleotide excision repair activity. *Nature protocols*, *15*(12), 3844–3878. https://doi.org/10.1038/s41596-020-0401-x

Weeden, C. E., Asselin-Labat, M. L. (2018). Mechanisms of DNA damage repair in adult stem cells and implications for cancer formation. *Biochimica et biophysica acta. Molecular basis of disease*, *1864*(1), 89–101. https://doi.org/10.1016/j.bbadis.2017.10.015

Wehrle, A., Witkos, T. M., Unger, S., Schneider, J., Follit, J. A., Hermann, J., Welting, T., Fano, V., Hietala, M., Vatanavicharn, N., Schoner, K., Spranger, J., Schmidts, M., Zabel, B., Pazour, G. J., Bloch-Zupan, A., Nishimura, G., Superti-Furga, A., Lowe, M., Lausch, E. (2019). Hypomorphic mutations of TRIP11 cause odontochondrodysplasia. *JCI insight*, *4*(3), e124701. https://doi.org/10.1172/jci.insight.124701

Wei, J. H., Seemann, J. (2009). Mitotic division of the mammalian Golgi apparatus. *Seminars in cell & developmental biology*, *20*(7), 810–816. https://doi.org/10.1016/j.semcdb.2009.03.010

Wheeler, R. J., Hyman, A. A. (2018). Controlling compartmentalization by non-membrane-bound organelles. *Philosophical transactions of the Royal Society of*

London. Series B, Biological sciences, *373*(1747), 20170193. https://doi.org/10.1098/rstb.2017.0193

Wilson, C., Venditti, R., Rega, L. R., Colanzi, A., D'Angelo, G., De Matteis, M. A. (2011). The Golgi apparatus: an organelle with multiple complex functions. *The Biochemical journal*, *433*(1), 1–9. https://doi.org/10.1042/BJ20101058

Wing, C. E., Fung, H. Y. J., Chook, Y. M. (2022). Karyopherin-mediated nucleocytoplasmic transport. *Nature reviews. Molecular cell biology*, *23*(5), 307–328. https://doi.org/10.1038/s41580-021-00446-7

Witkos, T. M., Lowe, M. (2016). The Golgin Family of Coiled-Coil Tethering Proteins. *Frontiers in cell and developmental biology*, *3*, 86. https://doi.org/10.3389/fcell.2015.00086

Wong, M., Gillingham, A. K., Munro, S. (2017). The golgin coiled-coil proteins capture different types of transport carriers via distinct N-terminal motifs. *BMC biology*, *15*(1), 3. https://doi.org/10.1186/s12915-016-0345-3

Woodrick, J., Gupta, S., Camacho, S., Parvathaneni, S., Choudhury, S., Cheema, A., Bai, Y., Khatkar, P., Erkizan, H. V., Sami, F., Su, Y., Schärer, O. D., Sharma, S., Roy, R. (2017). A new sub-pathway of long-patch base excision repair involving 5' gap formation. *The EMBO journal*, *36*(11), 1605–1622. https://doi.org/10.15252/embj.201694920

Wu, S., Shi, Y., Mulligan, P., Gay, F., Landry, J., Liu, H., Lu, J., Qi, H. H., Wang, W., Nickoloff, J. A., Wu, C., Shi, Y. (2007). A YY1-INO80 complex regulates genomic stability through homologous recombination-based repair. *Nature structural & molecular biology*, *14*(12), 1165–1172. https://doi.org/10.1038/nsmb1332

Yamada, K., Ono, M., Perkins, N. D., Rocha, S., Lamond, A. I. (2013). Identification and functional characterization of FMN2, a regulator of the cyclin-dependent kinase inhibitor p21. *Molecular cell*, *49*(5), 922–933. https://doi.org/10.1016/j.molcel.2012.12.023

Yamamoto, H., Kakuta, S., Watanabe, T. M., Kitamura, A., Sekito, T., Kondo-Kakuta, C., Ichikawa, R., Kinjo, M., Ohsumi, Y. (2012). Atg9 vesicles are an important membrane source during early steps of autophagosome formation. *The Journal of cell biology*, *198*(2), 219–233. https://doi.org/10.1083/jcb.201202061

Ye, J., DeBose-Boyd, R. A. (2011). Regulation of cholesterol and fatty acid synthesis. *Cold Spring Harbor perspectives in biology*, *3*(7), a004754. https://doi.org/10.1101/cshperspect.a004754

Yoon, S., Choi, J. H., Shah, M., Kwon, S. M., Yang, J., Park, Y. N., Wang, H. J., Woo, H. G. (2021). USO1 isoforms differentially promote liver cancer progression by dysregulating the ER-Golgi network. *Carcinogenesis*, *42*(9), 1208–1220. https://doi.org/10.1093/carcin/bgab067

Zappa, F., Failli, M., De Matteis, M. A. (2018). The Golgi complex in disease and therapy. *Current opinion in cell biology*, *50*, 102–116. https://doi.org/10.1016/j.ceb.2018.03.005

Zhao, Y. G., & Zhang, H. (2020). Phase Separation in Membrane Biology: The Interplay between Membrane-Bound Organelles and Membraneless Condensates. *Developmental cell*, *55*(1), 30–44. https://doi.org/10.1016/j.devcel.2020.06.033

Appendix

Supplementary figures

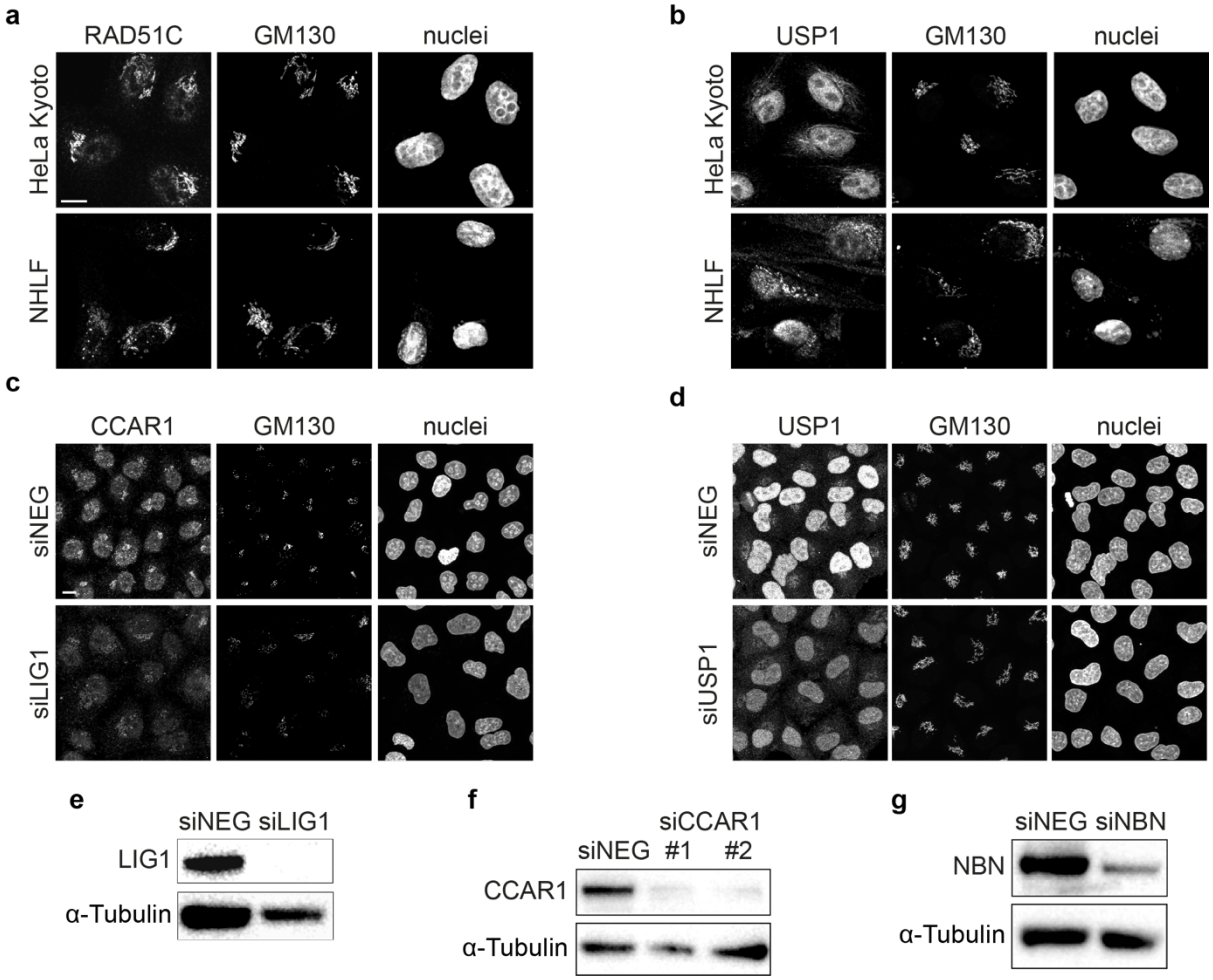

Supplementary Figure 1. Validation experiments for Golgi-nuclear localised proteins. (a-b) Representative images of the dual-localised DDR proteins RAD51C and USP1 in HeLa Kyoto and NHLF cells, which were fixed and stained with antibodies against RAD51C, USP1 and Golgi marker GM130; nuclei were stained with Hoechst 33342. **(c-d)** Example images of antibody validation experiments for antibodies against LIG1 and USP1. HeLa Kyoto cells were transfected with control NEG9, LIG1 and USP1 siRNAs for 72 hours, then fixed and stained with antibodies against LIG1, USP1 and Golgi marker GM130; nuclei were stained with Hoechst 33342, scale bars, 10 μm. **(e-g)** Western blots showing proteins levels of LIG1, CCAR1 and NBN in HeLa Kyoto cells, which were transfected with control NEG9, LIG1, CCAR1 and NBN siRNAs for 72 hours, then fixed and stained with antibodies against LIG1, CCAR1 and NBN and protein loading marker α-Tubulin.

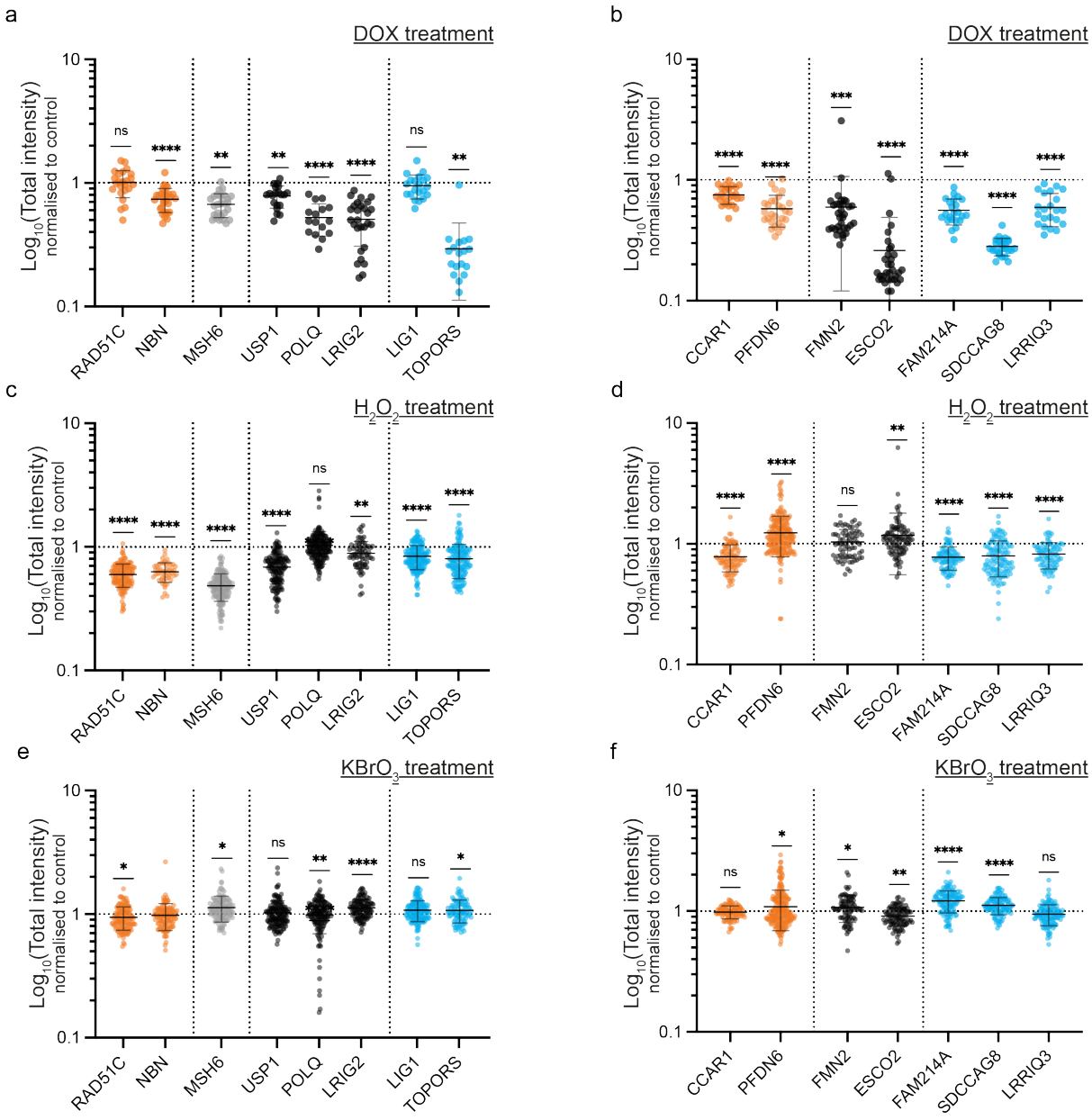

Supplementary Figure 2. Quantifications of the relative total intensity of DDR proteins upon induction of DNA damage with DOX, H2O2 and $KBrO_3$. (a-b) HeLa Kyoto cells were treated with 40 µM Doxorubicin for 3 hours; **(c-d)** 5 mM H_2O_2 for 20 minutes and let for 15 minutes recover; **(e-f)** 5 mM $KBrO_3$ for 3 hours, prior to cells being fixed and stained with antibodies against RAD51C, NBN, MSH6, LRIG2, POLQ, USP1, TOPORS, LIG1, CCAR1, PFDN6, FMN2, ESCO2, FAM214A, SDCCAG8, LRRIQ3 and Golgi marker GM130. Quantification of the normalised total intensity of DDR proteins untreated control versus treated. Error bars represent the mean ± SD (n=3 independent biological replicates).

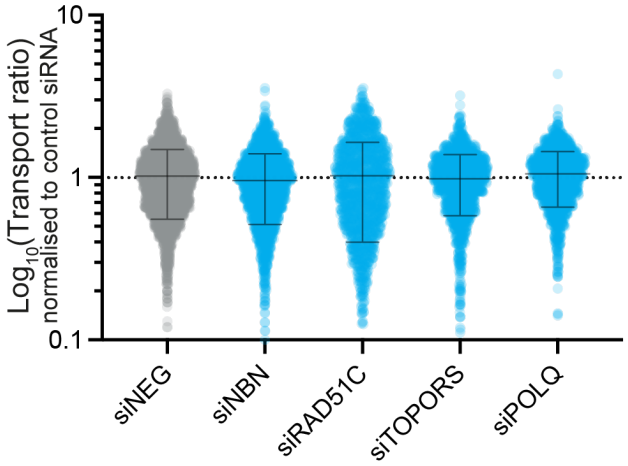

Supplementary Figure 3. Quantifications of VSV-G transport assay. HeLa Kyoto cells were transfected with control NEG9, NBN, RAD51C, TOPORS and POLQ siRNAs for 48 hours, followed by VSV-G assay, then fixed and stained with antibodies against VSV-G protein, cell nuclei were stained with Hoechst 33342. Quantifications present a normalised ratio of VSV-G (A647 signal) intensity at the plasma membrane and total VSV-G (YFP) intensity. Error bars represent the mean ± SD (n=3 independent biological replicates).

Supplementary tables

IP sample	Gene	logFC	P value
NBN	DBI	1.0455	0.0230
	MYDGF	1.0156	0.0034
	PRRC1	1.0406	0.0009
MSH6	DBI	1.0233	0.0254
	MYDGF	1.0972	0.0020
USP1	TMF1	3.8110	<0.0001
LIG1	ARF5	1.0069	0.0073
	DBI	1.5411	0.0025
	GDI1	1.2697	0.0056
	HMGB1	1.1723	0.0071
	HPD	1.0211	0.0041
	MYDGF	1.3673	0.0004
CCAR1	ARF5	1.0495	0.0057
	DBI	1.1599	0.0137
	GDI1	1.2503	0.0061
	MYDGF	1.4075	0.0003
	TMED10	1.1246	0.0054
ESCO2	GOLIM4	1.4786	<0.0001
	MYDGF	1.0185	0.0033
SDCCAG8	GOLM1	1.2773	<0.0001

Supplementary Table 1. MS-IP analysis of DDR proteins results. Data represents Golgi localising proteins from Gene Ontology (GO) analysis of interaction data from DDR IP samples**.** Summarized data of two independent replicates. Data normalised to the control sample without antibodies present.

IP sample	Gene	logFC	P value
CUX1	DMAP1	1.9532	0.0003
	LIG3	1.9548	0.0003
	RPA1	1.7907	0.0008
	RPA3	1.8914	0.0004
	TERF2	3.1626	<0.0001
	TERF2IP	2.5442	<0.0001
	XRCC1	1.7785	0.0009
Giantin	ATRX	1.4696	0.0648
	MRE11A	1.6393	0.0391
	NBN	1.5928	0.0451
	RAD50	1.9276	0.0151
	SMCHD1	1.3401	0.0927
	TNKS1BP1	1.7382	0.0286
	ZBTB1	3.3779	<0.0001
GMAP-210	CRIP1	1.0943	<0.0001
	NOP53	1.6963	<0.0001
	UBR5	1.5356	<0.0001
GOLGA7	YY1	1.1038	<0.0001
GOLGIN-245	PLK1	1.0297	0.0293
GOGIN-97	RNF138	1.0788	<0.0001

Supplementary Table 2. MS-IP analysis of Golgin family proteins results. Data represents DDR proteins indicated by Gene Ontology (GO) analysis of interaction data from Golgin IP samples**.** Shown preliminary data from one MS-IP experiment. Data normalised to the control sample without antibodies present.

Cell Profiler Pipeline

CellProfiler Pipeline: http://www.cellprofiler.org
Version:5
DateRevision:413
GitHash:
ModuleCount:38
HasImagePlaneDetails:False

Images:[module_num:1|svn_version:'Unknown'|variable_revision_number:2|show_window:False|notes:['To begin creating your project, use the Images module to compile a list of files and/or folders that you want to analyze. You can also specify a set of rules to include only the desired files in your selected folders.']|batch_state:array([], dtype=uint8)|enabled:True|wants_pause:False]
    :
    Filter images?:Images only
    Select the rule criteria:and (extension does isimage) (directory doesnot containregexp "[\\\\/]\\.")

NamesAndTypes:[module_num:3|svn_version:'Unknown'|variable_revision_number:8|show_window:False|notes:['The NamesAndTypes module allows you to assign a meaningful name to each image by which other modules will refer to it.']|batch_state:array([], dtype=uint8)|enabled:True|wants_pause:False]
    Assign a name to:Images matching rules
    Select the image type:Grayscale image
    Name to assign these images:DNA
    Match metadata:[]
    Image set matching method:Order
    Set intensity range from:Image metadata
    Assignments count:3
    Single images count:0
    Maximum intensity:255.0
    Process as 3D?:No
    Relative pixel spacing in X:1.0
    Relative pixel spacing in Y:1.0
    Relative pixel spacing in Z:1.0
    Select the rule criteria:and (file does contain "0001")
    Name to assign these images:h33342
    Name to assign these objects:Cell
    Select the image type:Grayscale image
    Set intensity range from:Image metadata
    Maximum intensity:255.0
    Select the rule criteria:and (file does contain "0000")
    Name to assign these images:gm130
    Name to assign these objects:Nucleus
    Select the image type:Grayscale image
    Set intensity range from:Image metadata
    Maximum intensity:255.0
    Select the rule criteria:and (file does contain "0002")
    Name to assign these images:rad51c
    Name to assign these objects:Cytoplasm
    Select the image type:Grayscale image
    Set intensity range from:Image metadata
    Maximum intensity:255.0

IdentifyPrimaryObjects:[module_num:5|svn_version:'Unknown'|variable_revision_number:14|show_window:False|notes:[]|batch_state:array([], dtype=uint8)|enabled:True|wants_pause:False]
    Select the input image:h33342
    Name the primary objects to be identified:intial_seg_nuclei
    Typical diameter of objects, in pixel units (Min,Max):20,200
    Discard objects outside the diameter range?:Yes
    Discard objects touching the border of the image?:Yes
    Method to distinguish clumped objects:Shape
    Method to draw dividing lines between clumped objects:Intensity
    Size of smoothing filter:10
    Suppress local maxima that are closer than this minimum allowed distance:7.0
    Speed up by using lower-resolution image to find local maxima?:Yes
    Fill holes in identified objects?:After both thresholding and declumping
    Automatically calculate size of smoothing filter for declumping?:Yes

Automatically calculate minimum allowed distance between local maxima?:Yes
Handling of objects if excessive number of objects identified:Continue
Maximum number of objects:500
Display accepted local maxima?:No
Select maxima color:Blue
Use advanced settings?:Yes
Threshold setting version:12
Threshold strategy:Global
Thresholding method:Minimum Cross-Entropy
Threshold smoothing scale:1.3488
Threshold correction factor:1.0
Lower and upper bounds on threshold:0.001,1.0
Manual threshold:0.01
Select the measurement to threshold with:None
Two-class or three-class thresholding?:Two classes
Log transform before thresholding?:No
Assign pixels in the middle intensity class to the foreground or the background?:Foreground
Size of adaptive window:50
Lower outlier fraction:0.05
Upper outlier fraction:0.05
Averaging method:Mean
Variance method:Standard deviation
# of deviations:2.0
Thresholding method:Otsu

IdentifySecondaryObjects:[module_num:6|svn_version:'Unknown'|variable_revision_number:10|show_window:False|notes:[]|batch_state:array([], dtype=uint8)|enabled:True|wants_pause:False]
Select the input objects:intial_seg_nuclei
Name the objects to be identified:intiation_cell_segmentation
Select the method to identify the secondary objects:Distance - N
Select the input image:gm130
Number of pixels by which to expand the primary objects:35
Regularization factor:0.05
Discard secondary objects touching the border of the image?:No
Discard the associated primary objects?:No
Name the new primary objects:FilteredNuclei
Fill holes in identified objects?:No
Threshold setting version:12
Threshold strategy:Global
Thresholding method:Minimum Cross-Entropy
Threshold smoothing scale:0.0
Threshold correction factor:1.0
Lower and upper bounds on threshold:0.0,1.0
Manual threshold:0.0
Select the measurement to threshold with:None
Two-class or three-class thresholding?:Two classes
Log transform before thresholding?:No
Assign pixels in the middle intensity class to the foreground or the background?:Foreground
Size of adaptive window:50
Lower outlier fraction:0.05
Upper outlier fraction:0.05
Averaging method:Mean
Variance method:Standard deviation
# of deviations:2.0
Thresholding method:Otsu

EnhanceOrSuppressFeatures:[module_num:7|svn_version:'Unknown'|variable_revision_number:7|show_window:False|notes:[]|batch_state:array([], dtype=uint8)|enabled:True|wants_pause:False]
Select the input image:gm130
Name the output image:golgi_background_subt
Select the operation:Enhance
Feature size:10
Feature type:Speckles
Range of hole sizes:1,10
Smoothing scale:2.0
Shear angle:0.0
Decay:0.95

Enhancement method:Tubeness
Speed and accuracy:Fast
Rescale result image:No

ExpandOrShrinkObjects:[module_num:9|svn_version:'Unknown'|variable_revision_number:2|show_window:False|notes:[]|batch_state:array([], dtype=uint8)|enabled:True|wants_pause:False]
Select the input objects:intiation_cell_segmentation
Name the output objects:shrunken_cell_segmentation
Select the operation:Shrink objects by a specified number of pixels
Number of pixels by which to expand or shrink:1
Fill holes in objects so that all objects shrink to a single point?:No

ConvertObjectsToImage:[module_num:10|svn_version:'Unknown'|variable_revision_number:1|show_window:False|notes:[]|batch_state:array([], dtype=uint8)|enabled:True|wants_pause:False]
Select the input objects:shrunken_cell_segmentation
Name the output image:CellImage
Select the color format:Binary (black & white)
Select the colormap:Default

IdentifyPrimaryObjects:[module_num:11|svn_version:'Unknown'|variable_revision_number:14|show_window:False|notes:[]|batch_state:array([], dtype=uint8)|enabled:True|wants_pause:False]
Select the input image:CellImage
Name the primary objects to be identified:cells
Typical diameter of objects, in pixel units (Min,Max):10,200
Discard objects outside the diameter range?:No
Discard objects touching the border of the image?:No
Method to distinguish clumped objects:Intensity
Method to draw dividing lines between clumped objects:Intensity
Size of smoothing filter:0
Suppress local maxima that are closer than this minimum allowed distance:0
Speed up by using lower-resolution image to find local maxima?:No
Fill holes in identified objects?:After both thresholding and declumping
Automatically calculate size of smoothing filter for declumping?:No
Automatically calculate minimum allowed distance between local maxima?:No
Handling of objects if excessive number of objects identified:Continue
Maximum number of objects:500
Display accepted local maxima?:No
Select maxima color:Blue
Use advanced settings?:Yes
Threshold setting version:12
Threshold strategy:Global
Thresholding method:Manual
Threshold smoothing scale:1.3488
Threshold correction factor:1.0
Lower and upper bounds on threshold:0.0,1.0
Manual threshold:0.9
Select the measurement to threshold with:None
Two-class or three-class thresholding?:Two classes
Log transform before thresholding?:No
Assign pixels in the middle intensity class to the foreground or the background?:Foreground
Size of adaptive window:50
Lower outlier fraction:0.05
Upper outlier fraction:0.05
Averaging method:Mean
Variance method:Standard deviation
# of deviations:2.0
Thresholding method:Otsu

MaskImage:[module_num:12|svn_version:'Unknown'|variable_revision_number:3|show_window:False|notes:[]|batch_state:array([], dtype=uint8)|enabled:True|wants_pause:False]
Select the input image:h33342
Name the output image:h33342_masked
Use objects or an image as a mask?:Objects
Select object for mask:cells
Select image for mask:None
Invert the mask?:No

MaskImage:[module_num:13|svn_version:'Unknown'|variable_revision_number:3|show_window:False|notes:[]|batch_state:array([], dtype=uint8)|enabled:True|wants_pause:False]
    Select the input image:golgi_background_subt
    Name the output image:gm130_masked
    Use objects or an image as a mask?:Objects
    Select object for mask:cells
    Select image for mask:None
    Invert the mask?:No

MaskImage:[module_num:14|svn_version:'Unknown'|variable_revision_number:3|show_window:False|notes:[]|batch_state:array([], dtype=uint8)|enabled:True|wants_pause:False]
    Select the input image:rad51c
    Name the output image:rad51c_masked
    Use objects or an image as a mask?:Objects
    Select object for mask:cells
    Select image for mask:None
    Invert the mask?:No

IdentifyPrimaryObjects:[module_num:15|svn_version:'Unknown'|variable_revision_number:14|show_window:False|notes:[]|batch_state:array([], dtype=uint8)|enabled:True|wants_pause:False]
    Select the input image:h33342_masked
    Name the primary objects to be identified:nuclei_final
    Typical diameter of objects, in pixel units (Min,Max):20,200
    Discard objects outside the diameter range?:Yes
    Discard objects touching the border of the image?:No
    Method to distinguish clumped objects:Shape
    Method to draw dividing lines between clumped objects:Intensity
    Size of smoothing filter:10
    Suppress local maxima that are closer than this minimum allowed distance:7.0
    Speed up by using lower-resolution image to find local maxima?:Yes
    Fill holes in identified objects?:After both thresholding and declumping
    Automatically calculate size of smoothing filter for declumping?:Yes
    Automatically calculate minimum allowed distance between local maxima?:Yes
    Handling of objects if excessive number of objects identified:Continue
    Maximum number of objects:500
    Display accepted local maxima?:No
    Select maxima color:Blue
    Use advanced settings?:Yes
    Threshold setting version:12
    Threshold strategy:Global
    Thresholding method:Minimum Cross-Entropy
    Threshold smoothing scale:1.3488
    Threshold correction factor:1.0
    Lower and upper bounds on threshold:0.0044,1.0
    Manual threshold:0.0
    Select the measurement to threshold with:None
    Two-class or three-class thresholding?:Two classes
    Log transform before thresholding?:No
    Assign pixels in the middle intensity class to the foreground or the background?:Foreground
    Size of adaptive window:50
    Lower outlier fraction:0.05
    Upper outlier fraction:0.05
    Averaging method:Mean
    Variance method:Standard deviation
    # of deviations:2.0
    Thresholding method:Otsu

IdentifyPrimaryObjects:[module_num:16|svn_version:'Unknown'|variable_revision_number:14|show_window:False|notes:[]|batch_state:array([], dtype=uint8)|enabled:True|wants_pause:False]
    Select the input image:gm130_masked
    Name the primary objects to be identified:golgi
    Typical diameter of objects, in pixel units (Min,Max):2,50
    Discard objects outside the diameter range?:Yes
    Discard objects touching the border of the image?:No
    Method to distinguish clumped objects:Intensity
    Method to draw dividing lines between clumped objects:Intensity
    Size of smoothing filter:10

Suppress local maxima that are closer than this minimum allowed distance:7.0
Speed up by using lower-resolution image to find local maxima?:Yes
Fill holes in identified objects?:After both thresholding and declumping
Automatically calculate size of smoothing filter for declumping?:Yes
Automatically calculate minimum allowed distance between local maxima?:Yes
Handling of objects if excessive number of objects identified:Continue
Maximum number of objects:500
Display accepted local maxima?:No
Select maxima color:Blue
Use advanced settings?:Yes
Threshold setting version:12
Threshold strategy:Global
Thresholding method:Minimum Cross-Entropy
Threshold smoothing scale:1.3488
Threshold correction factor:1.0
Lower and upper bounds on threshold:0.005,1.0
Manual threshold:0.0
Select the measurement to threshold with:None
Two-class or three-class thresholding?:Two classes
Log transform before thresholding?:No
Assign pixels in the middle intensity class to the foreground or the background?:Foreground
Size of adaptive window:50
Lower outlier fraction:0.05
Upper outlier fraction:0.05
Averaging method:Mean
Variance method:Standard deviation
# of deviations:2.0
Thresholding method:Otsu

MaskImage:[module_num:17|svn_version:'Unknown'|variable_revision_number:3|show_window:False|notes:[]|batch_state:array([], dtype=uint8)|enabled:True|wants_pause:False]
Select the input image:rad51c_masked
Name the output image:nuclei_golgi_removed
Use objects or an image as a mask?:Objects
Select object for mask:golgi
Select image for mask:None
Invert the mask?:Yes

MaskImage:[module_num:18|svn_version:'Unknown'|variable_revision_number:3|show_window:False|notes:[]|batch_state:array([], dtype=uint8)|enabled:True|wants_pause:False]
Select the input image:nuclei_golgi_removed
Name the output image:nuclei_only_final
Use objects or an image as a mask?:Objects
Select object for mask:nuclei_final
Select image for mask:None
Invert the mask?:No

MaskImage:[module_num:19|svn_version:'Unknown'|variable_revision_number:3|show_window:False|notes:[]|batch_state:array([], dtype=uint8)|enabled:True|wants_pause:False]
Select the input image:rad51c_masked
Name the output image:golgi_rad51c_mask
Use objects or an image as a mask?:Objects
Select object for mask:golgi
Select image for mask:None
Invert the mask?:No

MaskImage:[module_num:20|svn_version:'Unknown'|variable_revision_number:3|show_window:False|notes:[]|batch_state:array([], dtype=uint8)|enabled:True|wants_pause:False]
Select the input image:golgi_rad51c_mask
Name the output image:golgi_only_without_nucleus
Use objects or an image as a mask?:Objects
Select object for mask:nuclei_final
Select image for mask:None
Invert the mask?:Yes

MeasureObjectIntensity:[module_num:21|svn_version:'Unknown'|variable_revision_number:4|show_window:False|notes:[]|batch_state:array([], dtype=uint8)|enabled:True|wants_pause:False]

Select images to measure:golgi_only_without_nucleus
Select objects to measure:cells

MeasureObjectIntensity:[module_num:22|svn_version:'Unknown'|variable_revision_number:4|show_window:Fals
e|notes:[]|batch_state:array([], dtype=uint8)|enabled:True|wants_pause:False]
Select images to measure:nuclei_only_final
Select objects to measure:cells

OverlayOutlines:[module_num:31|svn_version:'Unknown'|variable_revision_number:4|show_window:False|notes:
[]|batch_state:array([], dtype=uint8)|enabled:True|wants_pause:False]
Display outlines on a blank image?:No
Select image on which to display outlines:markers_overlay_rescaled
Name the output image:rad51c_overlay_cell
Outline display mode:Color
Select method to determine brightness of outlines:Max of image
How to outline:Inner
Select outline color:#FC8008
Select objects to display:cells

OverlayOutlines:[module_num:32|svn_version:'Unknown'|variable_revision_number:4|show_window:False|notes:
[]|batch_state:array([], dtype=uint8)|enabled:True|wants_pause:False]
Display outlines on a blank image?:No
Select image on which to display outlines:rad51c_overlay_cell
Name the output image:marker_overlay_cell_nucleus
Outline display mode:Color
Select method to determine brightness of outlines:Max of image
How to outline:Inner
Select outline color:#FC8008
Select objects to display:intial_seg_nuclei

OverlayOutlines:[module_num:33|svn_version:'Unknown'|variable_revision_number:4|show_window:False|notes:
[]|batch_state:array([], dtype=uint8)|enabled:True|wants_pause:False]
Display outlines on a blank image?:No
Select image on which to display outlines:marker_overlay_cell_nucleus
Name the output image:marker_overlay_all
Outline display mode:Color
Select method to determine brightness of outlines:Max of image
How to outline:Inner
Select outline color:#FC8008
Select objects to display:golgi

DisplayDataOnImage:[module_num:34|svn_version:'Unknown'|variable_revision_number:6|show_window:False|
notes:[]|batch_state:array([], dtype=uint8)|enabled:True|wants_pause:False]
Display object or image measurements?:Object
Select the input objects:cells
Measurement to display:Number_Object_Number
Select the image on which to display the measurements:marker_overlay_all
Text color:#F40007
Name the output image that has the measurements displayed:DisplayImage_marker_identifier
Font size (points):10
Number of decimals:0
Image elements to save:Image
Annotation offset (in pixels):0
Display mode:Text
Color map:Default
Display background image?:Yes
Color map scale:Use this image's measurement range
Color map range:0.0,1.0

DisplayDataOnImage:[module_num:35|svn_version:'Unknown'|variable_revision_number:6|show_window:False|
notes:[]|batch_state:array([], dtype=uint8)|enabled:True|wants_pause:False]
Display object or image measurements?:Object
Select the input objects:cells
Measurement to display:Number_Object_Number
Select the image on which to display the measurements:rad51c_rescaled
Text color:#FEFEFE

Name the output image that has the measurements displayed:DisplayImage_rad51c_cell_identifier
Font size (points):10
Number of decimals:0
Image elements to save:Image
Annotation offset (in pixels):0
Display mode:Text
Color map:Default
Display background image?:Yes
Color map scale:Use this image's measurement range
Color map range:0.0,1.0

ExportToSpreadsheet:[module_num:36|svn_version:'Unknown'|variable_revision_number:13|show_window:False|notes:[]|batch_state:array([], dtype=uint8)|enabled:True|wants_pause:False]
Select the column delimiter:Comma (",")
Add image metadata columns to your object data file?:No
Add image file and folder names to your object data file?:No
Select the measurements to export:Yes
Calculate the per-image mean values for object measurements?:No
Calculate the per-image median values for object measurements?:No
Calculate the per-image standard deviation values for object measurements?:No
Output file location:Elsewhere...|/Location_for_analysis_files
Create a GenePattern GCT file?:No
Select source of sample row name:Metadata
Select the image to use as the identifier:None
Select the metadata to use as the identifier:None
Export all measurement types?:Yes
Press button to select measurements:cells|Intensity_MeanIntensity_nuclei_only_final,cells|Intensity_MeanIntensity_golgi_only_without_nucleus,cells|Intensity_IntegratedIntensity_nuclei_only_final,cells|Intensity_IntegratedIntensity_golgi_only_without_nucleus,cells|Intensity_MedianIntensity_nuclei_only_final,cells|Intensity_MedianIntensity_golgi_only_without_nucleus,cells|Number_Object_Number,cells
Representation of Nan/Inf:NaN
Add a prefix to file names?:Yes
Filename prefix:analysis_nbn_dox+ipz
Overwrite existing files without warning?:No
Data to export:cells
Combine these object measurements with those of the previous object?:No
File name:DATA.csv
Use the object name for the file name?:No

SaveImages:[module_num:37|svn_version:'Unknown'|variable_revision_number:15|show_window:False|notes:[]|batch_state:array([], dtype=uint8)|enabled:True|wants_pause:False]
Select the type of image to save:Image
Select the image to save:DisplayImage_marker_identifier
Select method for constructing file names:Sequential numbers
Select image name for file prefix:None
Enter file prefix:image_markers_
Number of digits:2
Append a suffix to the image file name?:Yes
Text to append to the image name:segmentation_
Saved file format:jpeg
Output file location:Elsewhere...|/Location_for_analysis_files
Image bit depth:8-bit integer
Overwrite existing files without warning?:No
When to save:Every cycle
Record the file and path information to the saved image?:No
Create subfolders in the output folder?:No
Base image folder:Elsewhere...|
How to save the series:T (Time)

SaveImages:[module_num:38|svn_version:'Unknown'|variable_revision_number:15|show_window:False|notes:[]|batch_state:array([], dtype=uint8)|enabled:True|wants_pause:False]
Select the type of image to save:Image
Select the image to save:DisplayImage_rad51c_cell_identifier
Select method for constructing file names:Sequential numbers
Select image name for file prefix:None
Enter file prefix:image_rad51c_

Number of digits:2
Append a suffix to the image file name?:Yes
Text to append to the image name:rad51c_
Saved file format:jpeg
Output file location:Elsewhere...|/Location_for_analysis_files
Image bit depth:8-bit integer
Overwrite existing files without warning?:No
When to save:Every cycle
Record the file and path information to the saved image?:No
Create subfolders in the output folder?:No
Base image folder:Elsewhere...|
How to save the series:T (Time)